AD-A095 368 NORTHWESTERN UNIV EVANSTON IL F/G 7/4

NONLINEAR OPTICAL EFFECTS IN LIQUID CRYSTALS.(U)

DEC 80 G K WONG DAAG29-77-G-0009

UNCLASSIFIED ARO-14280.4-P NL

1 OF 2

AD A095 368

UNCLASSIFIED

SECURITY CLASSIFICATION OF THIS PAGE (When Data Entered)

REPORT DOCUMENTATION PAGE		READ INSTRUCTIONS BEFORE COMPLETING FORM
1. REPORT NUMBER (19) 14280.4-P (18) ARO	2. GOVT ACCESSION NO. AD-A095	3. RECIPIENT'S CATALOG NUMBER 368
4. TITLE (and Subtitle) NONLINEAR OPTICAL EFFECTS IN LIQUID CRYSTALS. (6)		5. TYPE OF REPORT & PERIOD COVERED (9) FINAL repts
		6. PERFORMING ORG. REPORT NUMBER
7. AUTHOR(s) (10) George K./Wong (12) 114		8. CONTRACT OR GRANT NUMBER(s) (15) DAAG29-77-G-0009
9. PERFORMING ORGANIZATION NAME AND ADDRESS Northwestern University Evanston, IL 60201		10. PROGRAM ELEMENT, PROJECT, TASK AREA & WORK UNIT NUMBERS (11) 10 Dec 80
11. CONTROLLING OFFICE NAME AND ADDRESS U. S. Army Research Office Post Office Box 12211 Research Triangle Park, NC 27709		12. REPORT DATE December 10, 1980
		13. NUMBER OF PAGES 113
14. MONITORING AGENCY NAME & ADDRESS(if different from Controlling Office)		15. SECURITY CLASS. (of this report) Unclassified
		15a. DECLASSIFICATION/DOWNGRADING SCHEDULE

LEVEL II

16. DISTRIBUTION STATEMENT (of this Report)

Approved for public release; distribution unlimited.

DTIC ELECTE FEB 19 1981 S D C

17. DISTRIBUTION STATEMENT (of the abstract entered in Block 20, if different from Report)

NA

18. SUPPLEMENTARY NOTES

The view, opinions, and/or findings contained in this report are those of the author(s) and should not be construed as an official Department of the Army position, policy, or decision, unless so designated by other documentation.

19. KEY WORDS (Continue on reverse side if necessary and identify by block number)

Non linear optics, Liquid crystals, Phase-matching, Nonlinear susceptibilities, Lasers, Nematic, Cholesteric, Flexoelectric, Second-harmonic generation

20. ABSTRACT (Continue on reverse side if necessary and identify by block number)

SEE REVERSE SIDE

DD FORM 1 JAN 73 1473 EDITION OF 1 NOV 65 IS OBSOLETE

D.C.-field induced optical second-harmonic generation in nematic and cholesteric liquid crystals is investigated. In addition, flexo-electric induced second-harmonic generation in nematic MBBA is studied.

The experiments involve the detection of optical radiation at second-harmonic frequency when aligned thin film liquid crystals samples are irradiated with laser beam at the fundamental frequency. The laser used in a Q-switched Nd-YAG laser. Sample alignment is achieved either with rubbing technique or by coating glass spacers with 100 Å thick of SiO_2.

Experiments on nematic liquid crystals show that the temperature dependence of nematic order parameters can be obtained from the measurement of d.c.-induced second-harmonic generation. It is also demonstrated that flexoelectric effect can give rise to second-harmonic generation in nematic liquid crystal and the birefringence of nematic crystal can be used to achieve phase-matching. In the cholesteric liquid crystal, it is demonstrated that the lattice momentum associated with the one dimensional periodicity of cholesteric structure can be used to achieve phase-matching.

Comparison of the measured temperature dependence of nematic order parameters with the predictions of the existing statistical theories of nematic ordering indicates that these theories are not quantitatively reliable. The phase-matchability of liquid crystals shows that these media may be useful as practical optical harmonic generators.

NONLINEAR OPTICAL EFFECTS
IN LIQUID CRYSTALS

Abstract

D. C.-field-induced optical second-harmonic generation in nematic and cholesteric liquid crystals is investigated. In addition, flexo-electric induced second-harmonic generation in nematic MBBA is studied.

The experiments involve the detection of optical radiation at second-harmonic frequency when aligned thin film liquid crystals samples are irradiated with laser beam at the fundamental frequency. The laser used is a Q-switched Nd-YAG laser. Sample alignment is achieved either with rubbing technique or by coating glass spacers with 100 Å thick of SiO_2.

Experiments on nematic liquid crystals show that the temperature dependence of nematic order parameters can be obtained from the measurement of d. c.-induced second-harmonic generation. It is also demonstrated that flexoelectric effect can give rise to second-harmonic generation in nematic liquid crystal and the birefringence of nematic crystal can be used to achieve phase-matching. In the cholesteric liquid crystal, it is demonstrated that the lattice momentum associated with the one dimensional periodicity of cholesteric structure can be used to achieve phase-matching.

Comparison of the measured temperature dependence of nematic order parameters with the predictions of the existing statistical theories of nematic ordering indicates that these theories are not quantitatively reliable. The phase-matchability of liquid crystals shows that these media may be useful as practical optical harmonic generators.

TABLE OF CONTENTS

PUBLICATIONS

"Investigation of Nematic ordering using Electric-field-induced Second-harmonic Generation", S.K. Saha and George K. Wong, Applied Physics Letters 34, 423 (1979).

"Phase-matched Electric-field-induced Second-harmonic Generation in a Nematic Crystal", S.K. Saha and George K. Wong. Optics Communications 30, 119 (1979).

"Flexoelectric-induced Second-harmonic Generation in a Nematic Liquid Crystal", S.G. Gu, S.K. Saha, and George K. Wong, Molecular Crystals and Liquid Crystals, in press.

PARTICIPATING SCIENTIFIC PERSONNEL

Name:	Position:	Degree Granted:
Santosh K. Saha	Research Assistant	Ph.D., Physics
Jagmohan Bajaj	Research Assistant	
Hsin-Hsin Chou	Postdoc	
Shi-Jie Gu	Visiting Scholar	
George K. Wong	Associate Professor	

1. INTRODUCTION

Nonlinear optics[1] deals with optical phenomena arising from material polarization which is nonlinear in the amplitudes of the applied electromagnetic fields. The nonlinear material response to electromagnetic fields is described by expanding the polarization[2] in a power series in the field. For the pure electric dipole case one has for example,

$$\vec{P} = \overleftrightarrow{\Gamma} \cdot \vec{E} + \overleftrightarrow{\Gamma} : \vec{E}\,\vec{E} + \overleftrightarrow{\Gamma} \vdots\, \vec{E}\,\vec{E}\,\vec{E} + \cdots\cdots\cdots\cdots$$

The first term defines the usual linear susceptibility, the second term the lowest order nonlinear susceptibility, and so on. This procedure is useful because the optical nonlinearities are small. In fact, it can be shown the ratio of the magnitudes of the polarization in successive order is $\simeq |E|/|E_{at}|$ where $|E|$ is the electric field amplitude of the light wave and $|E_{at}|$ is the electric field inside the atom. Since $|E_{at}|$ is $\simeq 10^8$ volt/cm and $|E|$ is $\simeq 10^6$ volt/cm for a moderately intense beam with a power density of 10^9 watt/cm^2, the nonlinearities are usually quite small. However, due to excellent discrimination available in optical experiments, these nonlinear optical effects can be readily detected. For example, when a laser beam at frequency ω is incident on a material, the polarization quadratic in the field amplitude leads to optical radiation at 2ω. This is known as optical second-harmonic generation (SHG). For a medium with centrosymmetry, the second-order nonlinearity vanishes and SHG is forbidden. However, in the presence of an applied dc field the second-harmonic can still be observed. This is known as dc-field-induced second-harmonic generation (FISHG) and it is described by a polarization in the field amplitudes.

Over the past two decades, the field of nonlinear optics has grown rapidly. The main research effort has been to achieve an understanding of nonlinear optical effects in solids, liquids, and gases, to construct useful nonlinear optical devices using these media[3,4,5] and more recently to use nonlinear optical measurements to study the properties of materials. However, there have been only a few investigations of the nonlinear optical effects in liquid crystals.

Liquid crystals[6] are materials composed of elongated molecules with strong anisotropy. The molecular shape and intermolecular forces tend to make these molecules align parallel to one another against thermal agitation. As a result, new phases, known as mesomorphic phases, appear between the liquid phase and solid phase. In these phases, the molecules are more or less aligned with long range structural order. According to their ordering, they can be classified into nematic, smectic, and cholesteric phases (shown in Fig. 1). Among these phases, the nematic phase has the least ordering. In this phase, the long axes of the elongated molecules are oriented in a certain direction but the center of mass of the molecules are arranged at random. These molecules are free to translate and rotate about their long axes. The smectic phase has additional order. In this phase, the centers of mass of the molecules are arranged in equidistant planes. The molecules still retain their mobility in two dimensions (in the equidistant plane) and rotate about their long axes. Additional ordering within the two dimensional plane exists and smectic phases can be classified further[6]. The cholesteric phase can be considered as a twisted nematic phase. In this phase, the molecules form layers. In each layer, the long axes of the molecules are aligned parallel to each other and also parallel to the layer. But as the layers advance, the direction of the alignment gradually rotates. As a result, the material has an overall helical structure.

During the last decade, the physics of liquid crystals has grown rapidly. This area has been investigated because of the potential of liquid crystals in practical applications and the interesting physics involved, such as phase transitions and critical phenomena[7,8]. However, the nonlinear optical properties of liquid crystals have been sparsely studied. With the exception of the chiral smectic C phase, all mesomorphic phases possess overall centrosymmetry. Hence SHG is not expected to occur in liquid crystal phases. In fact, the experimental verifications that the SHG is absent in these mesomorphic phases provides stringent proof that there is no polarity associated with the director $\hat{n}$ (the macroscopic symmetry axis of the liquid crystals) and $\hat{n}$ and $-\hat{n}$ are physically indistinguishable. The third-order optical nonlinearity in liquid crystals is, however, quite large. Because of the strong molecular anisotropy, even an optical field can induce appreciable molecular alignment along the field. The induced alignment, which is proportional to the order parameter, gives rise to an induced birefringence proportional to $|E|^2$ or the optical intensity. In the isotropic phase, this effect, known as the optical Kerr effect, is closely analogous to a paramagnetic spin system responding to an applied magnetic field. Here the light intensity plays the role of the magnetic field and the induced birefringence is equivalent to the induced magnetization. Thus one expects that the induced birefringence Δn in the isotropic phase should obey the Curie law. Also the induced alignment should show a critical slowing down behavior, i.e., the relaxation time of Δn diverges near the isotropic to nematic phase transition. Indeed, this pretransitional behavior has been observed by Wong and Shen[4]. Other third-order nonlinear optical effects that have been observed in liquid crystals are third-harmonic generation and self-focusing[3].

In this dissertation, d. c.-field-induced second-harmonic generation (FISHG) in liquid crystals is investigated theoretically and experimentally for the first time. In Chapter 2, a detailed description of the experimental techniques and apparatus is given. In Chapter 3, we derive a relationship between the third-order macroscopic nonlinearity of a nematic crystal and its microscopic order parameters. We show that measurement of the temperature dependence of third-order nonlinearities can yield the temperature dependence of nematic order parameters. Experimental results obtained from two nematic liquid crystal 5CB and MBBA are then presented and compared with those obtained from polarized Raman scattering measurements. In Chapter 4, phase-matched FISHG in cholesteric liquid crystals is discussed. Finally, we present in Chapter 5 the observation of flexoelectric induced second-harmonic generation in a nematic liquid crystal.

REFERENCES

Chapter 1

1. J. D. Jackson, Classical Electrodynamics, 2nd edition (Wiley, New York, 1975), p. 17.
2. N. Bloembergen, Nonlinear Optics, 2nd edition (Benjamin Press, New York, 1977).
3. Y. R. Shen, Rev. Mod. Phys. 48, 1 (1976).
4. G. K. Wong and Y. R. Shen, Phys. Rev. Lett. 30, 895 (1973); Phys. Rev. A 10, 1277 (1974).
5. R. W. Hellwarth, Prog. Quantum Electron. 5, 1 (1977).
6. P. G. De Gennes, Physics of Liquid Crystals (Clarendon, Oxford, 1974); S. Chandrasekhar, Liquid Crystals (Cambridge University Press, Cambridge, 1977).
7. K. Miyano and J. B. Ketterson, in Physical Acoustics 14, edited by W. P. Mason and R. N. Thurston (Academic Press, New York, 1979), p. 93.
8. C. W. Woo, in Quantum Fluids and Solids, edited by S. B. Trickey, E. D. Adams, and J. W. Dufty (Plenum Press, New York, 1977), p. 265.

FIGURE CAPTIONS

Chapter 1

1. Molecular arrangement in various liquid crystalline phases. Liquid crystal molecules are schematically represented as rods.

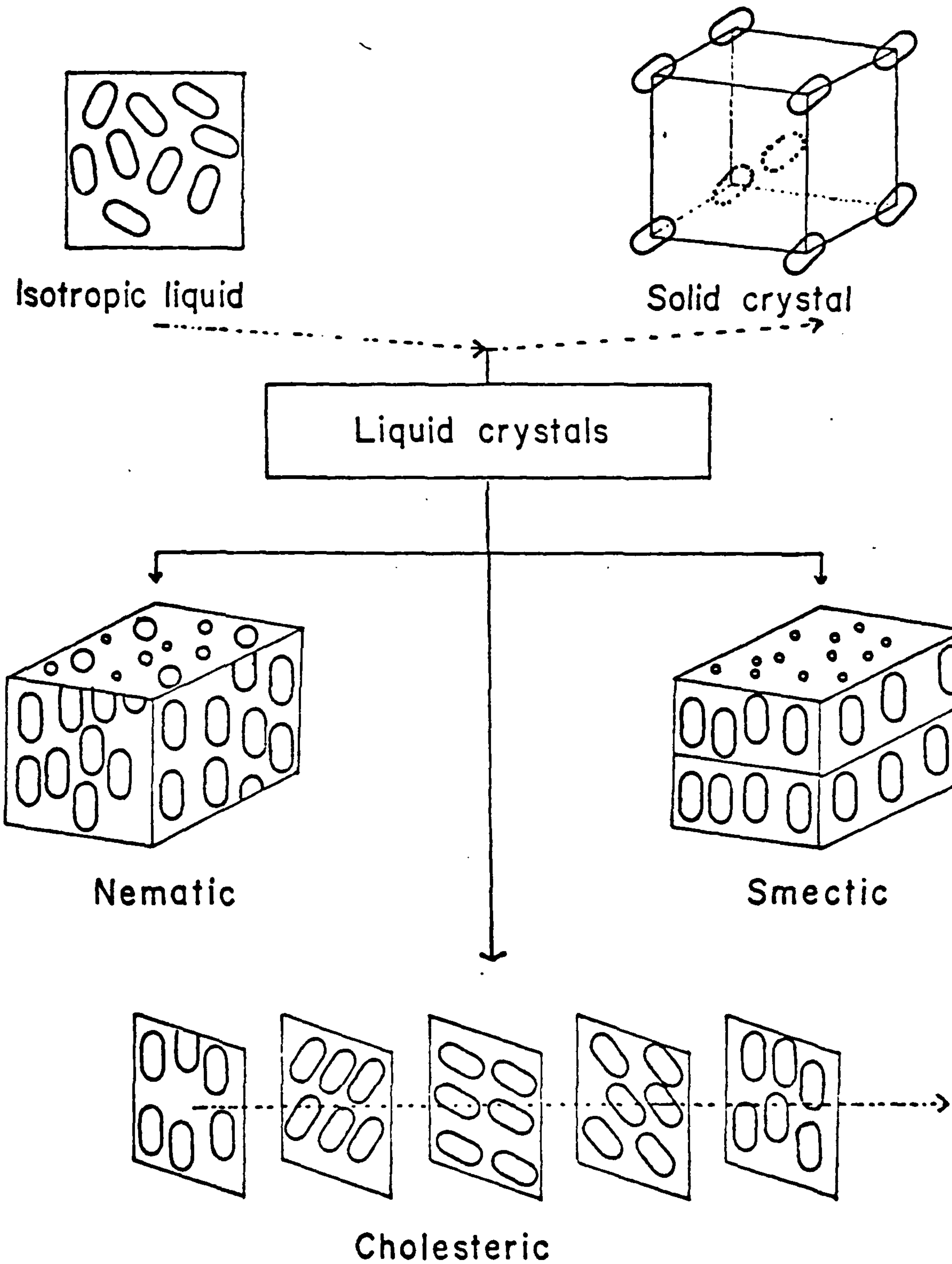
Isotropic liquid
Solid crystal
Liquid crystals
Nematic
Smectic
Cholesteric

FIG. 1

2. EXPERIMENTAL TECHNIQUES

In order to study field-induced second-harmonic generation we need a high power pulsed laser with suitable wavelength and a high voltage pulsed generator to apply a d.c. electric field to the medium in synchronization with the laser pulse. In addition, we also need a highly sensitive detection system. Between the laser and detection system there are optical components to define the direction of the laser beam and its polarization, a sample cell containing the liquid crystals to be studied, and filters to extract signal from the transmitted laser beam.

Figure 1 shows a typical arrangement for observing field-induced second-harmonic generation. Laser light at suitable wavelength propagates through the medium to which a high voltage pulse is applied. The detection system picks up the second-harmonic quanta from the transmitted fundamental quanta. Each system is discussed in detail in the following sections.

2.1 Laser

To avoid linear absorption of the second-harmonic intensity by the liquid crystals, the experiments were done using a Q-switched Nd:YAG laser (Quanta-Ray, Diffraction-Coupled Resonator, DCR) at a fundamental wavelength of 1.064 μm. The laser pulse had a maximum peak power of 20 MW and its pulse width was 10 nsec. The beam was weakly focussed into the sample cell with a 100 cm focal length lens. The original beam diameter of 6.3 mm was focussed down to a spot of diameter 0.2 mm at the sample. With a 100 cm focal length lens, the beam wrist was sufficiently long that the laser beam in the focal region could well be approximated as pencil rays. Thus the angular spread of the wave vectors in the focal region can be neglected. This enabled us to observe clearly the coherence length effect so that coherence length for second-harmonic generation could be measured accurately. To avoid optical damage of samples, the laser power was attenuated to 500 kW by inserting heat absorbing glasses in the path of the fundamental beam. At the focus, the donut-shaped output of the laser was transformed into a beam profile described by Airy's function[1,2]. This beam profile was sufficiently smooth for efficient and stable second-harmonic generation.

2.2 High voltage pulse generator

In order to observe second-harmonic generation from nematic and cholesteric phase, a d.c. electric field is needed to break the centrosymmetry of these phases. In our experiments, a pulsed d.c. field of 3 μsec duration was used so that dynamic scattering[3] in the nematic phase and heating of samples due to current flow could be avoided. A high voltage pulse generator by Narda (Model 10003) was used to generate the pulsed d.c. field. This generator is a typical hard tube device. It uses a high vacuum tube with a control grid to switch the energy storage condenser. The pulse duration is determined by the characteristics of the driver circuit[4] consisting of a line-simulating network and a pulse transformer. This high voltage pulse generator delivers 5 kV peak voltage with a 2 mA average current capacity.

To avoid ringing, the output of the generator was terminated at the sample with a 100 kΩ resistor. The rise and fall times of the pulse were 30 nsec and 400 nsec respectively. The high voltage pulse was monitored on the oscilloscope using a Tektronix high voltage probe (Model P6013A with an attenuation factor of 10^3). In order to synchronize the high voltage pulse with the laser pulse, the high voltage pulse generator was operated in external triggering mode. Details of the synchronization scheme are discussed in the next section.

2.3 Detection system

All the experiments we report here consist of measurement of very weak signals at the wavelength 5320 Å in the strong background of the laser. Since second-harmonic radiation is coherent, it is transmitted in the same direction as the laser beam. To extract second-harmonic intensity we used a harmonic beamsplitter (CVI Laser Corp., BSR 106-5) It transmits 70% of the 5320 Å radiation and 0.5% of the fundamental radiation. Further discrimination was obtained by placing a cell containing saturated $CuSO_4$ solution[5] and an interference filter with a band width of 50 Å in front of the photomultiplier. Due to the insertion loss of these discriminators, only one out of five second-harmonic photons can reach the photomultiplier. The photomultiplier used was a low noise, high gain (10^7) RCA tube (8575). At 5320 Å , this tube has a quantum efficiency of 12%. Thus the overall efficiency of our system allows 3 photoelectrons to be generated for every 100 second-harmonic photons.

The output of the photomultiplier was measured with a home-built gated integrator whose gate was opened just before the laser pulse and was reset a few microseconds later. The advantage of using a gated integrator is that most of the dark current pulses of the photomultiplier tube can be eliminated without cooling the tube. The integrator chip in the homebuilt gated integrator, was made by Optical Electronics (Model 9080). A schematic of it is shown in Fig. 2. A very low leakage 100 pF condenser is used for integration. For each photoelectron, there is 16 mV output which is much larger than the noise of the integrator. Hence every photoelectron can be easily detected. The output of the integrator is buffered by an operational amplifier. There is a provision for fine offset voltage adjustment in the input to the amplifier so that the baseline can be adjusted. A RC integrator of time constant 0.5 sec was used to average the output of the gated integrator. For a repetition rate of 10 Hz, the 0.5 sec time constant allowed averaging of 300 pulses so that the fluctuation of the signal due to laser power fluctuation could be averaged out. Finally the output of this RC integrator was fed to a chart recorder.

To operate the gated integrator we need to sequence pulses to open the gate and reset it before the next event. Signals from the sequencer are shown in Fig. 3. The sequencer card is triggered by the time delay pulse (delay 263 μsec) of the lamp synchronized output of the laser. Once the sequencer is started, the timing is derived from a 10 MHz crystal oscillator. The sequencer determines the delay and duration of the integrator gate, integrator reset, and trigger output.

Fig. 4 shows the sequencer cricuit diagram. The input trigger pulse resets two sequencer counters (I.C. Chips 4 and 6) and an edge triggered flip-flop (I.C. Chip 1A) is set to 5. The output of a crystal oscillator is fed to a nand gate followed by a synchronized counter (I.C. Chips 4), a binary counter (I.C. Chip 6), and a demultiplexer

(I.C. Chip 5). The outputs of the demultiplexer are 1 μsec pulses. These output at successive points Q_1, Q_2, and Q_3 are delayed by 1 μsec from the preceding one and indicated by their respective subscripts. But the delay between Q_3 and Q_4 can be adjusted by a timer (I.C. Chip 7A). The timing sequence at Q_4, Q_5,.......Q_9 follow in the same way as Q_1, Q_2 and Q_3 and each is delayed by 1 μsec from the preceding one. The integrator gate, integrator reset, and trigger output are derived from the output of the demultiplexer.

The integrator gate is opened by the output of an edge trigger flip-flop (I.C. Chip 1B) which is triggered by the output from Q_1. The width of the gate can be adjusted by a timer (I.C. Chips 7A). The input pulse of this timer can be held low by a RC circuit with an appropriate time constant. The time constant of this RC circuit determines the gate width.

The reset pulse is obtained by feeding the sequence of pulses at Q_4 and Q_5 into a nand gate. In order to reset the integrator, the reset pulse should be within the integrator gate. This was achieved by using sequence pulse Q_9 to close the integrator gate.

The trigger output is obtained from a timer (I.C. Chips 7B) whose input is Q_2. The width is obtained by keeping the input pulse low by a RC circuit. In this case it was held to a fixed width of 18 μsec.

To synchronize the laser pulse with the H.V. pulse, the Q-switch of the laser and the H.V. pulse generator were triggered externally. The synchronization scheme used in our experiments is shown in Fig. 5. All the timing was derived from the lamp synchronized output from the laser. After a fixed delay of 250 us, the pulse is used to trigger the H.V.

pulse generator and another fixed time delay pulse is used to initiate the sequencer card. The trigger output of the integrator was delayed by using a pulse generator with a fine variable delay (10 nsec to 1 μsec), and then the output of the pulse generator was then used to trigger the Q-switch of the laser.

To eliminate the variation of second-harmonic signal due to fluctuation in the power of the fundamental laser beam, 8% of the fundamental beam was split off by inserting a beamsplitter in the fundamental beam path. This split-off beam was focussed onto a wedge-shaped quartz crystal to generate second-harmonic. The second-harmonic from quartz was measured with another identical gated integrator. The signals from the two gated integrators were then ratioed by a ratiometer.

2.4 Cell design

The design of the glass cell is shown in Fig. 6. It is similar to that described by Bethea in reference 6. In order to measure the macroscopic third order nonlinearity, main consideration was given to the following matters: 1) uniform field in the sample region, 2) minimization of d. c.-field-induced third order nonlinearity of glass spacers, 3) provision for continuous change of the sample length, and 4) stable regulation of the sample temperature.

Uniform electric field (~15 kV/cm) was obtained by keeping the glass spacers perpendicular to the electrodes. The contribution of the field-induced second-harmonic intensity from the glass was minimized by keeping the outer boundaries of the spacers away from the edges of the electrodes. At the laser power level used in our experiments, second-harmonic intensity from the glass spacers is below the noise level of our detection system. For continuous variation of the sample thickness, the cell was made into a wedge-shape by placing mylar (50 μ m) at one end of the spacers. The wedge angle was measured using the two reflected dots of He-Ne laser from the inner two surfaces of the spacers.

The spacers and electrodes were held together in a copper holder using nylon screws. A glass cell containing liquid crystal was placed at the bottom end of the spacers. By capillary action, the region between the spacers is automatically filled with liquid crystal. The temperature of the copper holder was regulated by a proportional temperature controller. To insure temperature stability and to keep the sample stable, the copper holder was placed in an optical dewar. After inserting sample in the glass cell, the optical dewar was pumped out and back filled with nitrogen gas.

2.5 Temperature control

A proportional temperature controller by Oven Industries Inc. (Model 5CX-220) was used in our experiments. The shematic circuit diagram is shown in Fig. 7. A resistance sensing bridge network is used with a thermistor sensor and a coarse and fine temperature adjustment potentiometer (R_1). The bridge network is driven by a sinusoidal input (60 Hz) from a function generator. The signal of the sensing bridge is an input signal to a differential amplifier. Zero crossing information is combined with the output of the differential amplifier through an AND gate to cause the power amplifier to conduct through a load. A fraction of the output of the AND gate is fed to the function generator. This loop acts as a negative feed back circuit and this feed back circuit causes the temperature controller to drive as a proportional controller. There is a provision to adjust the band width of the controller. This is done by shaping the square wave to a proper sinusoidal wave. The preset potentiometer (R_2) determines the temperature. Fig. 8 shows the signals of the temperature controller for three different situations.

In our experiments, we used a TXO model (Oven Industries Inc.) thermistor and a 50 W heater. By carefully adjusting the band width, we could achieve stable temperature control within $\pm$ 0.05° C.

2.6 Sample alignment

Samples of liquid crystal materials were placed between two carefully cleaned glass spacers. The glass spacers were made into a wedge-shaped cell by placing a mylar strip (50 μ m) at one end as shown in Fig. 6. Prior to assembling the cell, the glass spacers were cleaned in hot chromic acid and then rinsed several times in deionized water. The glass spacers were then dried by blowing nitrogen gas over them and then baked at temperatures above 100° C. To achieve homogeneous alignment (director in the surface of glass spacer), the surface of the glass spacer was either rubbed unidirectionally with tissue paper or coated with 100 Å of SiO_2 [7]. In the former treatment, it was found that rubbing with light strokes produced satisfactory homogeneous alignment while rubbing with hard strokes usually resulted in tilting of the director away from the glass surface. In the latter treatment, SiO_2 was evaporated obliquely with an incident angle of 60° onto the glass spacer surface[8]. The glass spacer was oriented in such a way that the glass spacer surface is perpendicular to the incident plane. This procedure consistently produced good quality homogeneous alignment.

The quality of the alignment was checked by viewing the conoscopic figure[9] obtained by normal illumination of the samples between two crossed polarizers with a strongly focussed He-Ne beam. Typical interference patterns show families of hyperbola-like fringes. The geometrical appearance of these patterns unambiguously reflect the success of the alignment.

In summary, I have described in detail the experimental technique used in d.c. field-induced second-harmonic generation from the liquid crystals. Fig. 9 shows a schematic diagram of the apparatus and the layout required for FISHG. The optical dewar was placed on a translation mount (not shown in the figure). The temperature of the optical dewar was regulated by a temperature controller (not shown in the figure). This technique is useful for accurate determination of the macroscopic third-order nonlinearity of liquid crystals.

REFERENCES

Chapter 2

1. A. E. Siegman, Appl. Optics 23, 353 (1974).
2. R. L. Byer and R. L. Herbst, Laser Focus July, 48 (1978).
3. P. G. de Gennes, Physics of Liquid Crystals (Clarendon, Oxford, 1974).
4. Pulse Generator, Vol. 5 of MIT Radiation Laboratory Series: A Treatise, edited by G. N. Glasoe and J. V. Lebacoz (McGraw-Hill, New York, 1948).
5. S. F. Pellicori, Appl. Optics 3, 361 (1964).
6. C. G. Bethea, Appl. Optics 14, 1447 (1973).
7. J. L. Janning, Appl. Phys. Lett. 21, 173 (1973).
8. W. Urbach, M. Boix, and E. Guyon, Appl. Phys. Lett. 25, 479 (1974).
9. S. Jen, N. A. Clark, P. S. Pershan, and E. B. Priestly, J. Chem. Phys. 66, 4635 (1977).

FIGURE CAPTIONS

Chapter 2

1. Block diagram of experimental arrangement.
2. Schematic diagram of gated integrator.
3. Signals of sequencer circuits.
4. Schematic diagram of sequencer circuits.
5. Signals for synchronizing H. V. pulse with laser pulse.
6. A. Top view of the liquid crystal cell.

   B. Side view of the entire assembly of cell.
7. Schematic diagram of temperature control.
8. Signals of temperature control.
9. Experimental arrangement for field-induced second-harmonic generation in liquid crystals.

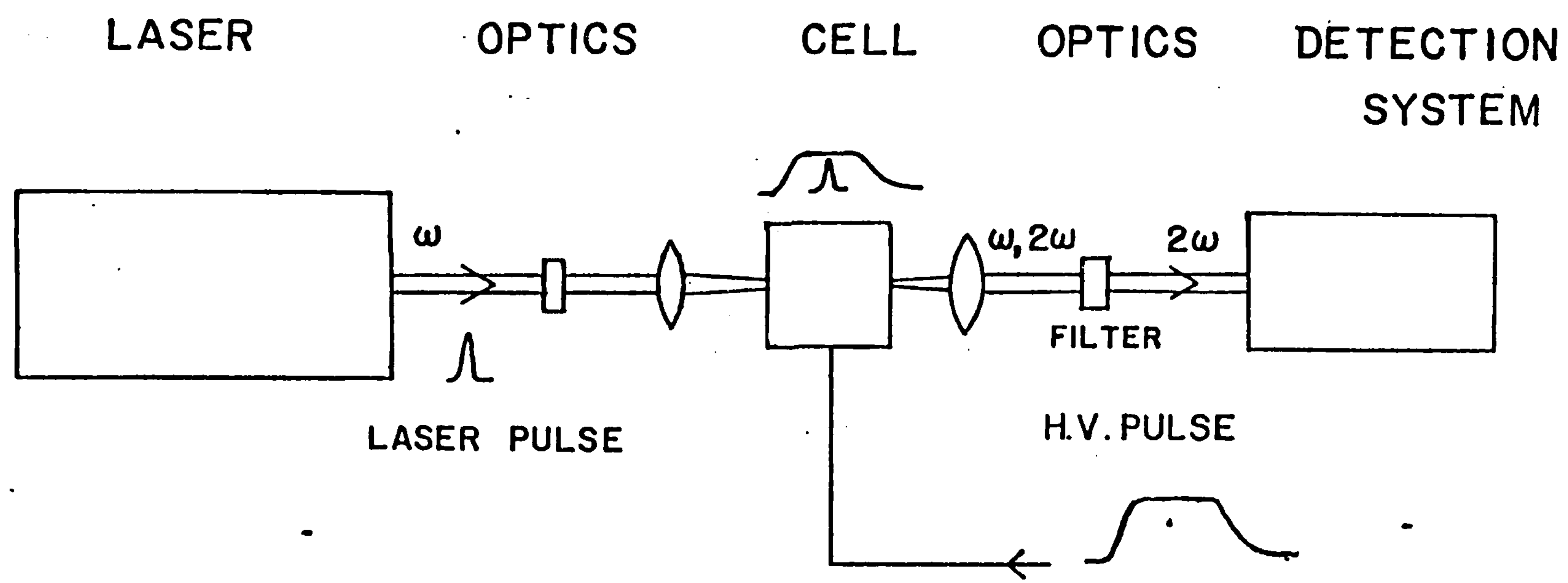
LASER
OPTICS
CELL
OPTICS
DETECTION SYSTEM
ω
ω,2ω
2ω
FILTER
LASER PULSE
H.V. PULSE

FIG. 1

GATED INTEGRATOR

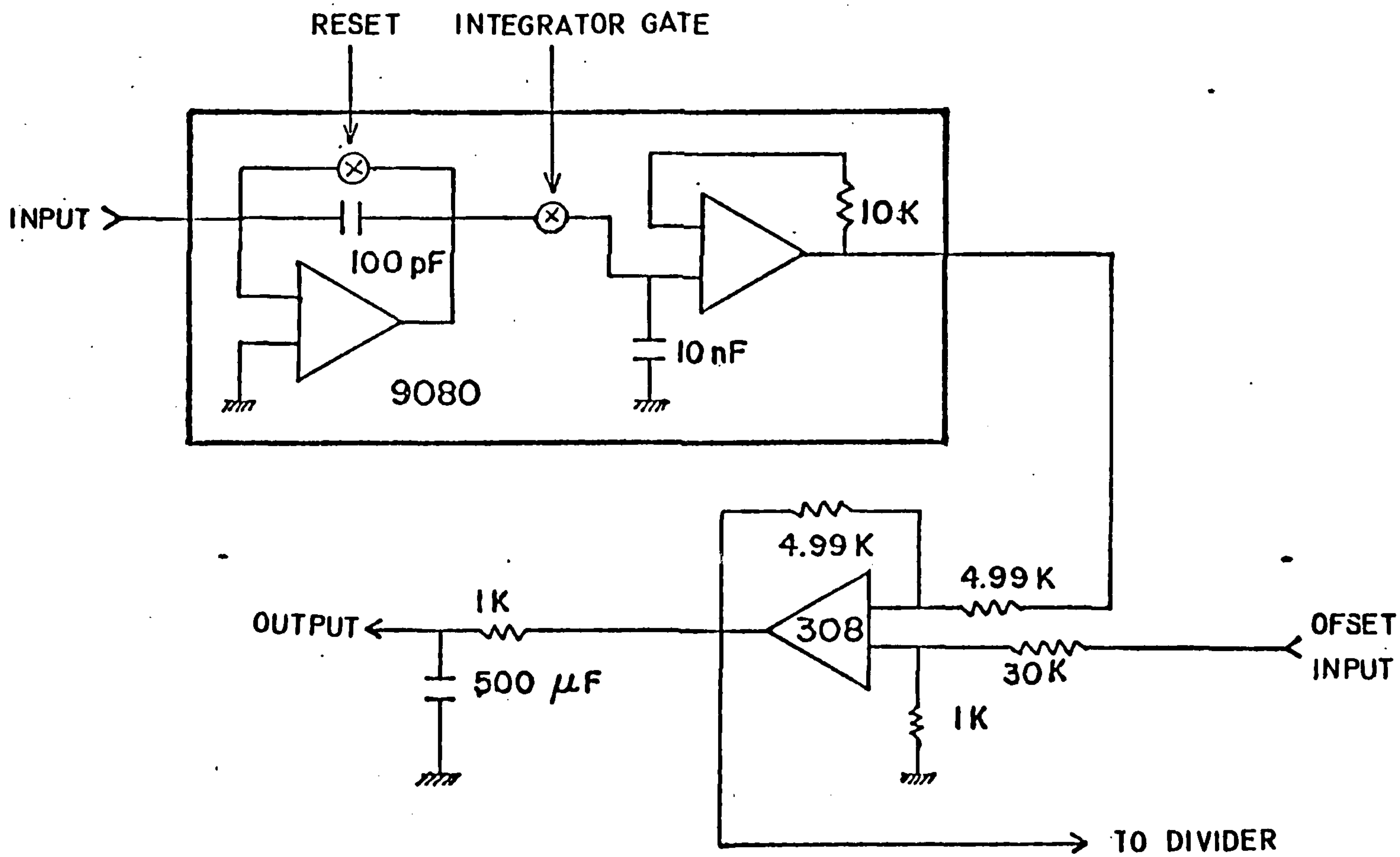

FIG. 2

SIGNALS OF SEQUENCER

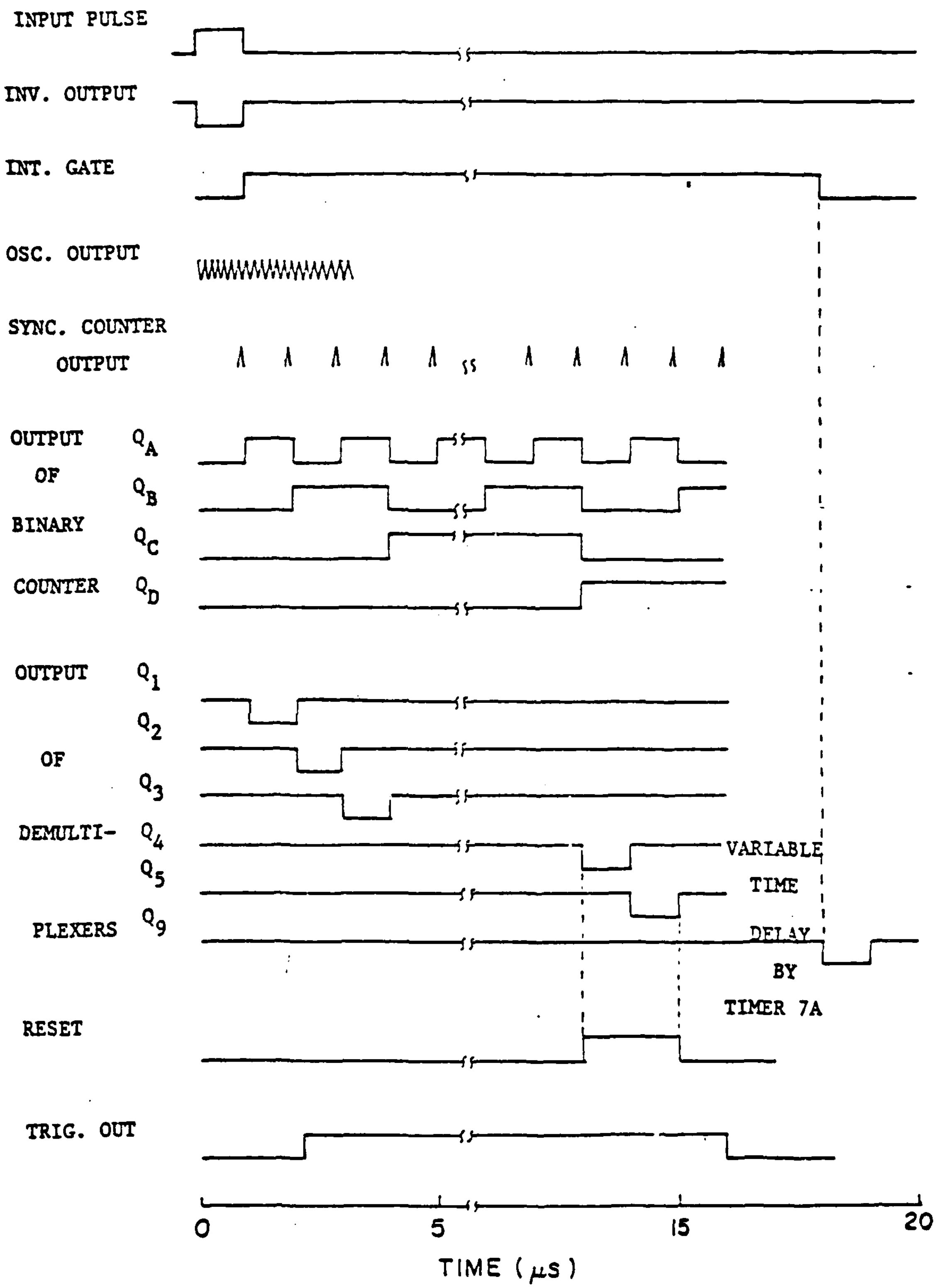

FIG. 3

SEQUENCER CIRCUITS

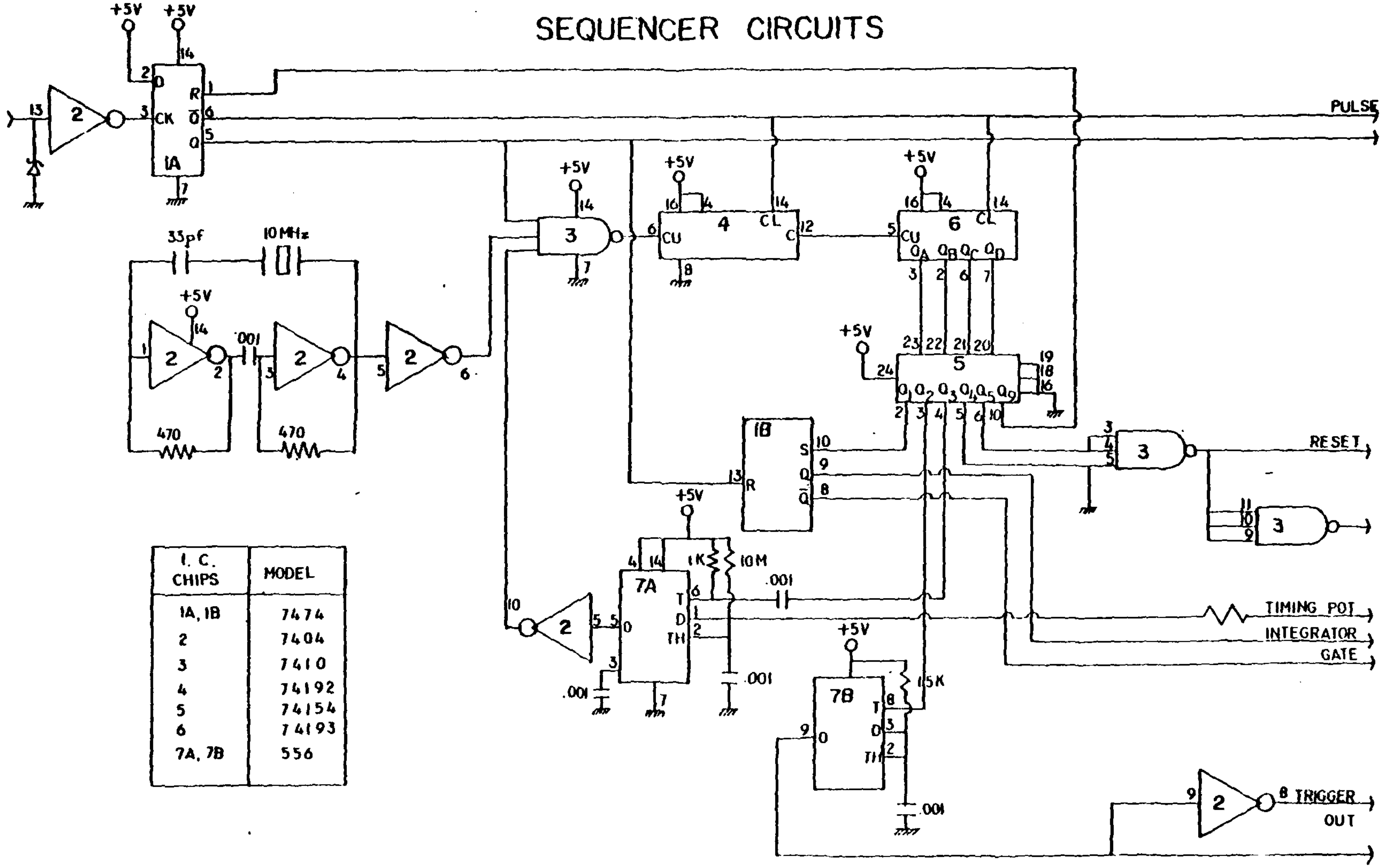

I. C. CHIPS	MODEL
1A, 1B	7474
2	7404
3	7410
4	74192
5	74154
6	74193
7A, 7B	556

FIG. 4

SIGNALS FOR SYNCHRONIZATION OF H.V. PULSE AND LASER PULSE

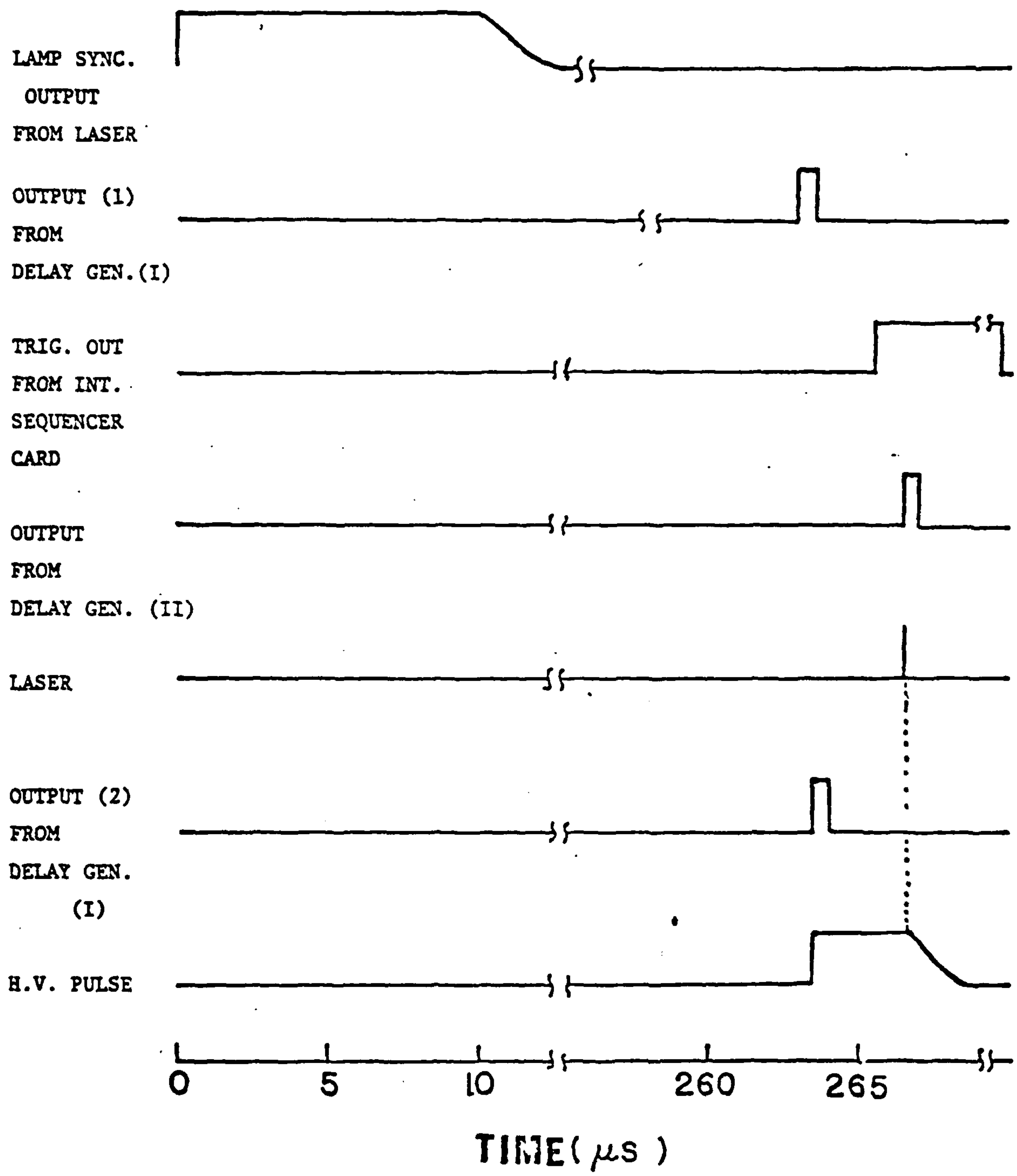

FIG. 5

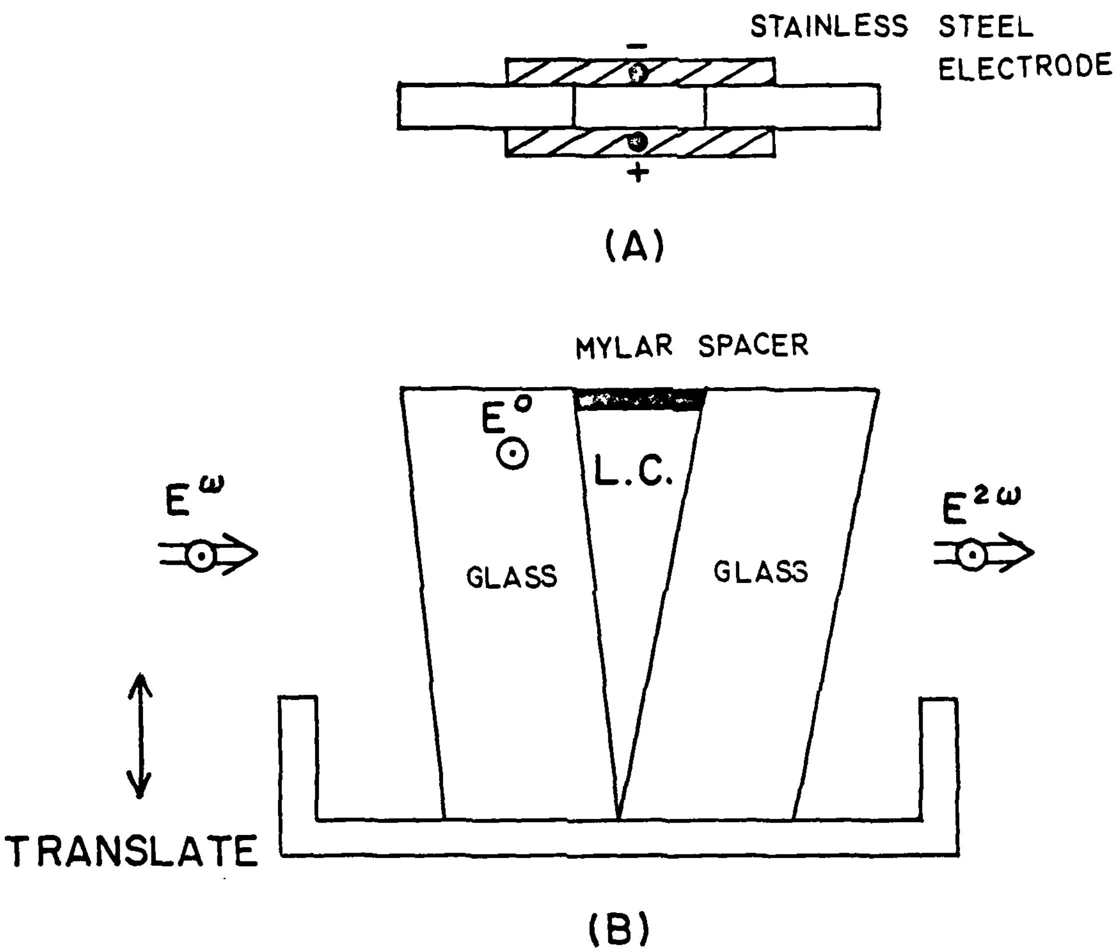
STAINLESS STEEL ELECTRODE
−
+
(A)
MYLAR SPACER
E^o
L.C.
E^ω
GLASS
GLASS
$E^{2\omega}$
TRANSLATE
(B)

FIG. 6

TEMPERATURE CONTROLLER

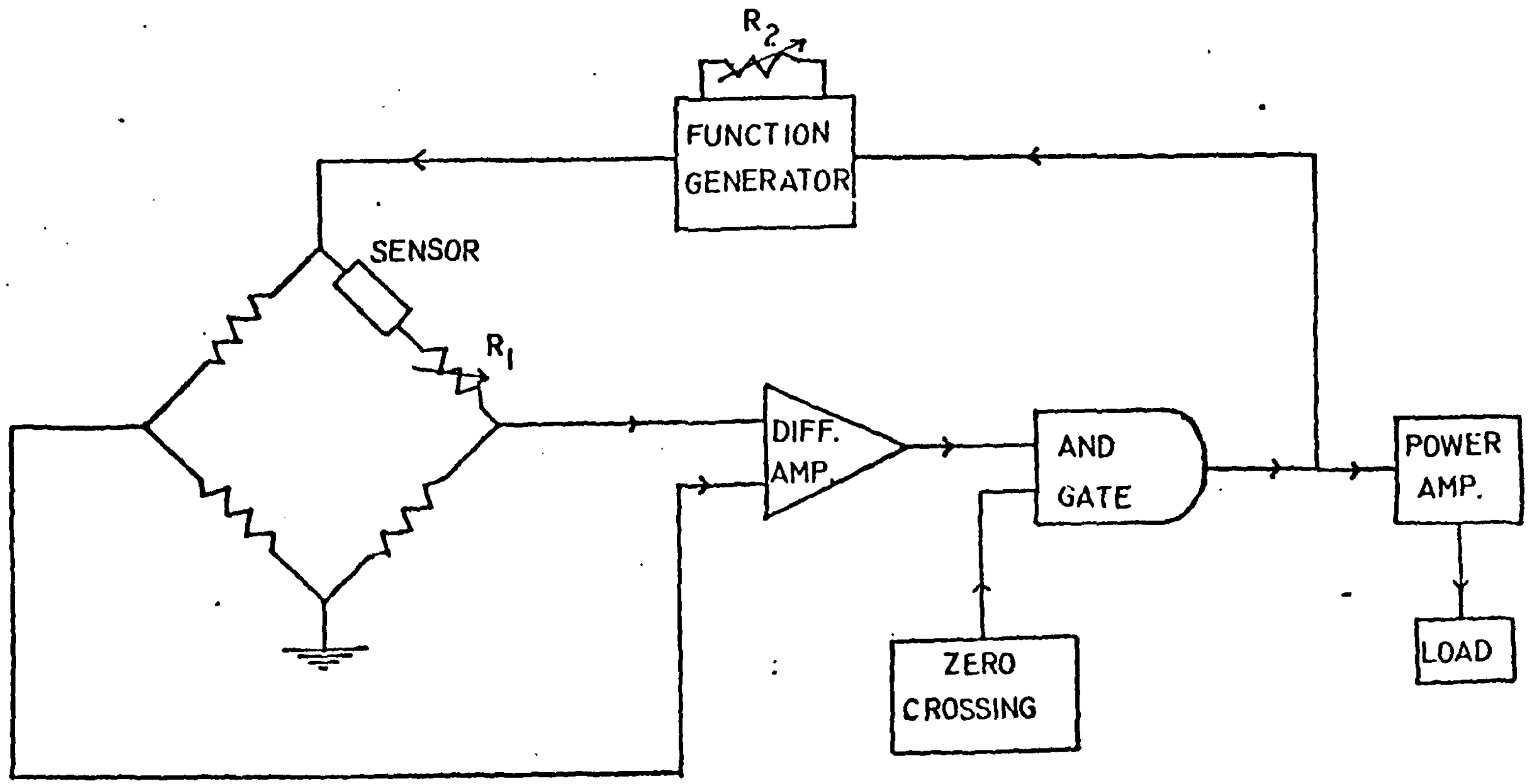

FIG. 7

SIGNALS OF TEMPERATURE CONTROLLER

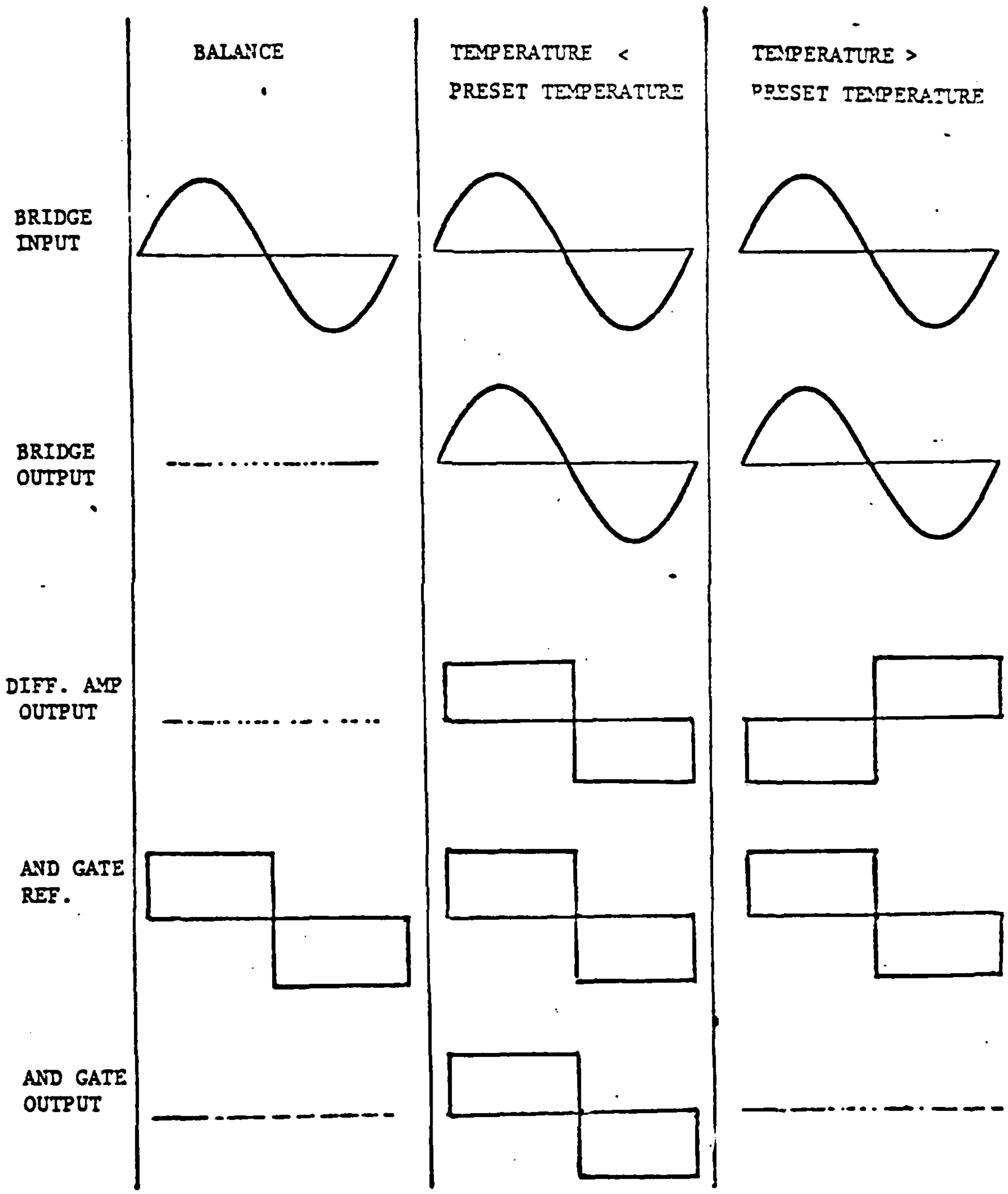

FIG. 8

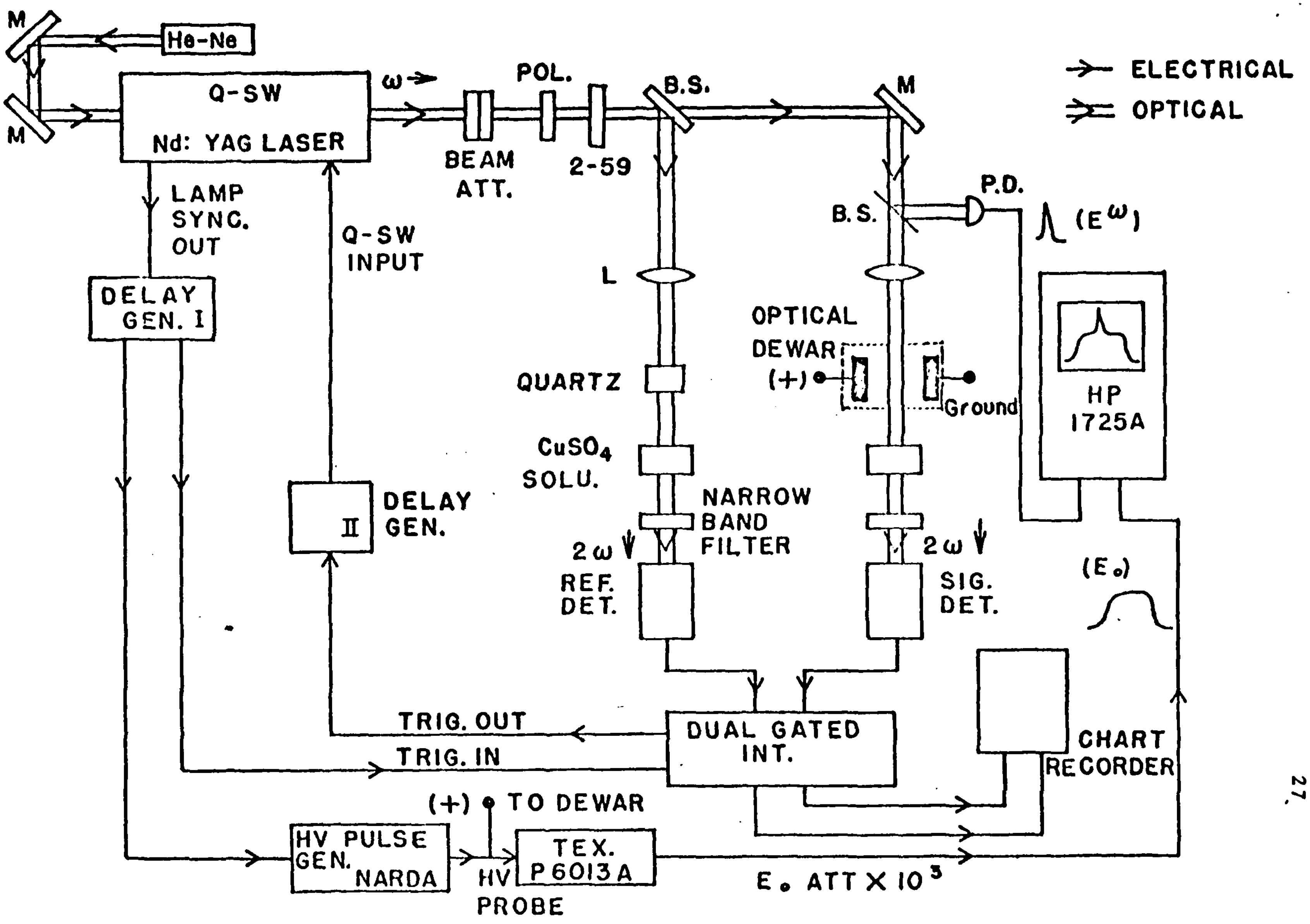
M
He-Ne
M
Q-SW
Nd: YAG LASER
ω
POL.
BEAM ATT.
2-59
B.S.
M
ELECTRICAL
OPTICAL
LAMP SYNC. OUT
Q-SW INPUT
P.D.
B.S.
(E^ω)
L
DELAY GEN. I
OPTICAL DEWAR
(+)
Ground
HP 1725A
QUARTZ
CuSO4 SOLU.
DELAY GEN. II
NARROW BAND FILTER
2ω
REF. DET.
2ω
SIG. DET.
(E₀)
TRIG. OUT
TRIG. IN
DUAL GATED INT.
CHART RECORDER
(+) TO DEWAR
HV PULSE GEN. NARDA
HV PROBE
TEX. P6013A
E₀ ATT X 10^3

FIG. 9

3. D. C.-FIELD-INDUCED SECOND-HARMONIC GENERATION IN NEMATIC LIQUID CRYSTALS

3.1 Investigation of nematic ordering

In the theoretical treatment of nematic ordering, it is usually assumed that the molecules are rigid and cylindrically symmetric. The aim of various theoretical efforts is then to calculate an anisotropic molecular orientation distribution function $f(\theta)$[1] which gives the probability that the symmetry axis of an individual molecule makes an angle θ with the macroscopic symmetry axis (the director $\hat{n}$) of the nematic phase. The results of these statistical calculations are usually given as a theoretical prediction for the statistical average of the Legendre polynomial $P_\ell(\cos\theta)$ (ℓ being even integer)

$$\langle P_\ell(\cos\theta)\rangle = \int_{-1}^{1} P_\ell(\cos\theta)\ f(\theta)\ d(\cos\theta)$$

These averages are nonzero in the nematic phase and they are called orientational order parameters. Experimentally $\langle P_2\rangle$ can be obtained readily from measurements of any anisotropic properties described by tensors of the second rank. Among the various techniques, measurements of anisotropy of refractive indices and nuclear magnetic resonance[2] have been used extensively to obtain $\langle P_2\rangle$. In the literature, there is a large amount of data on $\langle P_2\rangle$ for comparison with theoretical calculations. $\langle P_4\rangle$, however, has only recently been measured with the technique of polarized Raman scattering[3,4]. In this section, we show that electric-field-induced second-harmonic generation[5] provides a new technique with which the temperature dependence of $\langle P_4\rangle$ can be measured.

3.1.1 Theory

In the presence of a d. c. electric field $\vec{E}(0)$ and a laser field $\vec{E}(\omega)$ at frequency ω, molecular dipoles at the second harmonic frequency 2ω will be induced.

$$p_i(2\omega) = \beta_{ijk} E_j(\omega) E_k(\omega) + \gamma_{ijk\ell} E_j(\omega) E_k(\omega) E_\ell(0) \qquad (1)$$

where $p_i(2\omega)$ is the i th component of the second-harmonic dipole moment of an individual molecule, $E(\omega)$ and $E(0)$ are the optical and d. c. local fields respectively, and β_{ijk}[6], $\gamma_{ijk\ell}$[6] are the second- and third-order hyperpolarizabilities of the molecule with i, j, k, = 1, 2, 3 axes of the molecular frame.

In order to obtain the second-harmonic polarization $P(2\omega)$ in the laboratory frame, one needs to know the orientational distribution function describing the orientation ordering of liquid crystal molecules. For rigid molecules with arbitrary shape, the distribution function should in principle be a function of the three Euler's angles θ, ϕ, ψ (see Fig. 1) which links the molecular axis of an individual molecule to the laboratory frame. For molecules with a threefold or greater axis of symmetry (the major molecular axis), it can be shown[4] that the molecular orientational distribution function for the nematic phase is of the simple form $f(\theta)$, where θ is the angle linking the major molecular axis to the average director $\hat{n}$. The conditions of rigidity and possession of a threefold or higher symmetry axis are satisfied by liquid crystal molecules only in a crude sense. However, this assumption has been made in almost all discussions of nematic ordering and it has worked quite well. We shall adopt the same assumption throughout our discussions.

The molecular orientational distribution function $f(\theta)$ can be expanded in terms of the Legendre polynomials $P_\ell(\cos\theta)$

$$f(\theta) = \sum_{\ell=\text{even}} \frac{2\ell + 1}{2} \langle P_\ell(\cos\theta)\rangle \; P_\ell(\cos\theta) \qquad (2)$$

where $$\langle P_\ell(\cos\theta)\rangle = \int_{-1}^{1} P_\ell(\cos\theta)\; f(\theta)\; d(\cos\theta) \qquad (3)$$

The expansion coefficients $\langle P_\ell(\cos\theta)\rangle$ vanish in the isotropic phase where $f(\theta)$ is a constant, take on nonzero values in the ordered phase, and become unity when the system is completely aligned. They are therefore the natural choice for the ordering parameters describing the ordering in a nematic phase. Since all the experimental evidence indicates the average director direction $\hat{n}$ is physically indistinguishable from $-\hat{n}$, only Legendre polynomials of even order appear in Eq. (2).

Knowing the molecular orientation distribution function, one can write the second-harmonic polarization $P(2\omega)$ in the laboratory frame as

$$P_F(2\omega) = N \iiint p_i(2\omega)\; \Phi_{iF}\; f(\theta, E(0), E(\omega))\; \frac{d(\cos\theta)}{2} \frac{d\phi}{2\pi} \frac{d\psi}{2\pi} \qquad (4)$$

where F stands for x, y, z axis of the laboratory frame, N is the number of molecules per cm^3, Φ_{iF} is the cosine of the angle between the i th molecular axis and the F th laboratory axis, and $f(\theta, E(0), E(\omega))$

is the molecular distribution function in the presence of d.c. and optical fields. θ, ϕ, ψ are the three Euler's angles describing an individual molecule with respect to the laboratory frame (see Fig. 1). In terms of these angles, the angle cosines, Φ_{IF}, are given by the matrix[7]

$$\Phi_{iF} = \begin{pmatrix} \cos\psi\cos\phi - \cos\theta\sin\phi\sin\psi & -\sin\psi\cos\phi - \cos\theta\sin\phi\cos\psi & \sin\theta\sin\phi \\ \cos\psi\sin\phi + \cos\theta\cos\phi\sin\psi & -\sin\psi\sin\phi + \cos\theta\cos\phi\cos\psi & -\sin\theta\cos\phi \\ \sin\theta\sin\psi & \sin\theta\cos\psi & \cos\theta \end{pmatrix} \tag{5}$$

To proceed further, a simplifying approximation will be made for $f(\theta, E(0), E(\omega))$. The interaction energy between the external fields and an individual molecule is expected to be much smaller than the interaction energy between the constituent molecules responsible for the existence of the nematic phase. Hence, within the framework of mean field theories, it is an excellent approximation that

$$f(\theta, E(0), E(\omega)) \approx f(\theta) \exp\left[\frac{\Phi_{\ell z}\mu_\ell E_z(0)}{kT}\right]$$

$$\approx f(\theta)\left[1 + \Phi_{\ell z}\mu_\ell \, E_z(0)/kT\right] \tag{6}$$

where $f(\theta)$ is the molecular orientation distribution function in the absence of external fields, μ_ℓ is the ℓ th component of the permanent electric dipole moment in the molecular frame, and the external field $E(0)$ is taken to be along the z axis.

In the following, explicit expressions for the second-harmonic polarization will be worked out for the two orientations of external fields that are of interest to our experiments.

Case 1. $\vec{E}(\omega)$ and $\vec{E}(0)$ are parallel to the director $\hat{n}$ (parellel to the z axis of the laboratory frame)

Inserting Eq. (1) into Eq. (2), one obtains

$$P_z(2\omega) = N E_z(\omega) E_z(\omega) E_z(0) \bar{\gamma}_{zzzz} \qquad (7)$$

where
$$\bar{\gamma}_{zzzz} = \iiint \Phi_{iz} \left[\frac{1}{E_z(0)} \beta_{ijk} \Phi_{jz} \Phi_{kz} + \gamma_{ijk\ell} \Phi_{jz} \Phi_{kz} \Phi_{\ell z} \right] \times f(\theta, E(0), E(\omega)) \times \frac{d(\cos\theta)}{2} \frac{d\phi}{2\pi} \frac{d\psi}{2\pi} \qquad (8)$$

Using Eq. (6) as an approximation for $f(\theta, E(0), E(\omega))$, one can show that

$$\bar{\gamma}_{zzzz} = \left[\gamma_{ijk\ell} + \frac{\mu_\ell \beta_{ijk}}{kT} \right] \langle \Phi_{iz} \Phi_{jz} \Phi_{kz} \Phi_{\ell z} \rangle \qquad (9)$$

where

$$\langle (\cdots\cdots\cdot) \rangle = \int_0^{2\pi} \int_0^{2\pi} \int_1^{-1} (\cdots\cdots\cdot) f(\theta) \frac{d(\cos\theta)}{2} \frac{d\phi}{2\pi} \frac{d\psi}{2\pi}$$

In arriving at (9), we have made use of the fact $\langle$ odd number of $\Phi_{iz} \rangle = 0$

because the molecular orientation distribution function for the nematic phase contains only Legendre polynomial of even-order. Without loss of generality, we can assume $\gamma_{iijj}=\gamma_{jjii}=\gamma_{ijij}=\gamma_{ijji}$ and $\beta_{ijj}=\beta_{jij}=\beta_{jji}$ [8]. Then the first part of Eq. (9) is

$$\langle \Phi_{iz}\Phi_{jz}\Phi_{kz}\Phi_{\ell z}\rangle \gamma_{ijk\ell} = \langle\Phi_{iz}^4\rangle \gamma_{iiii}$$

$$+ 3 \sum_{\substack{i,j \\ i\neq j}} \langle \Phi_{iz}^2 \Phi_{jz}^2\rangle \gamma_{iijj} \qquad (10)$$

In the appendix , explicit expression for $\langle\Phi_{iz}^4\rangle$ and $\langle\Phi_{iz}^2\Phi_{jz}^2\rangle$ are given. Inserting these expressions into Eq. (10), one obtains

$$\langle \Phi_{iz} \Phi_{jz} \Phi_{kz} \Phi_{\ell z}\rangle \gamma_{ijk\ell} =$$

$$\frac{1}{5}(\gamma_{1111}+\gamma_{2222}+\gamma_{3333}+2\gamma_{1122}+2\gamma_{2233}+2\gamma_{3311})$$

$$+\frac{2}{7}(2\gamma_{3333}-\gamma_{1111}-\gamma_{2222}-2\gamma_{1122}+2\gamma_{2233}+\gamma_{3311})\langle P_2\rangle$$

$$+\frac{1}{35}(8\gamma_{3333}+3\gamma_{1111}+3\gamma_{2222}+6\gamma_{1122}-24\gamma_{2233}-24\gamma_{3311})\langle P_4\rangle$$

Similarly the second part of Eq. (9) is

$$\langle\Phi_{iz}\Phi_{jz}\Phi_{kz}\Phi_{\ell z}\rangle \mu_\ell\beta_{ijk} = \mu_i\beta_{iii}\langle \Phi_{iz}^4\rangle + 3\mu_i\beta_{ijj}\langle \Phi_{iz}^2\Phi_{jz}^2\rangle$$

$$= \frac{1}{5} [(\mu_3\beta_{333} + \mu_1\beta_{111} + \mu_2\beta_{222} + \mu_1\beta_{122} + \mu_2\beta_{211} + \mu_3\beta_{322} + \mu_3\beta_{311}$$

$$+ \mu_1\beta_{133} \quad \mu_2\beta_{233}) + \frac{20}{7} (\mu_3\beta_{333} - \frac{1}{2}\mu_1\beta_{111} - \frac{1}{2}\mu_2\beta_{222} - \frac{1}{2}\mu_1\beta_{122}$$

$$- \frac{1}{2}\mu_2\beta_{211} + \frac{1}{4}\mu_3\beta_{311} + \frac{1}{4}\mu_3\beta_{322} + \frac{1}{4}\mu_1\beta_{133} + \frac{1}{4}\mu_2\beta_{233}) \langle P_2 \rangle$$

$$+ \frac{8}{7} (\mu_3\beta_{333} + \frac{3}{8}\mu_1\beta_{111} + \frac{3}{8}\mu_2\beta_{222} + \frac{3}{8}\mu_1\beta_{122} + \frac{3}{8}\mu_2\beta_{211} - \frac{3}{2}\mu_3\beta_{322}$$

$$- \frac{3}{2}\mu_3\beta_{311} - \frac{3}{2}\mu_1\beta_{133} - \frac{3}{2}\mu_2\beta_{233}) \langle P_4 \rangle]$$

Finally we can write

$$\bar{\gamma}_{zzzz} = \gamma_{iso} + \frac{2}{7}\alpha\langle P_2\rangle + \frac{8}{7}\beta\langle P_4\rangle \tag{11}$$

where γ_{iso}, α, and β are given by

$$\gamma_{iso} = \frac{1}{5} (\gamma_{1111} + \gamma_{2222} + \gamma_{3333} + 2\gamma_{1122} + 2\gamma_{3322} + 2\gamma_{3311})$$

$$+ \frac{1}{5kT} (\mu_3\beta_{333} + \mu_3\beta_{322} + \mu_3\beta_{311} + \mu_2\beta_{233} + \mu_2\beta_{222} + \mu_2\beta_{211}$$

$$+ \mu_1\beta_{133} + \mu_1\beta_{122} + \mu_1\beta_{111}) \tag{12}$$

$$\alpha = (2\gamma_{3333} - \gamma_{1111} - \gamma_{2222} - 2\gamma_{1122} + \gamma_{3322} + \gamma_{3311})$$

$$+ \frac{1}{kT}(2\mu_3\beta_{333} + \frac{1}{2}\mu_3\beta_{311} + \frac{1}{2}\mu_3\beta_{322} + \frac{1}{2}\mu_2\beta_{233} - \mu_2\beta_{222} - \mu_2\beta_{211}$$

$$+ \frac{1}{2}\mu_1\beta_{133} - \mu_1\beta_{122} - \mu_1\beta_{111}) \qquad (13)$$

and

$$\beta = \frac{1}{40}(8\gamma_{3333} + 3\gamma_{1111} + 3\gamma_{2222} + 6\gamma_{1122} - 24\gamma_{3311} - 24\gamma_{3322})$$

$$+ \frac{1}{5kT} (\mu_3\beta_{333} - \frac{3}{2}\mu_3\beta_{322} - \frac{3}{2}\mu_3\beta_{311} - \frac{3}{2} \mu_2\beta_{233} + \frac{3}{8}\mu_2\beta_{222} + \frac{3}{8}\mu_2\beta_{211}$$

$$- \frac{3}{2}\mu_1\beta_{133} + \frac{3}{8}\mu_1\beta_{122} + \frac{3}{8}\mu_1\beta_{111}) \qquad (14)$$

Case 2. Both the laser field $\vec{E}(\omega)$ and d. c. field $\vec{E}(0)$ are perpendicular to the director $\hat{n}$. We will take $\vec{E}(\omega)$ and $\vec{E}(0)$ to be along the x-axis of the laboratory frame.

Following the procedures described for case 1, one can easily obtain an expression for the second-harmonic polarization for this case. The x component of the second-harmonic polarization is

$$P_x(2\omega) = N E_x(\omega) E_x(\omega) E_x(0)\bar{\gamma}_{xxxx} \qquad (15)$$

where $\bar{\gamma}_{xxxx}$ is a statistical average of the hyperpolarizabilities of the molecules. The explicit expression for $\bar{\gamma}_{xxxx}$ is

$$\bar{\gamma}_{xxxx} = \left[\gamma_{ijk\ell} + \frac{\mu_\ell \beta_{ijk}}{kT}\right] < \phi_{ix}\phi_{jx}\phi_{kx}\phi_{\ell x} >$$

$$= \left[\gamma_{iiii} + \frac{\mu_i \beta_{iii}}{kT}\right] < \phi_{ix}^4 >$$

$$+ 3\left[\gamma_{iijj} + \frac{\mu_i \beta_{ijj}}{kT}\right] < \phi_{ix}^2 \phi_{jx}^2 > \qquad (16)$$

With the values of $<\phi_{ix}^4>$ and $<\phi_{ix}^2 \phi_{jx}^2>$ given in appendix , $\bar{\gamma}_{xxxx}$ can finally be put in the form

$$\bar{\gamma}_{xxxx} = \gamma_{iso} - \frac{1}{7}\alpha < P_2 > + \frac{3}{7}\beta < P_4 > \qquad (17)$$

where γ_{iso}, α, and β are the same constants given by Eqs. (12), (13), and (14).

As a check on the correctness of Eqs. (11) and (17), we note Eqs. (11) and (17) indeed reduce to the known expression for an isotropic medium[9] when $< P_2 >$ and $< P_4 >$ are set equal to zero. Furthermore, in the ideal nematic case, for which $< P_2 > = < P_4 > = 1$, Eqs. (11) and (17) reduce to the forms

$$\bar{\gamma}_{zzzz} = \gamma_{3333} + \frac{\mu_3 \beta_{333}}{kT} \qquad (18)$$

$$\bar{\gamma}_{xxxx} = \gamma_{1111} + \frac{\mu_1 \beta_{111}}{kT} \qquad (19)$$

which are expected on physical ground.

The generation of second-harmonic wave due to nonlinear polarization is governed by Maxwell's equations. For a current free and non-magnetic nonlinear medium, we have

$$\nabla\times\vec{E} + \frac{1}{c}\frac{\partial\vec{H}}{\partial t} = 0 \qquad (20)$$

$$\nabla\times\vec{H} - \frac{1}{c}\frac{\partial\vec{D}}{\partial t} = 0 \qquad (21)$$

with

$$\vec{D} = \vec{E} + 4\pi\vec{P} \qquad (22)$$

where $\vec{P}$ includes both the linear and nonlinear polarizations

$$\vec{P}(2\omega) = \vec{P}^{L}(2\omega) + \vec{P}^{NL}(2\omega) \qquad (23)$$

If there are N molecules per cubic centimeter, the linear polarization $\vec{P}^{L}(2\omega)$ is

$$\vec{P}^{L}(2\omega) = N\alpha\vec{E}(2\omega) \qquad (24)$$

where α is the linear polarization and $\vec{E}(2\omega)$ is the local field at frequency 2ω. Using Lorentz field model for local field correction, we have

$$\vec{E}(2\omega) = \vec{E}(2\omega) + \frac{4\pi}{3}\left[\vec{P}^{L}(2\omega) + \vec{P}^{NL}(2\omega)\right] \qquad (25)$$

Combining Eqs. (24) and (25), we get

$$\vec{P}^{L}(2\omega) = \frac{N\alpha}{1 - \frac{4\pi N\alpha}{3}} \left[\vec{E}(2\omega) + \frac{4\pi}{3}\vec{P}^{NL}(2\omega)\right] \qquad (26)$$

Substitution of Eq. (26) into (22) yields

$$\vec{D}(2\omega) = \varepsilon(2\omega)\vec{E}(2\omega) + 4\pi\,\frac{\varepsilon(2\omega) + 2}{3}\,\vec{P}^{NL}(2\omega) \qquad (27)$$

Combination of Eqs. (20), (21) and (27) leads to the wave equation

$$\nabla\times\nabla\times\vec{E}(2\omega) + \frac{\varepsilon(2\omega)}{c^2}\,\frac{\partial^2\vec{E}(2\omega)}{\partial t^2} = -\,\frac{4\pi}{c^2}\,\frac{\partial^2\vec{P}^{NLS}(2\omega)}{\partial t^2} \qquad (28)$$

where $\vec{P}^{NLS}(2\omega) = \frac{\varepsilon(2\omega)+2}{3}\,\vec{P}^{NL}(2\omega)$. Thus the effective nonlinear polarization source to be used in Maxwell's equations is $\frac{\varepsilon(2\omega) + 2}{3}$ times the true induced nonlinear polarization. For harmonic wave at 2ω, Eq. (28) reduces to

$$\nabla\times\nabla\times\vec{E} - \left(\frac{2\omega}{c}\right)^2 \varepsilon(2\omega)\vec{E} = 4\pi\left(\frac{2\omega}{c}\right)^2 \vec{P}^{NLS} \qquad (29)$$

In our experiments, both the polarization of the input fundamental wave and the applied d. c. field are either parallel to the director direction or perpendicular to it. For the former case, we have

$$\vec{E}(\omega, y) = E_z(\omega)\exp\,(ik_\omega y)\hat{z}$$
$$\vec{E}(0, y) = E_z(0, y)\,\hat{z}$$

where $\hat{z}$ is in the direction of the director and $\vec{k}_\omega$ is the wave vector at ω. The nonlinear polarization $\vec{P}^{NLS}$ for this case can be obtained with Eq. (17) as

$$P_z^{NLS}(2\omega,\ y) = N\ (f_{2\omega} f_\omega^2 f_0)\bar{\gamma}_{zzzz} E_z^2(\omega) E_z(o,y)\ \exp\ (i2k_\omega y) \quad (30)$$

where $f_{2\omega} = \dfrac{\varepsilon(2\omega) + 2}{3}$, $\quad f_\omega = \dfrac{(\ \varepsilon(\infty) + 2\ )\varepsilon(\omega)}{\varepsilon(\infty) + 2\varepsilon(\omega)}$ and

$f_0 = \dfrac{(\ \varepsilon(\infty) + 2\ )\varepsilon(0)}{\varepsilon(\infty) + 2\varepsilon(0)}$. f_ω, f_0 are Onsager local field factors which are needed to relate the local fields in Eq. (7) to the macroscopic fields. At the optical frequency $\omega, \varepsilon(\infty) = \varepsilon(\omega)$ and f_ω reduces to $f_\omega = \dfrac{\varepsilon(\omega) + 2}{3}$ as expected from the Lorentz local field treatment. Also, in arriving at Eq. (30) from Eq. (7), we have used the fact that the molecular dimension is very small compared to the wavelength at optical frequency and the spatial variation of the d. c. field.

Similarly, the nonlinear polarization $\vec{P}^{NLS}$ for the latter case can be obtained from Eq. (15) as

$$P_x^{NLS}(2\omega,y) = N(f_{2\omega} f_\omega^2 f_0)\bar{\gamma}_{xxxx}\ E_x^2(\omega) E_x(0,y)\ \exp\ (i2k_\omega y) \quad (31)$$

In principle, the local field factors $f_{2\omega}$, f_ω, and f_0 in Eq. (30) may be different from those in Eq. (31) since nematic phase is anisotropic. Quantitative theoretical calculations of these factors in the nematic phase are extremely difficult. However, there exists empirical evidence[10,11,12] which suggests that these factors are not significantly different from those in the isotropic phase. The explanation, as suggested in Ref. (10), is that the local field factors ultimately depend on the short-range correlations between molecules, and that these short-range correlations are not significantly different in the isotropic and nematic phases. In our discussions, we shall assume that the local field factors in Eq. (30) and Eq. (31) are the same.

The second-harmonic wave generated by the nonlinear polarizations in Eq. (30) and Eq. (31) can be calculated from Eq. (29) by assuming the second-harmonic wave to be an infinite plane wave with spatially varying field amplitude and propagating in the y direction. For the case when the polarization of the fundamental wave and the applied field are parallel to the director direction (along z), Eq. (29) reduces to

$$\left[\frac{d^2}{dy^2} + \left(\frac{2\omega}{c}\right)^2 \varepsilon_{\parallel}(2\omega)\right] E_{\parallel}(y,2\omega) = -4\pi\left(\frac{2\omega}{c}\right)^2 \Gamma_{\parallel} E^2_{\parallel}(\omega)\, E_{\parallel}(0,y) \exp(i2k_{\omega}y) \quad (32)$$

where $\parallel$ is used to denote the z direction since in this case all the fields are parallel to the director. $\Gamma_{\parallel}$ is defined as $\Gamma_{\parallel} = N(f_{2\omega} f^2_{\omega} f_0)\bar{\gamma}_{zzzz}$. The solution to Eq. (32) is the sum of a free wave $E_{f,\parallel}$ (homogeneous solution) and a bound wave (inhomogeneous solution) whose amplitude $E_{b,\parallel}(y)$ will vary because of the spatial variation of the nonlinear polarization due to the fringing field of E (0,y)

$$E_{\parallel}(2\omega,y) = E_{f,\parallel} \exp(ik_{f,\parallel}y) + E_{b,\parallel}(y) \exp(ik_{b,\parallel}y) \quad (33)$$

where $k_{f,\parallel} = \frac{2\omega}{c}(n_{2\omega})_\parallel$, $k_{b,\parallel} = \frac{2\omega}{c}(n_\omega)_\parallel$, $(n_{2\omega})_\parallel = \sqrt{\epsilon_\parallel}(2\omega)$ and $(n_\omega)_\parallel = \sqrt{\epsilon_\parallel}(\omega)$. Substitution of Eq. (33) into Eq. (32) gives an equation for $E_{b,\parallel}(y)$

$$\frac{d^2}{dy^2}E_{b,\parallel}(y) + 2ik_{b,\parallel}\frac{dE_{b,\parallel}}{dy} + (k^2_{f,\parallel} - k^2_{b,\parallel})\, \dot{E}_{b,\parallel}(y)$$

$$= -4\left(\frac{2\omega}{c}\right)^2 \Gamma_\parallel E^2_\parallel(\omega) E_\parallel(0,y) \qquad (34)$$

If the fringing field is slowly varying such that

$$\frac{1}{E_\parallel(0,y)} \frac{dE_\parallel(0,y)}{dy} << 2\Delta k = 2(k_{f,\parallel} - k_{b,\parallel})$$

and $$\frac{1}{E_\parallel(0,y)} \frac{d^2E_\parallel(0,y)}{dy^2} << 2(k^2_{f,\parallel} - k^2_{b,\parallel}),$$

the solution to $E_{b,\parallel}(y)$ can readily be seen to be

$$E_{b,\parallel}(y) = -\left(\frac{4\pi}{n^2_{2\omega,\parallel} - n^2_{\omega,\parallel}}\right)\Gamma_\parallel E^2_\parallel(\omega)\, E_\parallel(0,y) \qquad (35)$$

These conditions on the slowly varying d. c. field $E_\parallel(0,y)$ are well satisfied by our electrode geometry.

To calculate the second-harmonic power generated from the liquid crystal medium, we have to consider boundary conditions. Since all the liquid crystals we studied have much larger nonlinearity than that induced in the glass spacer due to the fringing d. c. field, we can neglect the second-harmonic field generated in the glass spacer and hence, there is no incident harmonic field at the front boundary of the liquid crystal medium[13]. We shall take the front boundary to be $y = 0$ and the back boundary at $y = \ell$ (See Fig. 2).

At the front boundary between glass and liquid crystal medium, there is only a reflected wave on the glass side

$$E_{R,\parallel}(2\ ,y) = E_{R,\parallel} \exp[-(ik_f^G y)]$$

where $k_f^G = \frac{2\omega}{c} n_{2\omega}^G$ and $n_{2\omega}^G$ is the refractive index of glass at frequency 2ω.

On the liquid crystal side, we have both bound and free waves.

$$E_{\parallel}(2\omega,\ y) = E_{f,\parallel} \exp\ (ik_{f,\parallel} y) + E_{b,\parallel} \exp\ (ik_{b,\parallel} y)$$

The amplitude of free wave generated in the liquid crystal can be calculated by solving the boundary conditions on $\vec{E}(2\omega)$ and $\vec{H}(2\omega)$ at $y=0$

$$E_{b,\parallel} + E_{f,\parallel} = E_R$$

$$n_{\omega,\parallel} E_{b,\parallel} + n_{2\omega,\parallel} E_{f,\parallel} = -\ n_{2\omega}^G E_R$$

Solving these Eqs., we obtain

$$E_{f,\parallel} = -\left(\frac{n_{2\omega}^G + n_{\omega,\parallel}}{n_{2\omega}^G + n_{2\omega,\parallel}}\right) E_{b,\parallel}(0) \qquad (36)$$

At the back boundary ($y=\ell$), there are reflected wave, bound wave, and free wave in the liquid crystal region. The boundary conditions on $\vec{E}(2\omega)$ and $\vec{H}(2\omega)$ are

$$E_{b,\parallel}(\ell)\exp(ik_{b,\parallel}\ell) + E_{f,\parallel}\exp(ik_{f,\parallel}\ell) + E_{R\parallel}\exp(ik_{f,\parallel}\ell)$$
$$= E^G_{f,\parallel}\exp(ik^G_f\ell)$$

$$n_{\omega,\parallel}E_{b,\parallel}(\ell)\exp(ik_{b,\parallel}\ell) + n_{2\omega,\parallel}E_{f,\parallel}\exp(ik_{f\parallel}\ell)$$
$$- n_{2\omega,\parallel}E_{R,\parallel}\exp(ik_{f\parallel}\ell) = n^G_{2\omega}E^G_{f,\parallel}\exp(ik^G_f\ell)$$

From these two Eqs. we obtain

$$E^G_{f,\parallel}\exp(ik^G_f\ell) = \left(\frac{n_{2\omega,\parallel} + n_{\omega,\parallel}}{n_{2\omega,\parallel} + n^G_{2\omega}}\right)E_{b,\parallel}(\ell)\exp(ik_{b,\parallel}\ell)$$
$$-\left(\frac{2n_{2\omega,\parallel}}{n_{2\omega,\parallel} + n^G_{2\omega}}\right)\left[\frac{n^G_{2\omega} + n_{\omega,\parallel}}{n^G_{2\omega} + n_{2\omega\parallel}}\right]E_{b,\parallel}(0)\exp(ik_{f\parallel}\ell) \tag{37}$$

where we used Eq. (36) for $E_{f,\parallel}$.

Since the liquid crystal medium is well within the electrodes, $E_\parallel(0,0) = E_\parallel(0,\ell) = E_\parallel(0)$. From Eq. (35) we have

$$E_{b,\parallel}(\ell) = E_{b,\parallel}(0) = -\left[\frac{4\pi}{n^2_{2\omega,\parallel} - n^2_{\omega,\parallel}}\right]\Gamma_\parallel E^2_\parallel(\omega)E_\parallel(0) \tag{35a}$$

Substitution of Eq. (35a) into Eq. (37) gives

$$E^{G}_{f,\parallel}(2\omega,\ \ell) = -\left[\frac{4\pi}{n^{2}_{2\omega,\parallel} - n^{2}_{\omega,\parallel}}\right]\left[\frac{n_{2\omega,\parallel} + n_{\omega,\parallel}}{n_{2\omega,\parallel} + n^{G}_{2\omega}}\right]\Gamma_{\parallel} E^{2}_{\parallel}(\omega) E_{\parallel}(0)$$

$$\left[\exp\,(ik_{f,\parallel}\ell) - \exp\,(ik_{b,\parallel}\ell)\right] \qquad (38)$$

where we have made the approximation

$$\left[\frac{2n_{2\omega,\parallel}}{n_{2\omega,\parallel} + n^{G}_{2\omega}}\right]\left[\frac{n^{G}_{2\omega} + n_{\omega,\parallel}}{n^{G}_{2\omega} + n_{2\omega,\parallel}}\right] \simeq \left[\frac{n_{2\omega,\parallel} + n_{\omega,\parallel}}{n_{2\omega,\parallel} + n^{G}_{2\omega}}\right]$$

The second-harmonic intensity produced by the liquid crystal medium is thus given by

$$\begin{aligned} I_{\parallel}(2\omega) &\propto \left|E^{G}_{\parallel f,}(2\omega,\ell\ )\right|^{2} \\ &\propto \ell^{2}_{c,\parallel}\Gamma^{2}_{\parallel}\sin^{2}\left(\frac{\pi\ell}{2\ell_{c,\parallel}}\right)|E_{\parallel}(2\omega)|^{4}|E_{\parallel}(0)|^{2} \end{aligned} \qquad (39)$$

where $\ell_{c,\parallel} = \dfrac{\pi}{k_{f,\parallel} - k_{b,\parallel}} = \dfrac{\pi}{\frac{2\omega}{c}(n_{2\omega,\parallel} - n_{\omega,\parallel})}$ is

known as coherence length. If $\Delta k_{\parallel} = k_{f,\parallel} - k_{b,\parallel} \neq 0$, we see that second-harmonic intensity oscillates as a function of the sample length. This periodic variation of second-harmonic intensity is known as Maker fringes. The second-harmonic intensity measured for a given fundamental beam intensity and d. c. applied field is given by

$$I_{\parallel}(2\omega) \propto (\ell_{c\parallel}\Gamma_{\parallel})^2 \qquad (40)$$

Similarly, when the polarization of the fundamental beam and d. c. applied field are perpendicular to the director, we have

$$I_{\perp}(2\omega) \propto (\ell_{c,\perp}\Gamma_{\perp})^2 \qquad (41)$$

where $\Gamma_{\perp}=N(f_{2\omega}f_{\omega}^2\ f_0)_{\perp}\bar{\gamma}_{xxxx}$, $\ell_{c,\perp}=\dfrac{\pi}{\frac{2\omega}{c}(n_{2\omega,\perp}-n_{\omega\perp})}$

with $n_{2\omega\perp}$ and $n_{\omega\perp}$ being the indices of refraction at 2ω and ω and for polarization perpendicular to the director. In the isotropic phase, $\langle P_2\rangle$ and $\langle P_4\rangle$ vanish and Eqs. (40) and (41) both reduce to

$$I_L(2\omega) \propto (\ell_c^L\Gamma^L)^2 \qquad (42)$$

where $\Gamma^L=N(f_{2\omega}f_{\omega}^2f_0)_L\gamma_{iso}$ with $(f_{2\omega}f_{\omega}^2f_0)_L$ being the local field factors for the isotropic phase and $\ell_c^L=\dfrac{\pi}{\frac{2\omega}{c}(n_{2\omega}^L-n_{\omega}^L)}$ with $n_{2\omega}^L$ and n_{ω}^L being the indices of refraction at 2ω and ω in the isotropic phase.

By measuring the second-harmonic intensity and the coherence length, we see from Eqs. (40), (41) and (42) that $\Gamma_{\parallel}$ $\Gamma_{\perp}$ and Γ^L can be determined. However, since it is difficult to make accurate measurement of the absolute values of intensities, only the ratio $I_{\parallel}(2\omega)/I_L(2\omega)$ and $I_{\perp}(2\omega)/I_L(2\omega)$ are measured in the experiments. Hence, only the ratio $R_{\parallel}=\Gamma_{\parallel}/\Gamma^L$ and $R_{\perp}=\Gamma_{\perp}/\Gamma^L$ will be determined experimentally. Using Eqs. (11) and (17) and making the approximation that the local field factors in the nematic phase and the isotropic phase are the same, we can write the ratios

$R_{\parallel} = \frac{\Gamma_{\parallel}}{\Gamma^{L}}$ and $R_{\perp} = \frac{\Gamma_{\perp}}{\Gamma^{L}}$ as

$$R_{\parallel} = 1 + \frac{2\alpha}{7\gamma_{iso}} \langle P_2 \rangle + \frac{8\beta}{7\gamma_{iso}} \langle P_4 \rangle \qquad (43)$$

$$R_{\perp} = 1 - \frac{\alpha}{7\gamma_{iso}} \langle P_2 \rangle + \frac{3\beta}{7\gamma_{iso}} \langle P_4 \rangle \qquad (44)$$

Neglecting the small temperature dependence of α, β, and γ_{iso}, we can use Eqs. (43) and (44) to obtain

$$\frac{\langle P_2 \rangle}{\langle P_2 \rangle'} = \frac{3R_{\parallel} - 8R_{\perp} + 5}{3R'_{\parallel} - 8R'_{\perp} + 5} \qquad (45)$$

$$\frac{\langle P_4 \rangle}{\langle P_4 \rangle'} = \frac{R_{\parallel} + 2R_{\perp} - 3}{R'_{\parallel} + 2R'_{\perp} - 3} \qquad (46)$$

where $\langle P_2 \rangle'$, $\langle P_4 \rangle'$, $R'_{\parallel}$ and $R'_{\perp}$ denote their values at a reference temperature. Thus, by measuring the temperature dependence of $R_{\parallel}$ and $R_{\perp}$, one can determine the temperature dependence of $\langle P_2 \rangle$ and $\langle P_4 \rangle$ of a nematic liquid crystal. The absolute values of $\langle P_2 \rangle$ and $\langle P_4 \rangle$, however, can not be determined with this method since there are four unknowns in Eqs. (45) and (46).

3.1.2 Experiments

All the experiments were performed on two nematic liquid crystals, MBBA (p-methoxy-bezylidene p-n-butylaniline) and 5CB (p-n-pentyl-p'-cyanobiphenyl). The MBBA samples were purchased from Atomergic Chemetals and 5CB samples from BDH Corporation. They were used without further purification. The clearing temperature (T_{NI}) for MBBA was 42.5°C and that for 5CB was 35°C. Both samples were sufficiently stable that the clearing temperatures remained unchanged during each measurement run.

To verify the observed second-harmonic was indeed due to FISHG, We measured the dependence of second-harmonic intensity on the fundamental beam intensity and the applied d. c. field. As can be seen from Figs. 3 and 4, the observed second-harmonic in 5CB dependes quadratically on the fundamental beam intensity and the applied d. c. field as expected for FISHG (see Eq. (39)). Similar results were also obtained for MBBA.

In order to measure the coherence length and the second-harmonic intensity at the peak of a Maker fringe, we need to vary the sample length continuously. This was done by translating the wedged liquid crystal cell across the laser beam. Fig. 5 shows typical variation of second-harmonic intensity as a function of the distance translated (L'). The coherence length was then determined from the separation L between two successive fringe mimima by using

$$\ell_c = \frac{L}{2} \tan \alpha$$

where α is the wedge angle of the cell. Typically we constructed the cells so that $\alpha \sim 10$ mr.

3.1.3 Experimental results and discussions

Figs. 6 and 7 show the temperature dependence of the peak intensity of a Maker fringe for 5CB and MBBA. $I_{\parallel}(2\omega)$ and $I_{\perp}(2\omega)$ are the measured second-harmonic intensities when the applied d. c. field and laser field are parallel and perpendicular to the director respectively. As is expected, $I_{\parallel}(2\omega)$ and $I_{\perp}(2\omega)$ have the same value when the sample was heated into the isotropic phase. The scattering loss of the fundamental and second-harmonic beams due to director fluctuation in the nematic phase is negligible for the sample length (up to ~ 100 μm) used in our experiments. Hence, no correction due to scattering loss were made to the data presented in Figs. 6 and 7. Figs. 8 and 9 show the measured coherence length as a function of temperature for 5CB and MBBA.

Knowing the second-harmonic intensities and the coherence lengths, we used Eq. (42) to calculate the macroscopic nonlinearity Γ. The results normalized to the value of Γ^L in the isotropic phase are shown in Figs. 10 and 11. Using Eqs. (45) and (46), we then deduced the relative values of $\langle P_2 \rangle$ and $\langle P_4 \rangle$. In order to compare our results with those obtained from polarized Raman scattering measurements,[3] we assigned our $\langle P_2 \rangle$ and $\langle P_4 \rangle$ at $T=(T_{NI}-10)^{\circ}C$ the absolute values determined by those experiments and at the same temperature. The absolute values of our $\langle P_2 \rangle$ and $\langle P_4 \rangle$ at other temperatures are then fixed. The results for 5CB is shown in Fig. 12 and those for MBBA in

Fig. 13. Our data agree surprisingly well with those obtained from polarized Raman scattering measurements[3,4]. Existing statistical theories[14] of nematic ordering can account very well for the temperature dependence of P_2 obtained from both measurements. However, these theories fail to explain the temperature dependence of $\langle P_4 \rangle$. In particular, all existing statistical theories of nematic ordering do not yield negative $\langle P_4 \rangle$ which is the case for 5CB near the transition temperature. To understand the significance of this disagreement, we plot in Fig. 14. the truncated orientational distribution function

$$f_3(\theta) = \frac{1}{2}\left[1 + 5\langle P_2\rangle P_2(\cos\theta) + 9\langle P_4\rangle P_4(\cos\theta)\right] \quad (47)$$

for 5CB at $\Delta T = 0.05^\circ C$. It is seen that near T_{NI} the 5CB molecules have a tendency to be tipped away from the nematic axis. This behavior is not predicted by existing theories. We believe the reason for the disagreement is probably that all existing theories have neglected short-range orientational intermolecular correlations. For example, dipole-dipole interactions can induce splay on a microscopic scale and these correlations have not been included in these theories.

3.1.4 Summary

The temperature dependence of second-harmonic intensities and coherence lengths of two nematic liquid crystals, MBBA and 5CB, were measured. These measurements were used to obtain macroscopic third-order nonlinearity of these liquid crystals. It is demonstrated that the temperature dependence of the ordering parameters $\langle P_2 \rangle$ and $\langle P_4 \rangle$

can be obtained from the temperature dependence of macroscopic third order nonlinearity. The results obtained with this method compare well with those obtained from polarized Raman scattering measurements. Comparison of our data with existing statistical theories of nematic ordering indicates that these theories are qualitatively useful for the understanding of gross features but they are not quantitatively reliable. A more realistic theory probably requires the inclusion of short-range orientational intermolecular correlations.

3.2 Phase-matched electric-field-induced second-harmonic generation

3.2.1 Introduction

As seen in the previous section, the second-harmonic intensity generated from a nonlinear medium varies periodically as a function of the sample length if $\Delta k = k_{2\omega} - k_{\omega} = \frac{2\omega}{c}(n_{2\omega} - n_{\omega}) \neq 0$. For efficient generation, it is important to achieve phase matching, i.e., $\Delta k = 0$. In a nonabsorbing isotropic medium, it is impossible to satisfy the phase matching condition because of the normal dispersion of the refractive index. However, for an anisotropic medium, phase matching can be achieved by requiring one or two of the waves involved to be ordinary rays and the rest extraordinary. Nematic liquid crystals exhibit large optical birefringence and phase matching can, in principle, be achieved in these media. In fact, this potential for efficient second harmonic generation is responsible for the original interest in the nonlinear optical properties of liquid crystals. In this chapter, we present the first experimental demonstration that phase matching for second-harmonic generation can indeed be achieved in nematic crystals.

Nematic liquid crystals are positive (optically) uniaxial crystals with the average director $\hat{n}$ being the optic axis. For 5CB, which was used in our experimental demonstration, we have $(n_o^{2\omega} - n_o^{\omega}) < (n_e^{\omega} - n_o^{\omega})$ where n_o and n_e are the ordinary and extraordinary indices of refraction at the frequency indicated. Phase-matching for this case is most easily achieved by having the fundamental wave as an extraordinary ray and the second-harmonic wave as an ordinary ray. The extraordinary refractive index at frequency ω with wave vector $\vec{k}_{\omega}$ making an angle θ with respect to the optic axis is given by

$$\left(\frac{1}{n_e^{\omega}(\theta)}\right)^2 = \frac{\cos^2\theta}{(n_o^{\omega})^2} + \frac{\sin^2\theta}{(n_e^{\omega})^2} \qquad (48)$$

At the phase-matching angle θ_m, $n_e^{\omega}(\theta_m) = n_o^{2\omega}$.

Thus, we get from Eq. (48),

$$\theta_m = \sin^{-1}\left[\frac{(n_o^{\omega})^{-2} - (n_o^{2\omega})^{-2}}{(n_o^{\omega})^{-2} - (n_e^{\omega})^{-2}}\right]^{\frac{1}{2}} \qquad (49)$$

Equivalently, the phase-matching angle can be obtained graphically from the intersection of the extraordinary and ordinary refractive index surfaces as shown in Fig. 15.

3.2.2. Experiments

In our experiment, the fundamental beam was provided by a Q-switched Nd:YAG laser operating at 1.064 μm. The liquid crystal used was 5CB. To calculate the phase matching angle θ_m, we need to know the refractive indices of 5CB at $\lambda_{\omega} = 1.064\ \mu m$ and $\lambda_{2\omega} = 5320$ Å. Since the refractive indices of 5CB at these two wavelengths had not been measured, the following procedure was used to determine their values. The refractive indices at 5320 Å was obtained by extrapolation using the reported values at 6328 Å and 5890 Å. The refractive indices at 1.064 μm were then determined by measuring the two coherence lengths defined below. When both the applied optical field and d. c. electric field are parallel to the optic axis, the coherence length is given by

$$\ell_{c,\parallel} = \frac{\lambda_\omega}{4(n_e^{2\omega} - n_e^{\omega})}$$

Similarly,

$$\ell_{c,\perp} = \frac{\lambda_\omega}{4(n_o^{2\omega} - n_o^{\omega})}$$

when fields are perpendicular to the optic axis. Thus by measuring $\ell_{c,\parallel}$, $\ell_{c,\perp}$ and knowing $n_e^{2\omega}$, $n_o^{2\omega}$, one can determine n_e^{ω} and n_o^{ω}. Table 1 shows the indices of refraction thus determined and the corresponding phase-matching angle calculated with Eq. (49).

Fig. 16 shows the design of the liquid cell used in our dc-field-induced second-harmonic measurements. The liquid crystal was sandwiched between two glass spacers of triangular shape. The inside boundaries of the glass spacers were coated with 100 Å thick of SiO_2 evaporated obliquely onto the glass surface[15]. Stable and defect free monodomain planar nematic films of thickness up to 150 μm can be routinely formed between the coated boundaries. The director $\hat{n}$ (which is also the optic axis) of the nematic film used in our experiment was parallel to the boundary. The dc electric field $\vec{E}(0)$ was applied perpendicular to the director by sandwiching the liquid cell shown in Fig. 16 between two stainless steel electrodes. A typical value of E(0) was 15 kV/cm. The use of triangular spacers was necessary so that θ could be varied between 25° and 32° covering the range of the calculated phase-matching angles shown in Table 1. Otherwise, refraction at the air to glass boundary will limit θ to values larger than 47.2°.

3.2.3. Experimental results and discussion

Fig. 17 shows the variation of second-harmonic intensity as a function of the angle θ at $T = 22^{\circ}C$. The second-harmonic intensity peaks at 25°, in good agreement with the calculated phase-matching angle of 25.2°. The theoretical phase-matching curve is also shown in the figure for comparison with the experimental data. The theoretical curve was calculated with the expression

$$\frac{I^{2\omega}(\theta)}{I^{2\omega}(\theta_m)} = \frac{\ell_c^2(\theta)}{\ell^2(\theta_m)} \left(\frac{2}{\pi}\right)^2 \sin^2\left[\frac{\pi}{2}\,\frac{\ell(\theta)}{\ell_c(\theta)}\right] \qquad (50)$$

where $\ell_c(\theta)$ is the angle dependent coherence length given by $\ell_c(\theta) = \dfrac{\lambda_\omega}{4(n_o^{2\omega} - n_e^{\omega}(\theta))}$, $\ell(\theta)$ is the angle dependent sample length which is related to the sample thickness d by $\ell = \dfrac{d}{\sin\theta}$. The thickness d of the liquid crystal film used in our experiment was 75 μm. The experimental peak is somewhat wider than the theoretical one. Also the two side minima were not observed. These were probably due to slight spatial variation of the director $\hat{n}$ in our sample. The phase-matching angles at several other temperatures have also been measured. The measured angles agree quite well with the calculated values as can be seen from Table 1. By calibrating against aniline, we determined the macroscopic linearity Γ of 5CB to be 40×10^{-14} esu at $34^{\circ}C$.

3.2.4. Conclusion

It has been demonstrated experimentally that the linear birefringence of nematic liquid crystals can be used to achieve phase-matching condition for harmonic generation. Since smectic and nematic liquid crystals have similar birefringence properties, smectic liquid crystals should also be phase-matchable. Despite its phase-matchability, a nematic liquid crystal is not expected to be useful as a practical second-harmonic generator because it is unlikely that single domain nematic liquid crystal samples with thickness greater than a few mm can be achieved. In addition, the scattering loss due to thermal fluctuation of the director would be prohibitive. The potential of smectic liquid crystals as practical optical frequency doublers, however deserves further investigation. First, smectic liquid crystals have very low scattering loss. Second, there exist ferroelectric smectic liquid crystals which, because of the lack of inversion symmetry, should possess second-order nonlinearity. Third, it appears possible that the director can be made to lie at an arbitrary angle with respect to the aligning surface if SiO_2 is evaporated onto the surface at an appropriate angle [16]. With this ability, one can orient the director in such a direction that phase-matching is achieved when the fundamental beam is propagating parallel to the aligning surfaces. Since it is known that single domain smectic liquid crystals can be formed between two aligning surfaces separated by a couple of mm, a lightly focused fundamental beam can be sent into the sample easily. For this geometry, a single domain sample length of several centimeters should also be ready obtainable. Thus it appears that smectic liquid crystals can be useful as practical harmonic generators.

Appendix

$$\langle \Phi^4_{3z} \rangle = \langle \cos^4\theta \rangle \; ; \quad \langle \Phi^4_{1z} \rangle = \langle \Phi^4_{2z} \rangle = \frac{3}{8} \langle \sin^4\theta \rangle$$

$$\langle \Phi^4_{1x} \rangle = \langle \Phi^4_{2x} \rangle = \frac{3}{64} [\; 3 + 2\langle \cos^2\theta \rangle + 3\langle \cos^4\theta \rangle \;]$$

$$\langle \Phi^4_{3x} \rangle = \frac{3}{8} \langle \sin^4\theta \rangle$$

$$\langle \Phi^2_{1z} \Phi^2_{2z} \rangle = \frac{1}{8} \langle \sin^4\theta \rangle$$

$$\langle \Phi^2_{3z} \Phi^2_{1z} \rangle = \langle \Phi^2_{3z} \Phi^2_{2z} \rangle = \frac{1}{2} \langle \cos^2\theta \sin^2\theta \rangle$$

$$\langle \Phi^2_{1x} \Phi^2_{2x} \rangle = \frac{1}{64} [\; 3 + 2\langle \cos^2\theta \rangle + 3\langle \cos^4\theta \rangle \;]$$

$$\langle \Phi^2_{3x} \Phi^2_{1x} \rangle = \langle \Phi^2_{3x} \Phi^2_{2x} \rangle = \frac{1}{16} [\; \langle \sin^2\theta \rangle + 3\langle \cos^2\theta \sin^2\theta \rangle \;]$$

$$\langle \Phi^2_{iF} \Phi^2_{jJ} \rangle = 0 \; ; \quad \langle \Phi_{iF} \Phi_{jF} \Phi_{kF} \Phi_{\ell F} \rangle = 0$$

$$\langle \cos^4\theta \rangle = \frac{1}{35} [\; 7 + 20\langle P_2 \rangle + 8\langle P_4 \rangle \;]$$

$$\langle \sin^4\theta \rangle = \frac{8}{105} [\; 7 - 10\langle P_2 \rangle + 3\langle P_4 \rangle \;]$$

$$\langle \cos^2\theta \rangle = \frac{1}{3} [\; 1 + 2\langle P_2 \rangle \;] \; ; \quad \langle \sin^2\theta \rangle = \frac{2}{3} [\; 1 - \langle P_2 \rangle \;]$$

$$\langle \cos^2\theta \sin^2\theta \rangle = \frac{1}{105} [\; 14 + 10\langle P_2 \rangle - 24\langle P_4 \rangle \;]$$

REFERENCES

Chapter 3

1. P. G. de Gennes, Physics of Liquid Crystals (Clarendon, Oxford, 1974).
2. M. J. Stephen, and J. P. Straley, Rev. Mod. Phys. 46, 617 (1974).
3. K. Miyano, J. Chem. Phys. 69, 4807 (1978).
4. S. Jen, N. A. Clark, P. S. Pershan, and E. B. Priestly, J. Chem. Phys. 66, 4635 (1977).
5. S. K. Saha, and G. K. Wong, Appl. Phys. Lett, 34, 423 (1979).
6. B. F. Levine, and C. G. Bethea, J. Chem. Phys. 63, 2666 (1975).
7. H. Goldstein, Classical Mechanics (Addison-Wesley, New York, 1959).
8. Without loss of generality, we assume Kleiman's conjecture holds for β_{ijk} and $\gamma_{ijk\ell}$. Other wise, a few more terms will appear in the expressions for γ_{iso}, α , and β.
9. S. Keilich, IEEE J. Quant. Electron QE-5, 562 (1969).
10. S. Jen, N. A. Clark, P. S. Pershan, and E. B. Priestly, Phys. Rev. Lett. 31, 1552 (1973).
11. S. Chandrasekhar, and N. V. Madhusudana, J. Phys. (Paris) Suppl. 30, C4-24 (1969).
12. M. F. Vuks, Optics Spectr. 20, 361 (1966).
13. If the nonlinearity of glass spacers is comparable to that of the medium under study, the boundary conditions at the air and glass should also be considered. For detailed discussion, see Ref. 6 and J. L. Ouder, J. Chem. Phys. 67, 446 (1977).
14. L. Feijoo, V. T. Rajan, C. W. Woo, Phys. Rev. A19, 1263 (1979).

15. W. Urbach, M. Boix and E. Guton, Appl. Phys. Lett. 25, 479 (1974).

16. E. P. Raynes, D. K. Rowell and I. A. Shanks, Mol. Crys. Liq. Crys. Lett. 34, 105 (1976).

Table 1. Refractive indices and phase-matching angle for 5CB at several temperatures. T_{NI} is the nematic to isotropic temperature and is $35^{o}C$ for our sample.

$T_{NI}-T$ (^{o}C)	1	3	5	7	10	13
n_o^2 (5320Å)	1.5400	1.5396	1.5360	1.5352	1.5345	1.5342
n_e^2 (5320Å)	1.6800	1.7007	1.7094	1.7156	1.7215	1.7250
n_o (1.064 m)	1.5110	1.5096	1.5090	1.5085	1.5083	1.5083
n_e (1.064 m)	1.6316	1.6491	1.6569	1.6621	1.6670	1.6699
θ_m(calculated)	30.8^{o}	28.2^{o}	26.9^{o}	26.2^{o}	25.6^{o}	25.2^{o}
θ_m(measured)	30.6^{o}	28^{o}	26.8^{o}	26.1^{o}	25.7^{o}	25^{o}

FIGURE CAPTIONS

Chapter 3

1. Schematic diagram of molecular frame and laboratory frame.
2. Boundaries associated with the liquid crystal cell.
3. Dependence of second-harmonic intensity in 5CB on d. c. field.
4. Dependence of second-harmonic intensity in 5CB on fundamental laser intensity.
5. Variation of second-harmonic intensity as a function of the translated distance of the liquid crystal cell. The solid line is the plot of $\sin^2(\frac{\pi}{2}\frac{2L'}{L})$.
6. Relative second-harmonic intensity as a function of temperature in 5CB.
7. Relative second-harmonic intensity as a function of temperature in MBBA.
8. Coherence length as a function of temperature in 5CB.
9. Coherence length as a function of temperature in MBBA.
10. Macroscopic third-order nonlinearity as a function of temperature in 5CB.
11. Macroscopic third-order nonlinearity as a function of temperature in MBBA.
12. Microscopic order parameters as a function of temperature in 5CB.
13. Microscopic order parameters as a function of temperature in MBBA.
14. Plot of truncated distribution function for 5CB at $\Delta T = 0.05^{\circ}$.

15. Index surfaces of the ordinary and extraordinary rays for a positive uniaxial crystal. The condition $n_o^{2\omega} = n_e^{\omega}(\theta)$ is satisfied at $\theta = \theta_m$.

16. Schematic of liquid crystal cell used in the experiment on phase-matched electric-field induced second-harmonic generation in a nematic liquid crystal.

17. Variation of second-harmonic intensity as a function of the angle between the director and the wave vector. The solid line is the theoretical phase-matching curve and circles are the experimental data points.

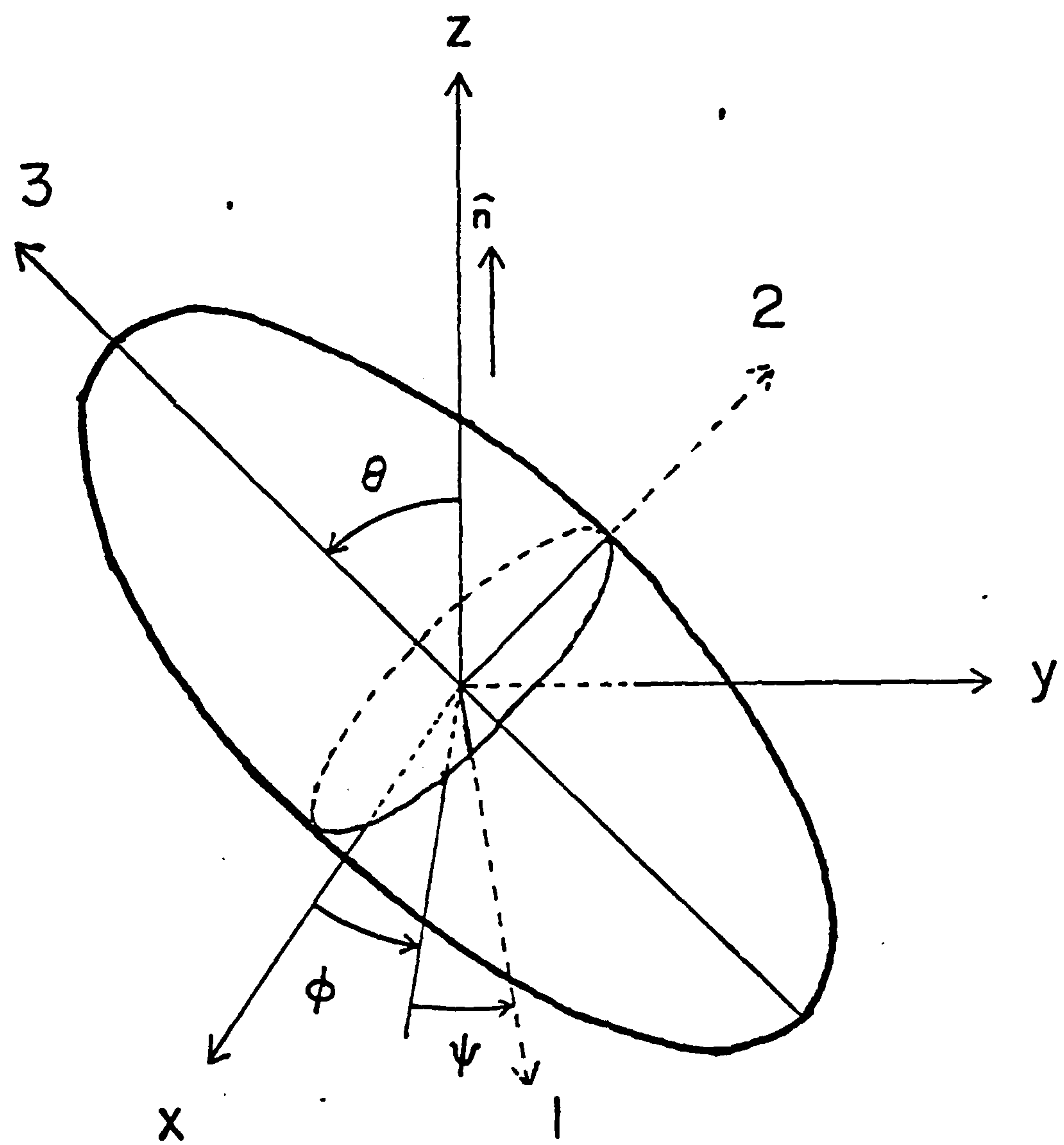

FIG. 1

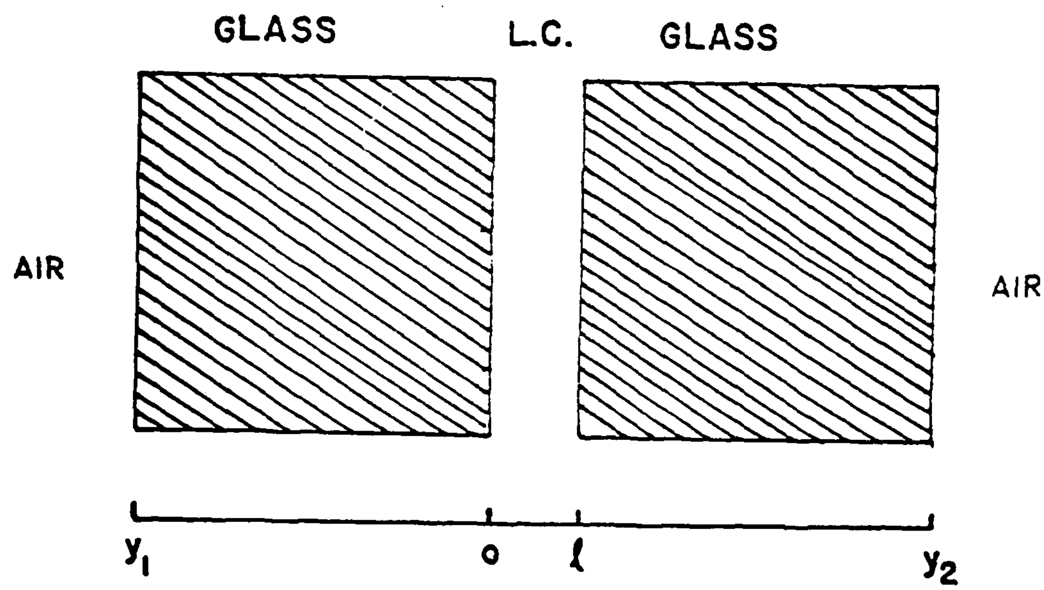

FIG. 2

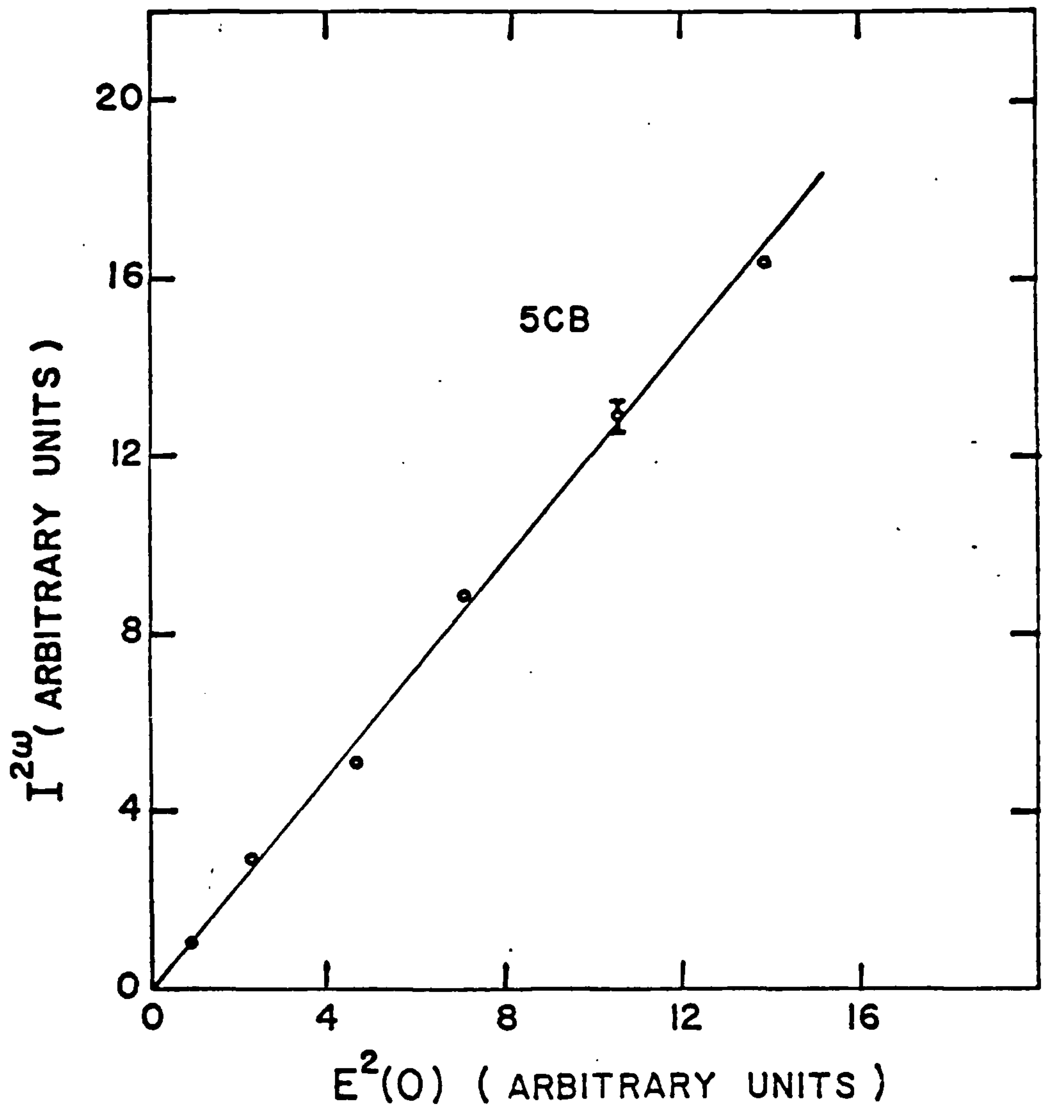

20
16
12
8
4
0
0
4
8
12
16
5CB
$I^{2\omega}$ (ARBITRARY UNITS)
$E^2(0)$ (ARBITRARY UNITS)

FIG. 3

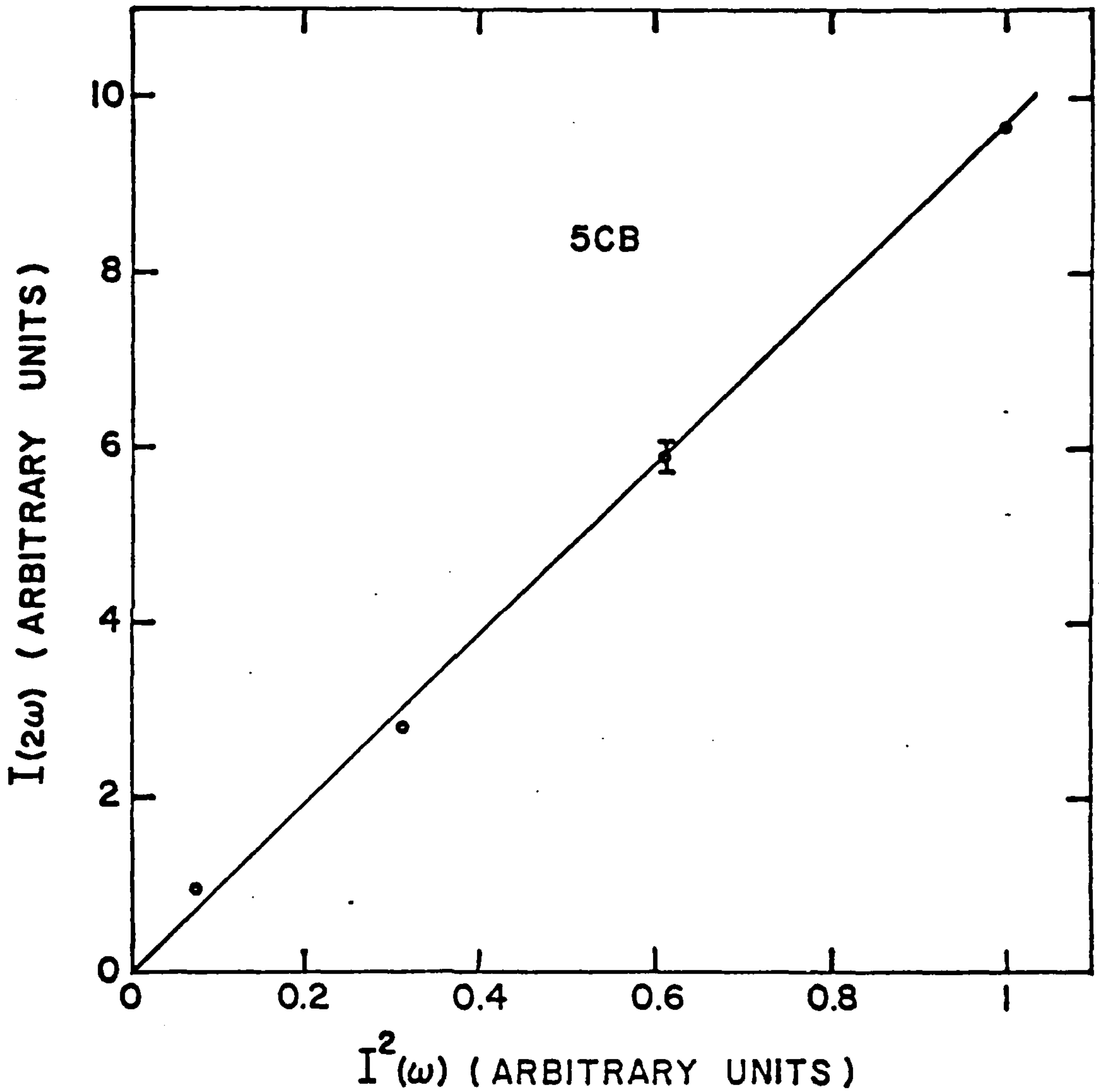
10
8
6
4
2
0
0
0.2
0.4
0.6
0.8
1
5CB
I(2ω) (ARBITRARY UNITS)
I²(ω) (ARBITRARY UNITS)

FIG. 4

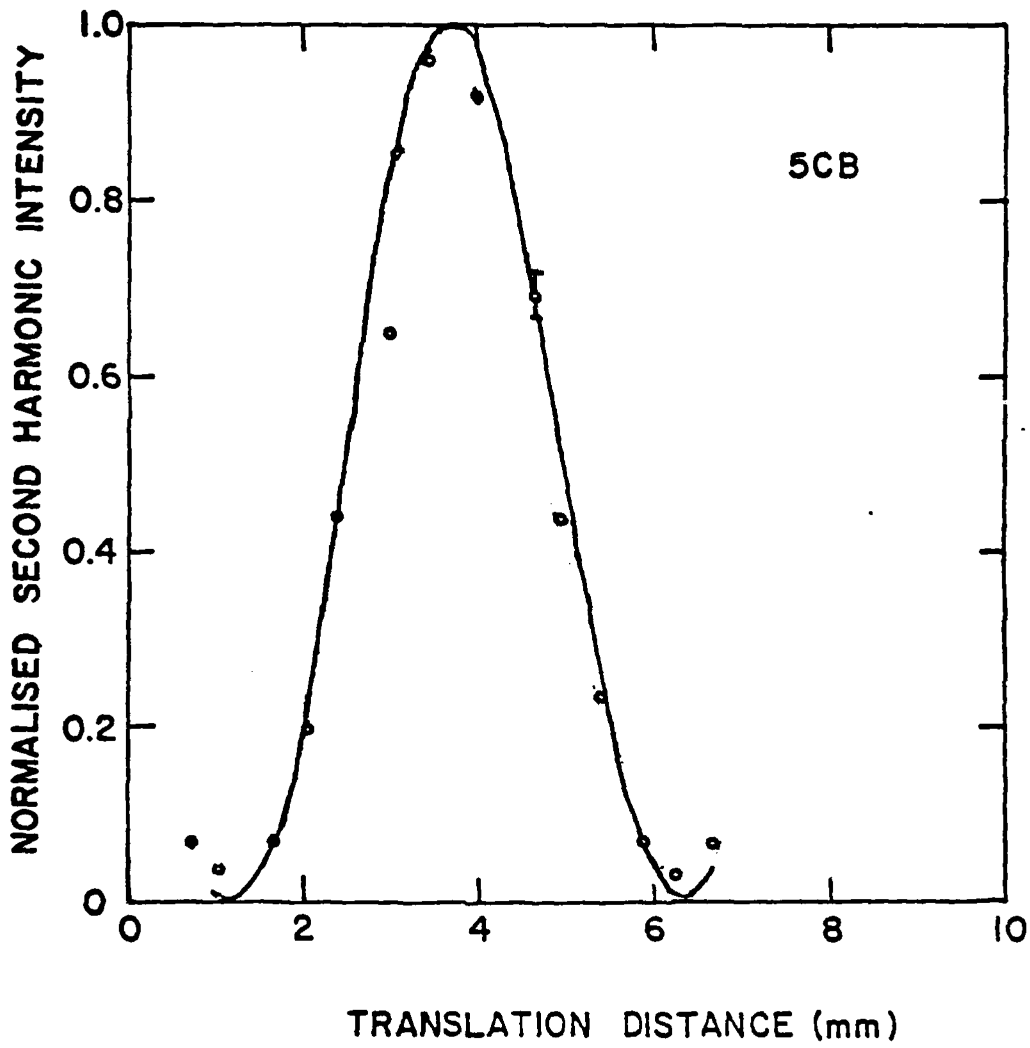
1.0
0.8
0.6
0.4
0.2
0
NORMALISED SECOND HARMONIC INTENSITY
5CB
0
2
4
6
8
10
TRANSLATION DISTANCE (mm)

FIG. 5

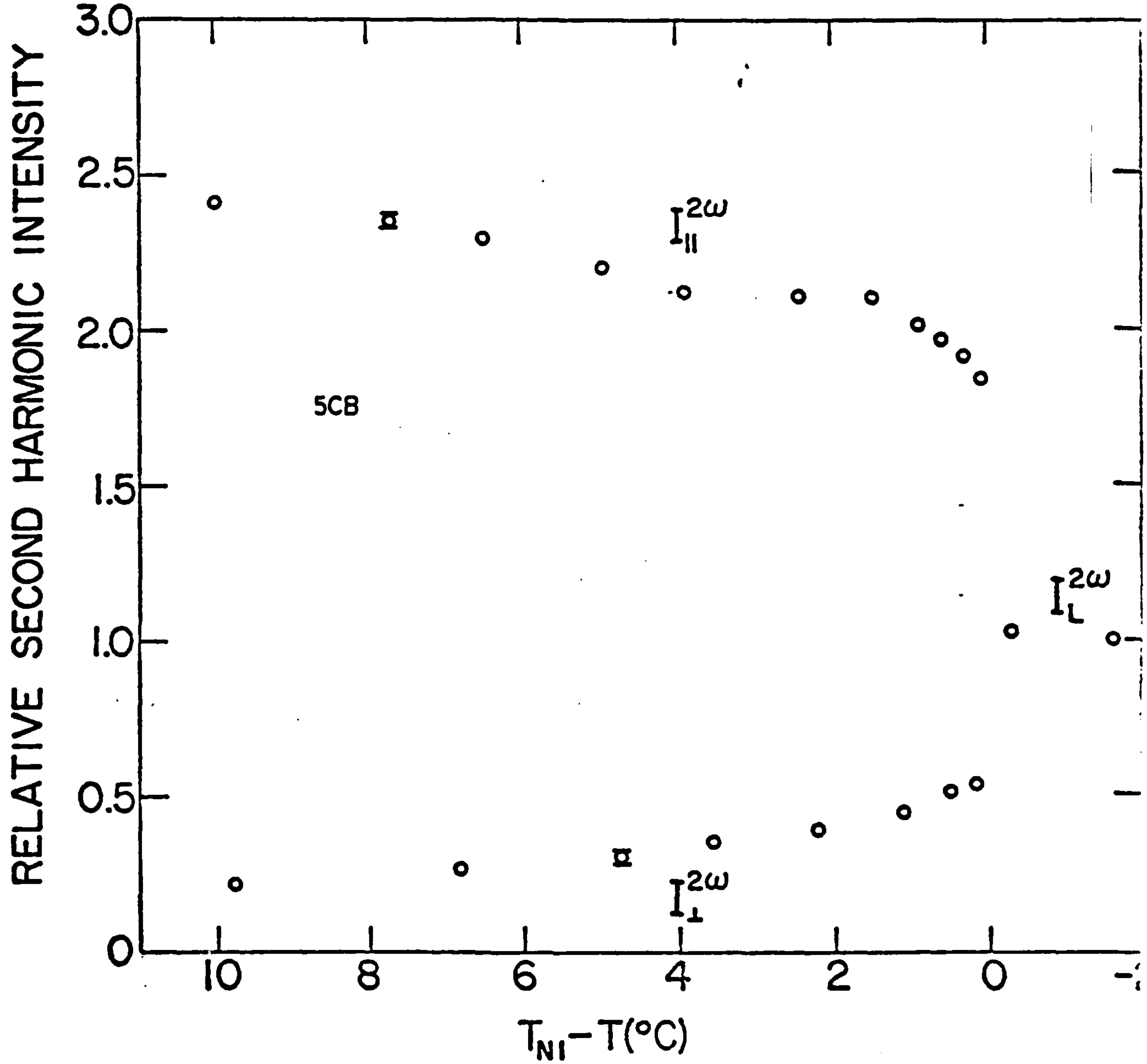
RELATIVE SECOND HARMONIC INTENSITY
3.0
2.5
2.0
1.5
1.0
0.5
0
5CB
$I_{\parallel}^{2\omega}$
$I_{\perp}^{2\omega}$
$I_{L}^{2\omega}$
10
8
6
4
2
0
$T_{NI}-T(°C)$

FIG. 6

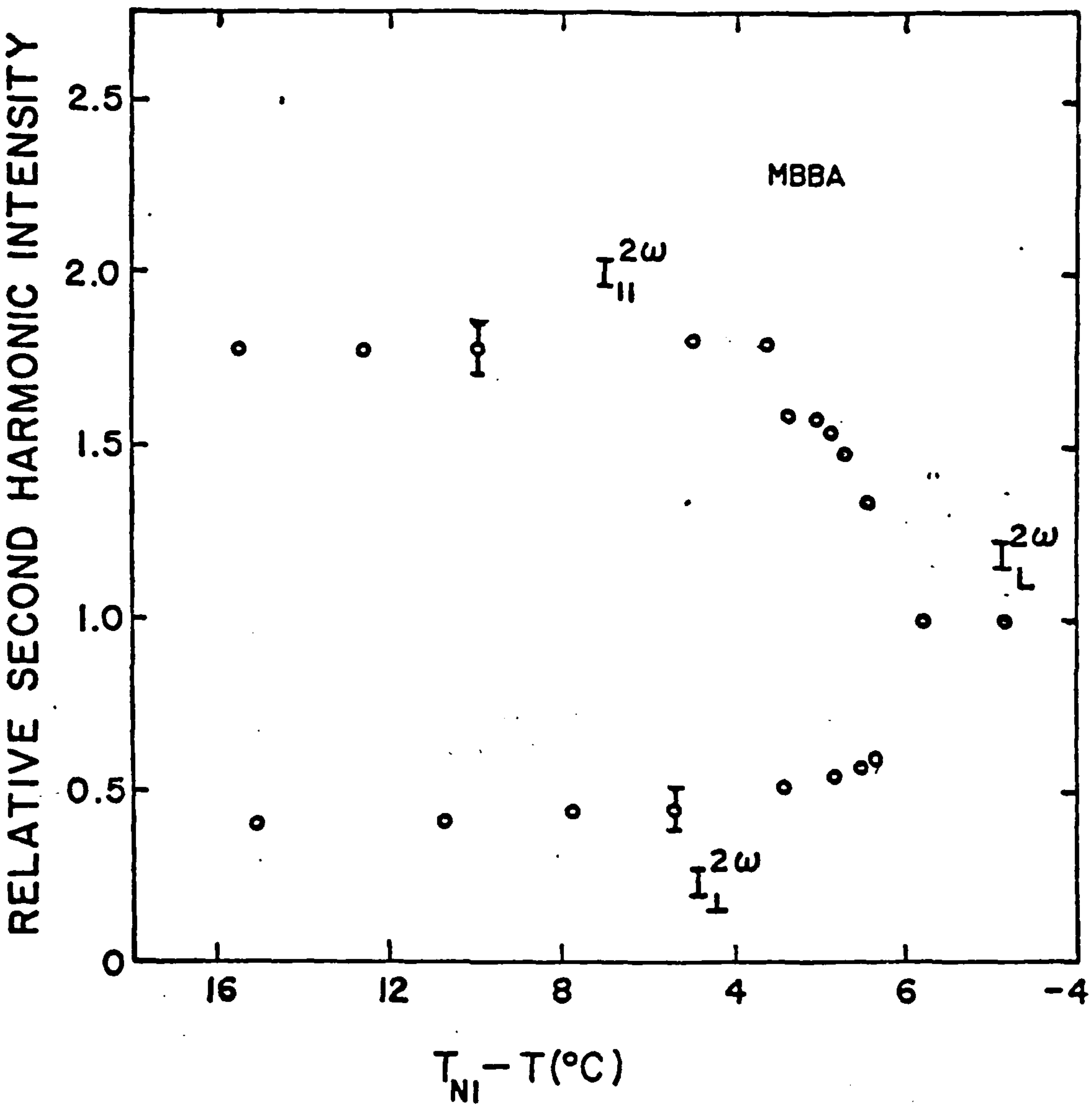
RELATIVE SECOND HARMONIC INTENSITY
2.5
2.0
1.5
1.0
0.5
0
MBBA
$I_{\parallel}^{2\omega}$
$I_{L}^{2\omega}$
$I_{\perp}^{2\omega}$
16
12
8
4
6
-4
$T_{NI}-T(°C)$

FIG. 7

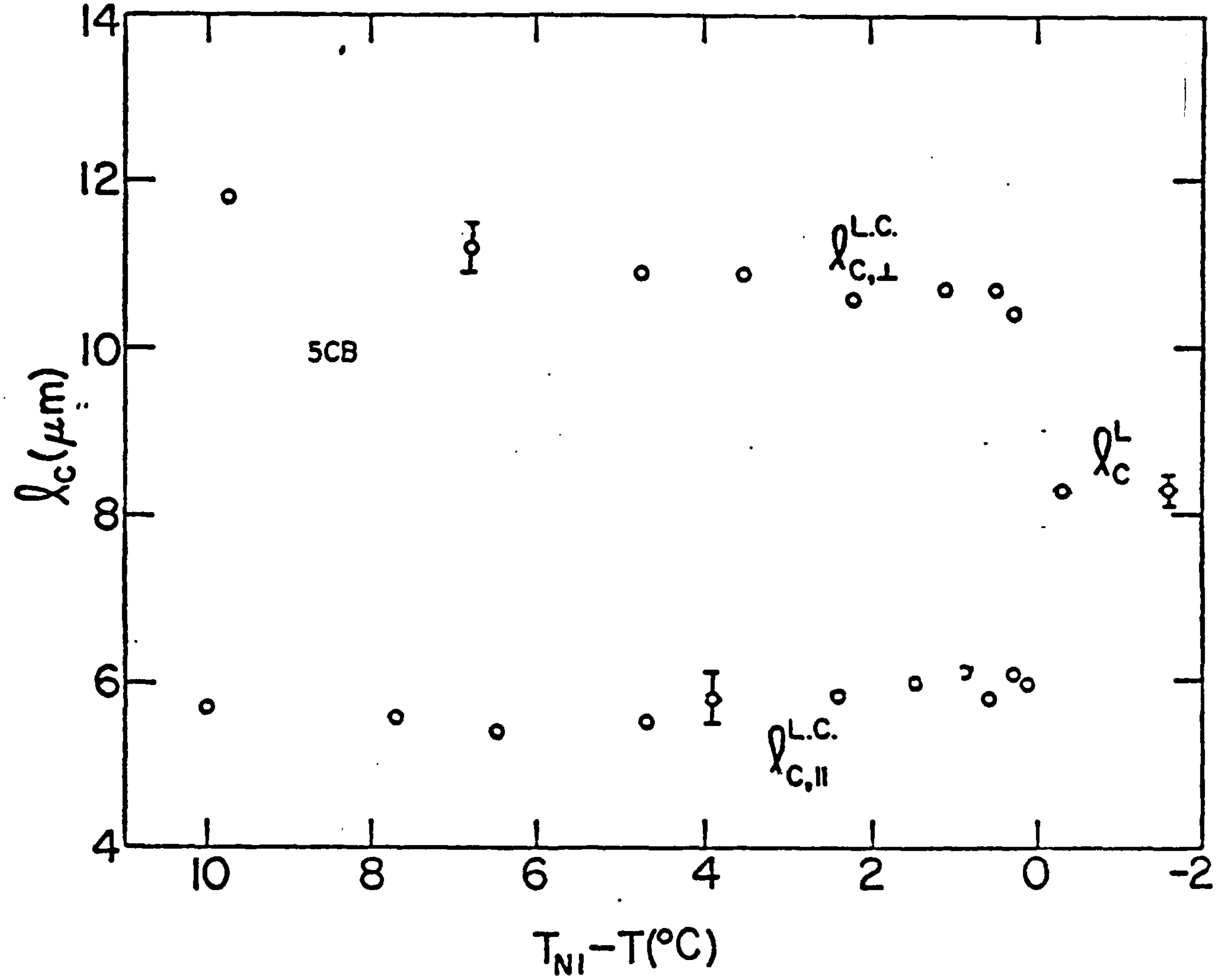
14
12
10
8
6
4
5CB
$\ell_{c,\perp}^{L.C.}$
ℓ_c^{L}
$\ell_{c,\parallel}^{L.C.}$
$\ell_c(\mu m)$
10
8
6
4
2
0
-2
$T_{NI}-T(°C)$

FIG. 8

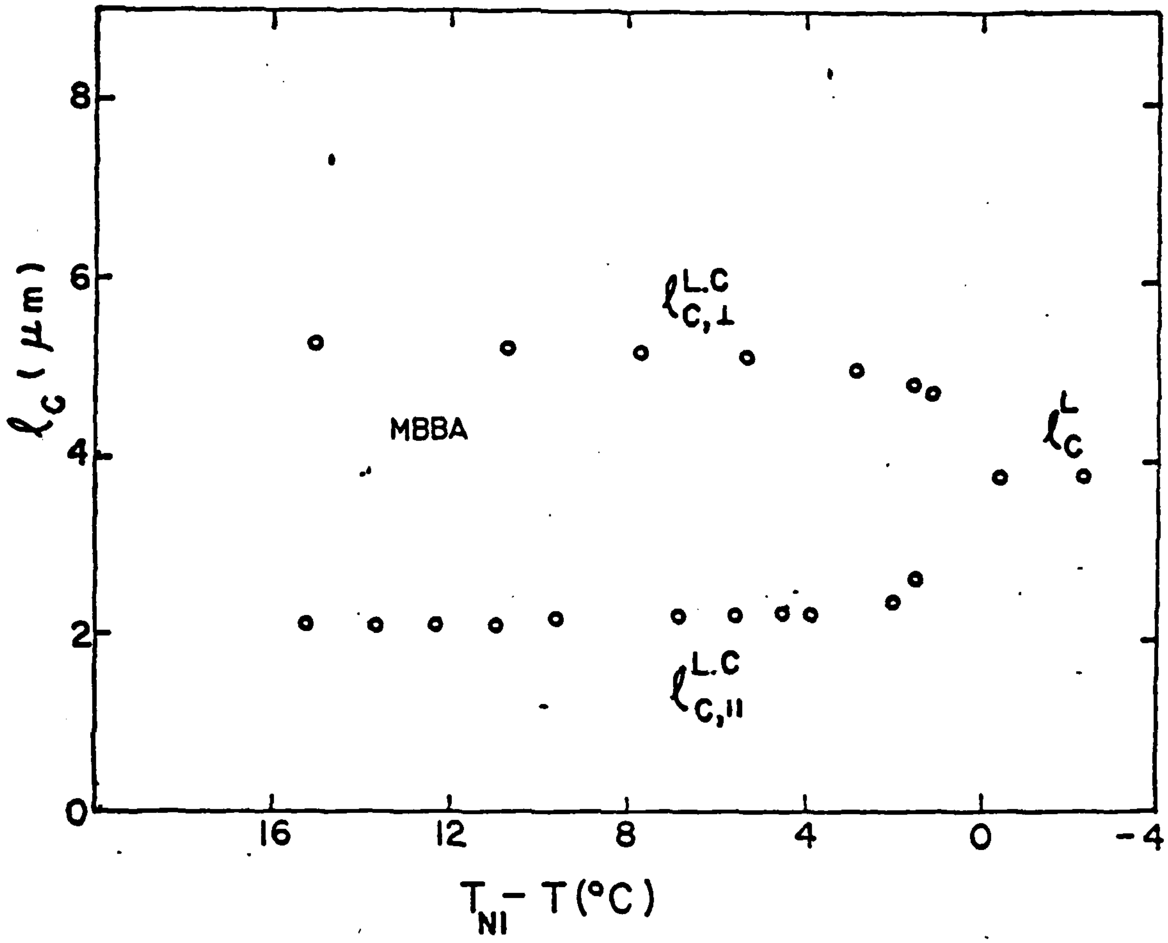

ℓ_c (μm)
$\ell^{L.C}_{c,\perp}$
MBBA
ℓ^{L}_{c}
$\ell^{L.C}_{c,\parallel}$
0
2
4
6
8
16
12
8
4
0
-4
$T_{NI} - T$(°C)

FIG. 9

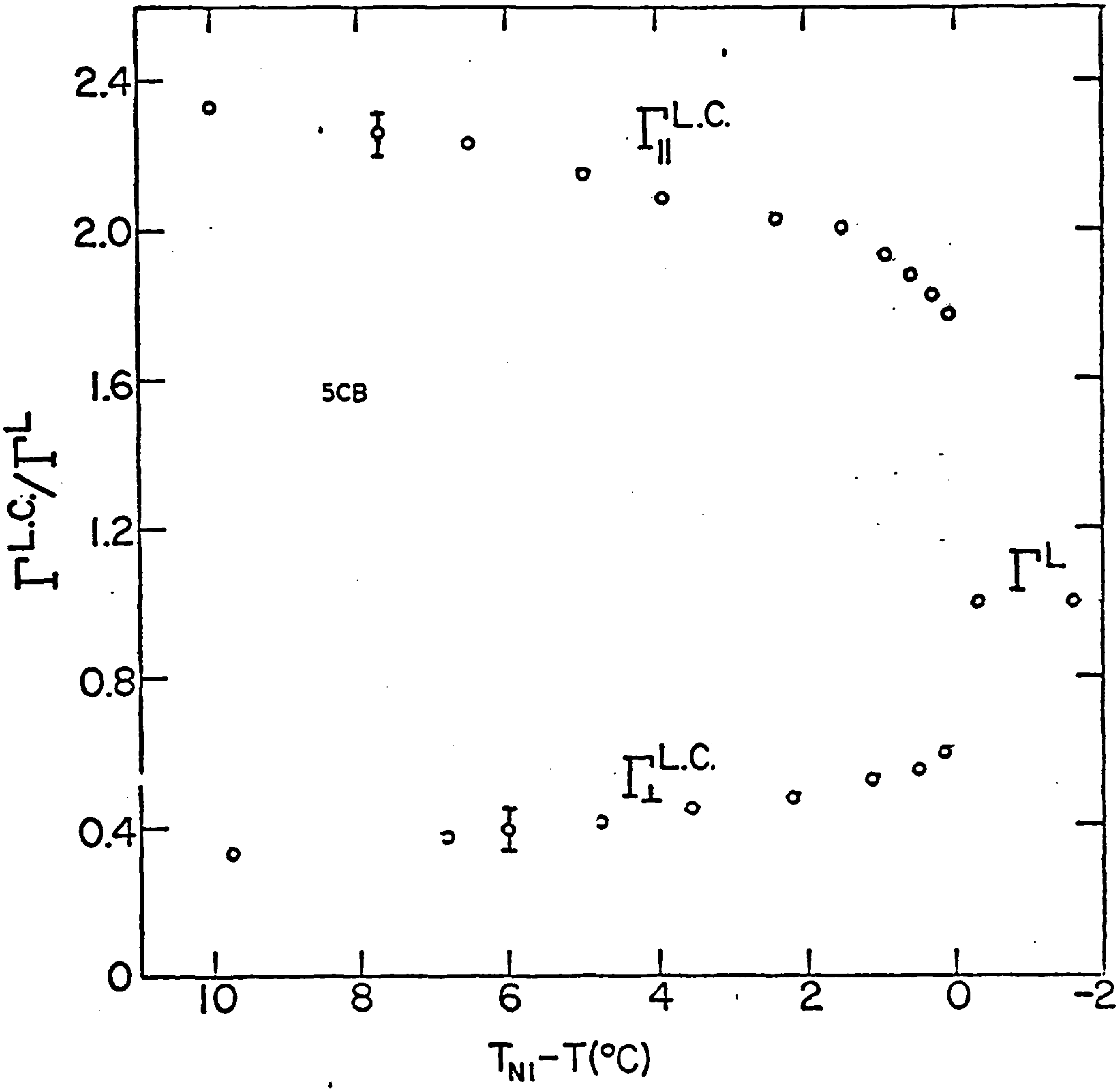
$\Gamma^{L.C.}/\Gamma^{L}$
2.4
2.0
1.6
1.2
0.8
0.4
0
$\Gamma_{\parallel}^{L.C.}$
5CB
Γ^{L}
$\Gamma_{\perp}^{L.C.}$
10
8
6
4
2
0
-2
$T_{NI}-T(°C)$

FIG. 10

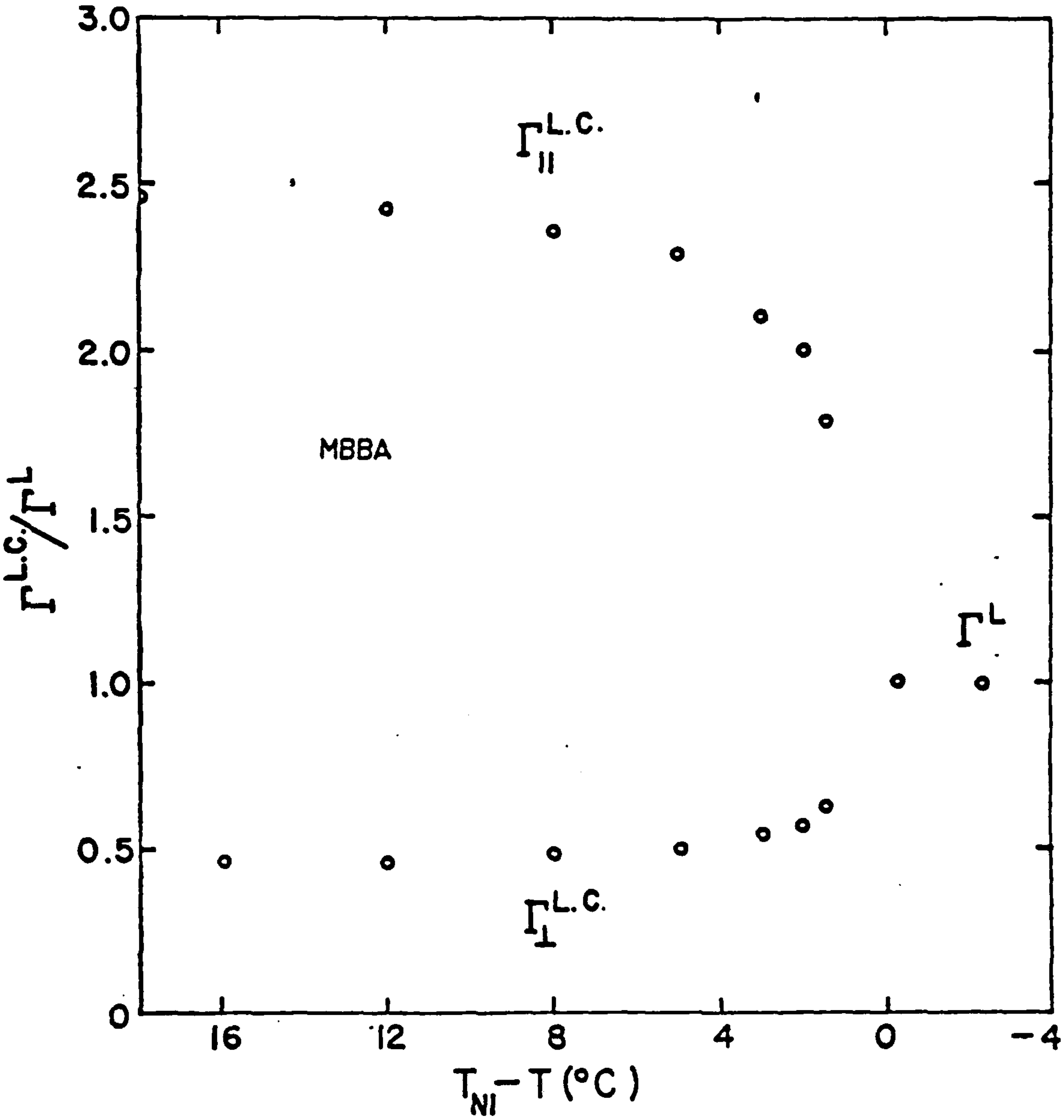

3.0
2.5
2.0
1.5
1.0
0.5
0
$\Gamma^{L.C.}/\Gamma^{L}$
$\Gamma_{\parallel}^{L.C.}$
MBBA
Γ^{L}
$\Gamma_{\perp}^{L.C.}$
16
12
8
4
0
−4
$T_{NI} - T$ (°C)

FIG. 11

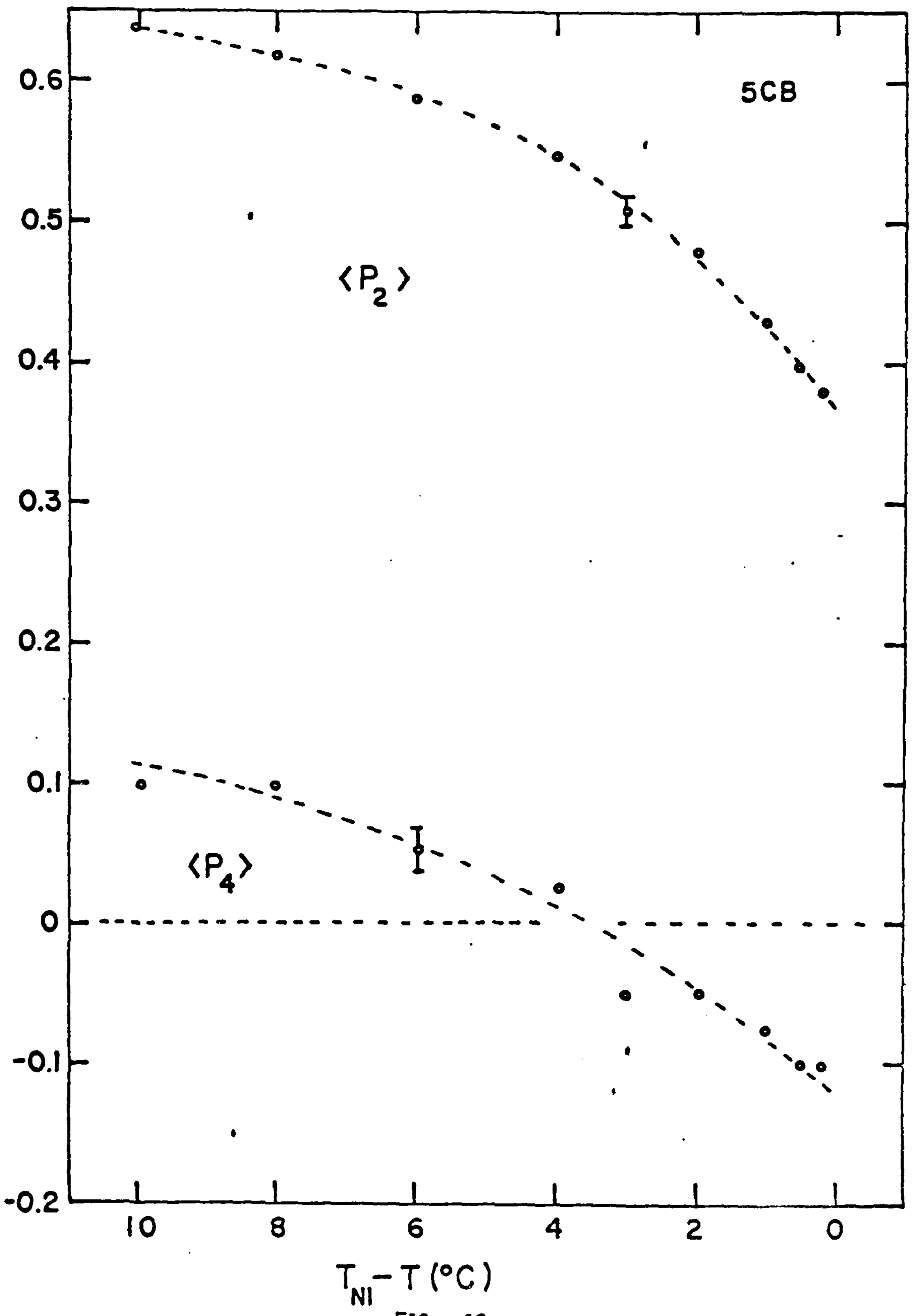

FIG. 12

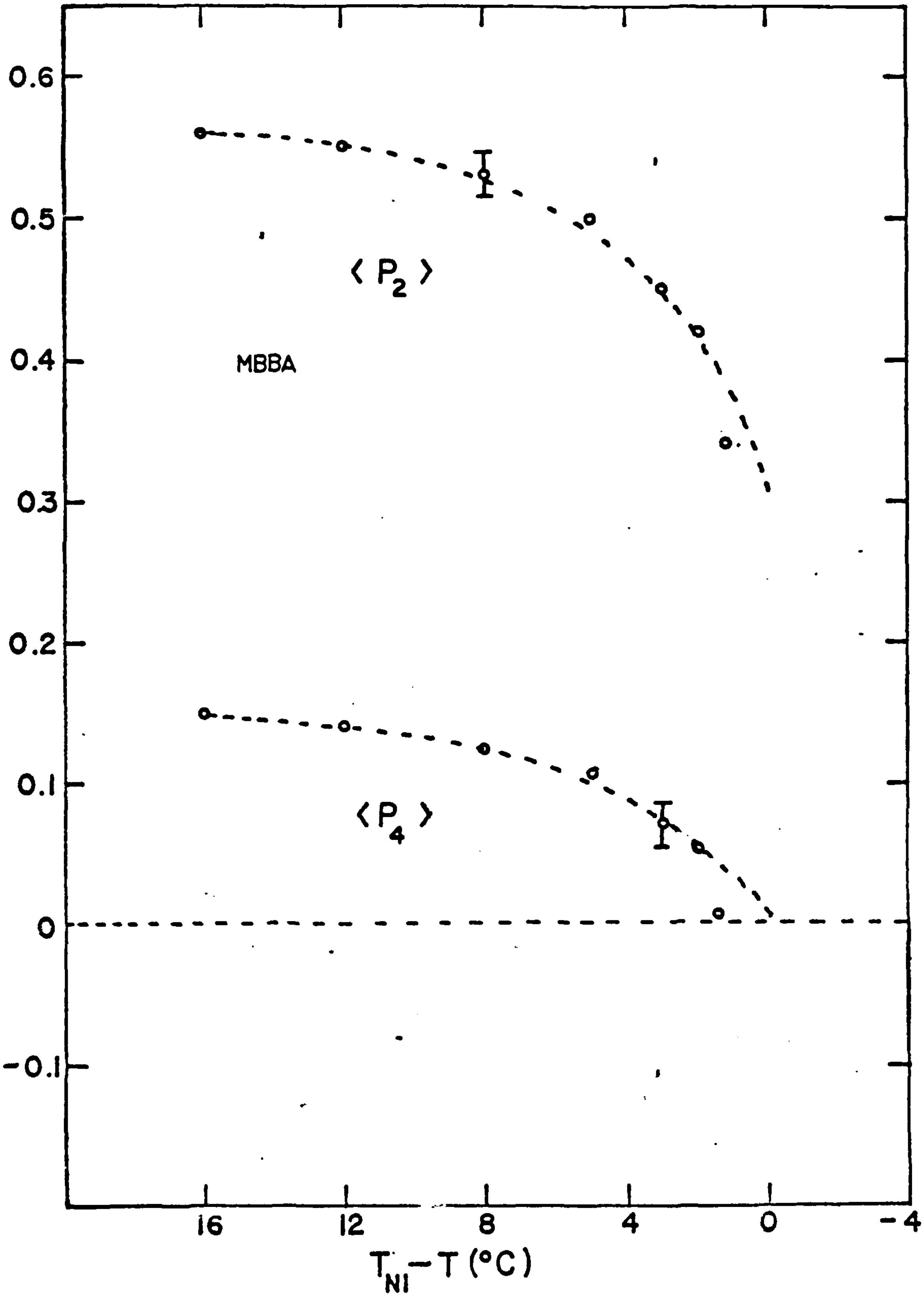

FIG. 13

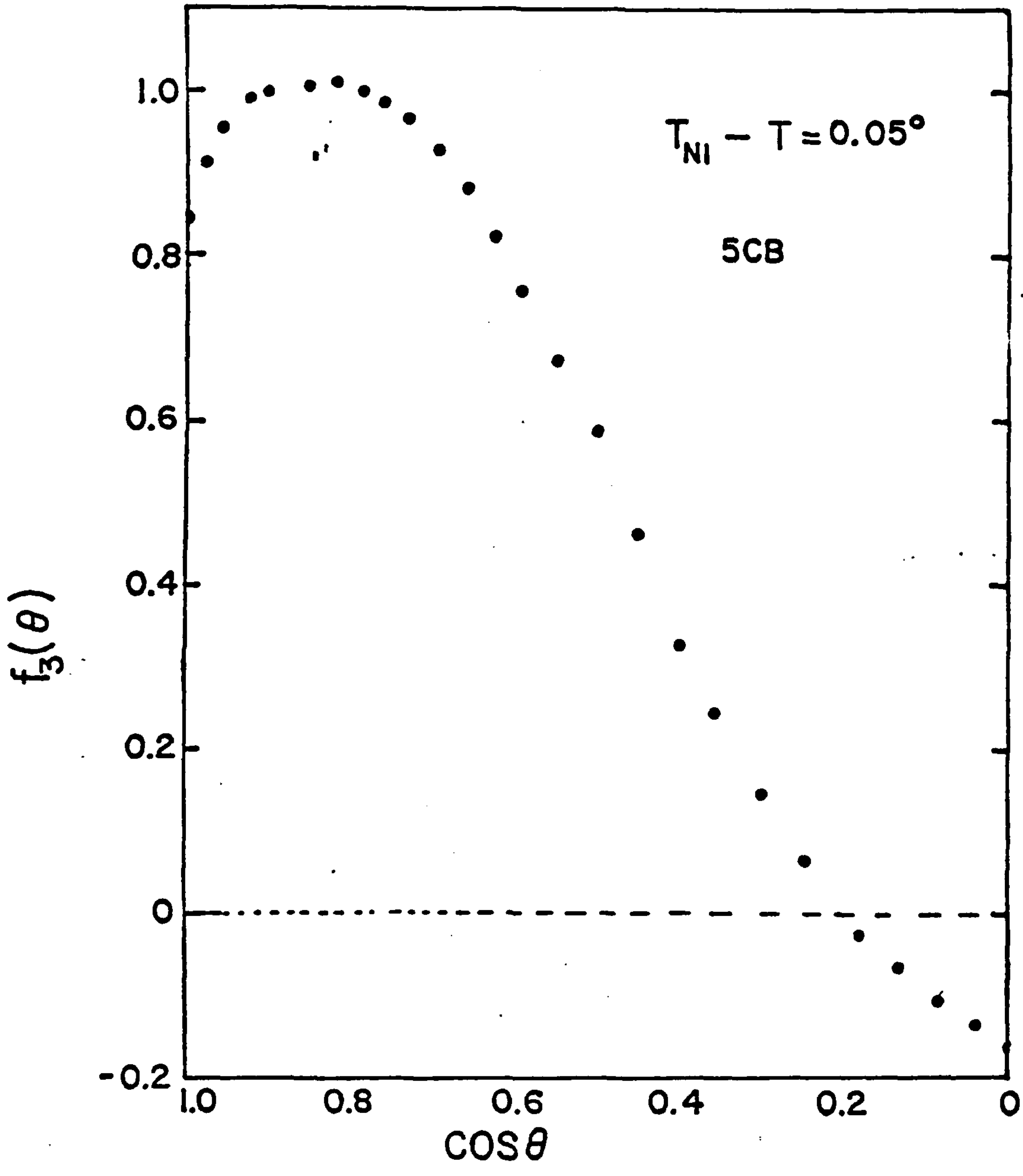

FIG. 14

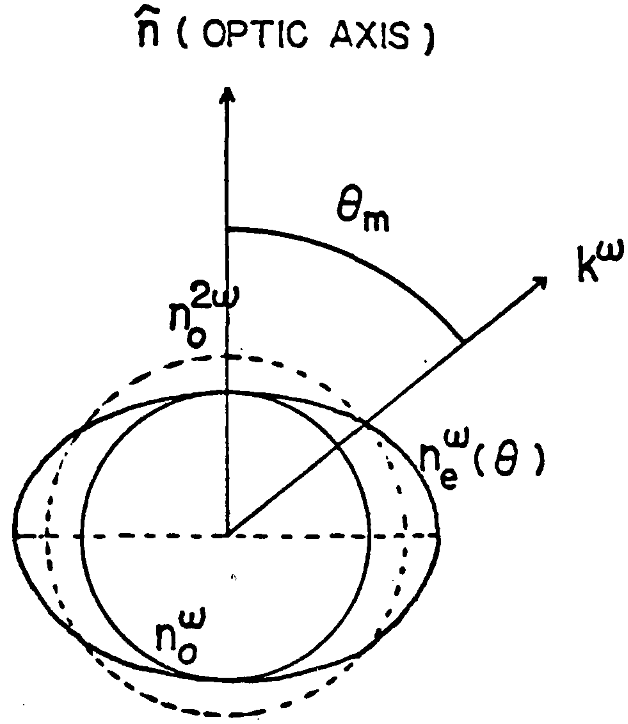
$\hat{n}$ (OPTIC AXIS)
θ_m
k^ω
$n_o^{2\omega}$
$n_e^\omega(\theta)$
n_o^ω

FIG. 15

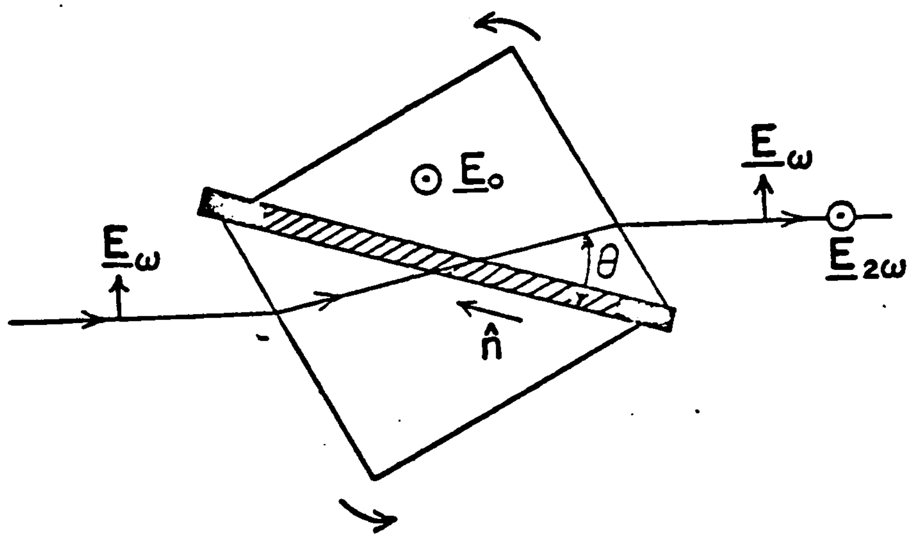

$\odot\ \underline{E}_0$
$\underline{E}_\omega$
$\underline{E}_\omega$
$\underline{E}_{2\omega}$
θ
$\hat{n}$

FIG. 16

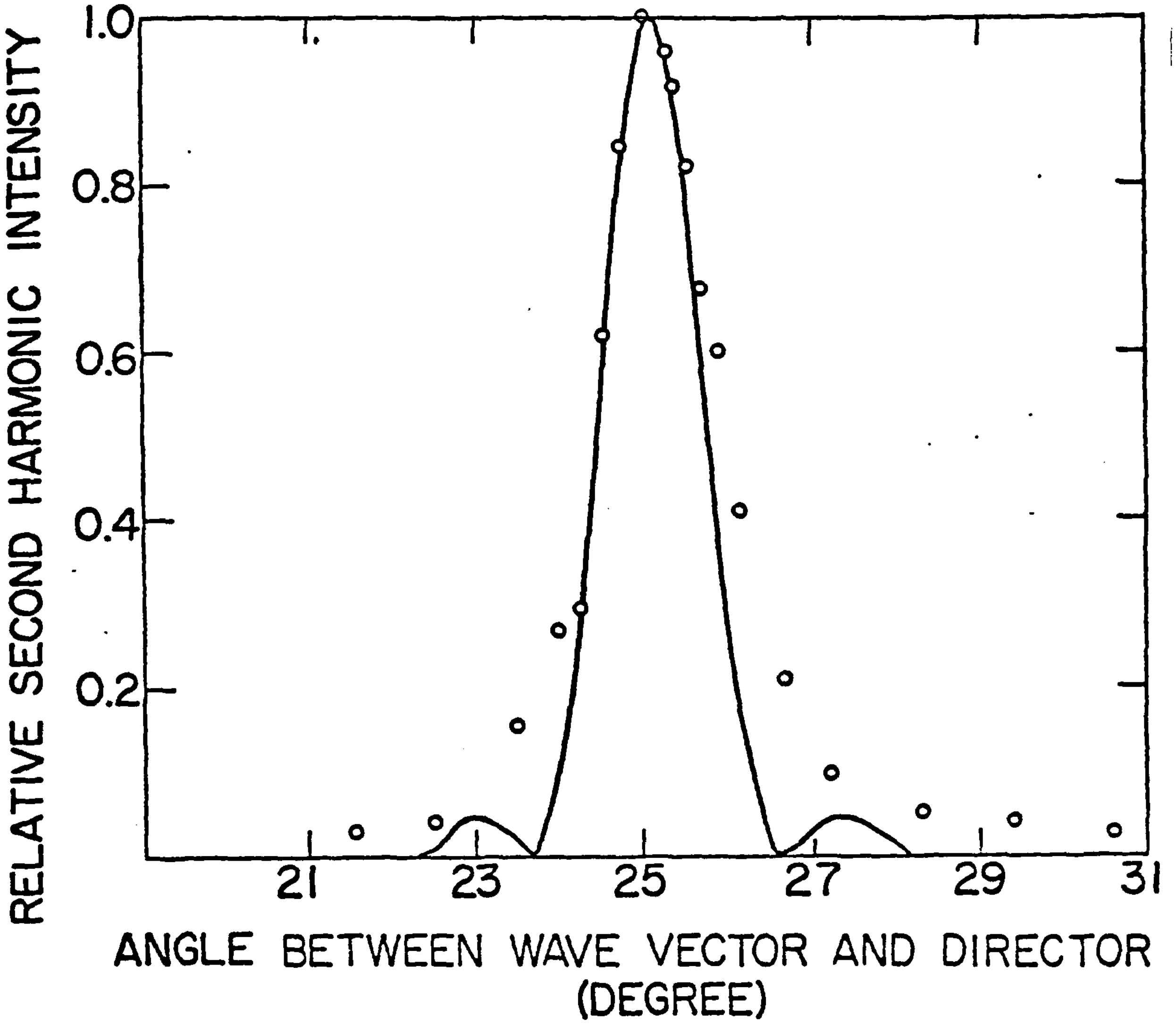
RELATIVE SECOND HARMONIC INTENSITY
1.0
0.8
0.6
0.4
0.2
21
23
25
27
29
31
ANGLE BETWEEN WAVE VECTOR AND DIRECTOR
(DEGREE)

FIG. 17

4. PHASE-MATCHED FIELD-INDUCED SECOND-HARMONIC GENERATION IN CHOLESTERIC LIQUID CRYSTALS

A cholesteric liquid crystal can be considered as a nematic liquid crystal twisted around an axis perpendicular to the direction of molecular alignment. The molecules form layers; in each layer the molecules are aligned parallel to the layer, but as the layers advances, the direction of alignment gradually rotates. As a result, the material has an over-all helical structure. The pitch of this helical structure varies as a function of temperature. The crystal momentum associated with this one-dimensional periodicity can thus be adjusted to compensate for the momentum mismatch between the fundamental and harmonic photons in a harmonic generation process. The possibility of achieving phase matching with this effect has been demonstrated for third-harmonic generation by Shelton and Shen [1]. In this chapter, we extend their theoretical consideration to the case of d. c.-field-induced second-harmonic generation. An experiment on a cholesteric mixture of cholesteryl chloride and cholesteryl myristate was performed to verify our theoretical results.

4.1 Theory

In order to develop theory for field-induced second-harmonic generation in cholesteric liquid crystals, we present a brief review of their linear optical properties. These results are needed in the discussion of field-induced second-harmonic generation (FISHG) in cholesteric liquid crystals.

The theory of linear wave propagation in a cholesteric liquid crystal has been well developed by Oseen[2] and Vries[3]. In their model, it is assumed that a cholesteric liquid crystal can be treated as a twisted birefringent medium characterized by a dielectric tensor $\overleftrightarrow{\varepsilon}_L$ periodic in z along the helical axis with a period equal to half of the helical pitch p.

$$\overleftrightarrow{\varepsilon}_L(z) = \begin{bmatrix} \bar{\varepsilon}\left[1+\alpha\cos(4\pi z/p)\right] & \bar{\varepsilon}\alpha\sin(4\pi z/p) & 0 \\ \bar{\varepsilon}\alpha\sin(4\pi z/p), & \bar{\varepsilon}\left[1-\alpha\cos(4\pi z/p)\right] & 0 \\ 0 & 0 & \varepsilon_\eta \end{bmatrix} \quad (1)$$

where $\bar{\varepsilon} = (\varepsilon_\xi + \varepsilon_\eta)/2$, $\alpha = (\varepsilon_\xi - \varepsilon_\eta)/2$. ε_ξ and ε_η are the principal dielectric constants in the directions parallel and perpendicular to the molecular alignment respectively.

Electromagnetic waves propagating in the z direction are then governed by the wave equation

$$\left[\frac{\partial^2}{\partial z^2} + \frac{\omega^2}{c^2}\overleftrightarrow{\varepsilon}_L(z)\right]\cdot \vec{E}_L(z) = 0 \ . \qquad (2)$$

where we have used the subscript L to denote $\overleftrightarrow{\varepsilon}_L$ and $\overleftrightarrow{E}_L$ are quantities referred to the laboratory frame.

To obtain solutions to Eq. (2), it is convenient to introduce a spatially rotating reference frame which twists with the cholesteric structure (see Fig. 1). We shall call this rotating frame the twisted frame and let its coordinates be ξ, η, z. An electric field vector in the laboratory frame is then related to the same vector in the twisted frame by

$$\vec{E}_L\ (x,y,z) = \overleftrightarrow{R}\ (z)\cdot \vec{E}_T\ (\xi,\eta,\ z) \qquad (3)$$

where

$$\overleftrightarrow{R}\ (\theta = 2\pi z/p) = \begin{pmatrix} \cos\theta & -\sin\theta & 0 \\ \sin\theta & \cos\theta & 0 \\ 0 & 0 & 1 \end{pmatrix} \qquad (4)$$

The dielectric tensor in the twisted frame is related to that in the laboratory frame by

$$\overleftrightarrow{\varepsilon}_T = \overleftrightarrow{R}^{-1} : \overleftrightarrow{\varepsilon}\,(z) : \overleftrightarrow{R} = \begin{pmatrix} \varepsilon_\xi & 0 & 0 \\ 0 & \varepsilon_\eta & 0 \\ 0 & 0 & \varepsilon_\pi \end{pmatrix} . \qquad (5)$$

The dielectric tensor $\overleftrightarrow{\varepsilon}_T$ now takes on the form for a simple birefringent medium because in the twisted frame the cholesteric medium appears as a simple birefringent materials. With these relationships, Eq. (2) can then be transformed into

$$\left[\frac{\partial^2}{\partial z^2} - \frac{4\pi}{p}\overleftrightarrow{\sigma}\frac{\partial}{\partial z} - \left(\frac{2\pi}{p}\right)^2 + \frac{\omega^2}{c^2}\overleftrightarrow{\varepsilon}_T(\omega)\right] \cdot \vec{E}_T = 0 , \qquad (6)$$

where

$$\overleftrightarrow{\sigma} = \begin{pmatrix} 0 & 1 & 0 \\ -1 & 0 & 0 \\ 0 & 0 & 1 \end{pmatrix} \qquad (7)$$

The two extra terms that appear in Eq. (6) are due to the spatial dependence of the transformation. The solutions to Eq. (6) can be determined by assuming a propagating wave of the form

$$\vec{E}_T = \begin{pmatrix} \mathcal{E}_\xi \\ \mathcal{E}_\eta \\ 0 \end{pmatrix} \exp\ (ikz - i\omega t) \qquad (8)$$

Substitution of Eq. (8) into Eq. (6) gives

$$\left[-k^2 - \left(\frac{2\pi}{p}\right)^2 + \frac{\omega^2}{c^2}\varepsilon_\xi\right]\mathcal{E}_\xi - ik\frac{4\pi}{p}\mathcal{E}_\eta = 0$$

$$+ ik\frac{4\pi}{p}\mathcal{E}_\xi + \left[-k^2 - \left(\frac{2\pi}{p}\right)^2 + \frac{\omega^2}{c^2}\varepsilon_\eta\right]\mathcal{E}_\eta = 0 \qquad (9)$$

Non-trivial solutions for $\mathcal{E}_\xi$ and $\mathcal{E}_\eta$ exist only when the determinant of their coefficients is zero. We then find

$$m_{\pm}^2 = (\lambda'^2 + 1) \pm (4\lambda'^2 + \alpha^2)^{1/2} \qquad (10)$$

$$\left.\frac{E_\eta}{E_\xi}\right)_{\pm} = \frac{i2m_{\pm}\lambda'}{m_{\pm}^2 + \lambda'^2 + \alpha - 1} = f_{\pm} \qquad (11)$$

where

$$m_{\pm}^2 = \frac{k_{\pm}^2 c^2}{\omega^2 \bar{\varepsilon}} \qquad (12)$$

$$\lambda' = \frac{2\pi c}{\omega p\, \bar{\varepsilon}^{1/2}} \qquad (13)$$

The solutions to Eq. (6) are thus of the form

$$\vec{E}_{T\pm} = \hat{e}_{\pm} E_{\pm} \exp(ik_{\pm}z - i\omega t) \qquad (14)$$

where

$$E_{\pm} = E_{\xi\pm}(1 + f_{\pm})^{1/2}$$

and

$$\hat{e}_{\pm} = (1 + f_{\pm})^{-1/2} (\hat{\xi} + i f_{\pm} \hat{\eta}) \qquad (14\text{-a})$$

D. C. field induced second harmonic generation is governed by the nonlinear wave equations (see Chapter 3),

$$\left[\frac{\partial^2}{\partial z^2} + \left(\frac{2\omega}{c}\right)^2 \overleftrightarrow{\varepsilon}_L(z,2\omega)\right] \cdot \vec{E}_L(z,2\omega) = -4\left(\frac{2\omega}{c}\right)^2 \vec{P}_L^{NLS}(z,2\omega) \qquad (15)$$

where the nonlinear polarization is given by

$$\vec{P}^{NLS}(z,2\omega) = \overleftrightarrow{\Gamma}_L : \vec{E}_L(z,\omega)\,\vec{E}_L(z,\omega)\,\vec{E}_L(z,0) \qquad (16)$$

where the macroscopic third order nonlinearity $\overleftrightarrow{\Gamma}_L$ is a function of z. As in the linear case, it is easier to obtain solutions to Eq. (15) by transforming it into the twisted frame.

$$\left[\frac{\partial^2}{\partial z^2} - \frac{4\pi}{p}\overleftrightarrow{\sigma}\frac{\partial}{\partial z} - \left(\frac{2\pi}{p}\right)^2 + \left(\frac{2\omega}{c}\right)^2 \overleftrightarrow{\varepsilon}_T(2\omega)\right] \cdot \vec{E}_T(2\omega)$$

$$= -\frac{4\pi(2\omega)^2}{c^2}\,\vec{P}_T^{NLS}(2\omega) \qquad (17)$$

where

$$\vec{P}_T^{NLS}(z,2\omega) = \overleftrightarrow{\Gamma}_T : \vec{E}_T(z,\omega)\,\vec{E}_T(z,\omega)\,\vec{E}_T(z,0)$$

$$\overleftrightarrow{\Gamma}_T = \overleftrightarrow{R}^{-1} : \overleftrightarrow{\Gamma}_L : \overleftrightarrow{R}\;\overleftrightarrow{R}\;\overleftrightarrow{R}\;, \qquad (17\text{-a})$$

and

$$\overleftrightarrow{\varepsilon}_T(z,2\omega) = \overleftrightarrow{R}^{-1} : \overleftrightarrow{\varepsilon}_L(z,2\omega) : \overleftrightarrow{R}$$

The transformed $\overleftrightarrow{\Gamma}_T$ is now independent of z and has the form for a birefringent material with four independent elements [4]. To solve Eq. (17), we use the usual slowly varying-amplitude approximation and let

$$\vec{E}_T(z,2\omega) = E_+(z,2\omega)\,\hat{e}_+(2\omega)\,\exp\left[ik_+(2\omega)z\right]$$
$$+E_-(z,2\omega)\,\hat{e}_-(2\omega)\,\exp\left[ik_-(2\omega)z\right] \qquad (18)$$

with
$$\left|\frac{\partial^2 E_+}{\partial z^2}\right| << \left|2k_+\frac{\partial E_+}{\partial z}\right|, \quad \left|\frac{\partial^2 E_-}{\partial z^2}\right| << \left|2k_-\frac{\partial E_-}{\partial z}\right|$$

and $\hat{e}_+$, $\hat{e}_-$ given by Eq. (14-a). Substitution of Eq. (18) into Eq. (17) gives

$$(2ik_+(2\omega) - \frac{4\pi}{p}\overleftrightarrow{\sigma})\cdot\hat{e}_+(2\omega)\,\exp\left[ik_+(2\omega)z\right]\frac{\partial E_+}{\partial z}(z,2\omega)$$
$$+\,(2ik_-(2\omega) - \frac{4\pi}{p}\overleftrightarrow{\sigma})\cdot\hat{e}_-(2\omega)\,\exp\left[ik_-(2\omega)z\right]\frac{\partial E_-}{\partial z}(z,2\omega) =$$
$$-\,4\pi\,(\frac{2\omega}{c})^2\,\vec{P}_T^{\,NLS}(z,2\omega) \qquad (19)$$

where we have neglected the second derivatives of E_+ and E_-. Forming the scalar products of $\hat{e}_+^{\,*}(2\omega)$ and $\hat{e}_-^{\,*}(2\omega)$ with Eq. (19), we obtain

$$A\,\exp\left[ik_+(2\omega)z\right]\frac{\partial E_+}{\partial z}(z,2\omega) + B\,\exp\left[ik_-(2\omega)z\right]\frac{\partial E_-}{\partial z}(z,2\omega) =$$
$$-\,4\pi(\frac{2\omega}{c})^2\,e_+^{\,*}(2\omega)\,\vec{P}_T^{\,NLS} \quad ,$$
$$C\,\exp\left[ik_+(2\omega)z\right]\frac{\partial E_+}{\partial z}(z,2\omega) + D\,\exp\left[ik_-(2\omega)z\right]\frac{\partial E_+}{\partial z}(z,2\omega) =$$
$$-\,4\pi(\frac{2\omega}{c})^2\,e_-^{\,*}(2\omega)\,\vec{P}_T^{\,NLS} \qquad (20)$$

where

$$A = 2ik_+(2\omega) - \frac{4\pi}{p} e_+^*(2\omega)\cdot\overleftrightarrow{\sigma}\cdot\hat{e}_-(2\omega)$$

$$B = \hat{e}_+^*(2\omega)\cdot\left[2ik_+(2\omega) - \frac{4\pi}{p}\overleftrightarrow{\sigma}\right]\cdot\hat{e}_-(2\omega)$$

$$C = \hat{e}_+^*(2\omega)\cdot\left[2ik_+(2\omega) - \frac{4\pi}{p}\overleftrightarrow{\sigma}\right]\cdot\hat{e}_+(2\omega) \qquad (21)$$

$$D = 2ik_-(2\omega) - \frac{4\pi}{p} e_-^*(2\omega)\cdot\overleftrightarrow{\sigma}\cdot\hat{e}_-(2\omega)$$

From Eq. (20), we readily obtain

$$\frac{\partial E_+}{\partial z}(z,2\omega) = 4\pi\left(\frac{2\omega}{c}\right)^2 \frac{D\hat{e}_+^*(2\omega)-Be_-^*(2\omega)}{AD - BC} \exp\left[-ik_+(2\omega)z\right]\vec{P}_T^{NLS}$$

$$\frac{\partial E_-}{\partial z}(z,2\omega) = 4\pi\left(\frac{2\omega}{c}\right)^2 \frac{A\hat{e}_-^*(2\omega)-Ce_+^*(2\omega)}{AD - BC} \exp\left[-ik_-(2\omega)z\right]\vec{P}_T^{NLS} \qquad (22)$$

Neglecting the small depletion in the driving field at the fundamental frequency ω, we can write $\vec{E}_T(\omega)$ as

$$\vec{E}_T(z,\omega) = \sum_{i=\pm} E_i(\omega)\hat{e}_i(\omega)\exp\left[ik_i(\omega)z\right] \qquad (23)$$

Since $\vec{E}_L(z,0) = (E^o,0,0)$, $\vec{E}_T(z,0)$ is obtained straight-forwardly as

$$\begin{aligned}\vec{E}_T(z,0) &= \overleftrightarrow{R}^{-1}\cdot\vec{E}(z,0)\\ &= E_+^o\ \hat{e}_+(0)\exp\left[i\frac{2\pi}{p}z\right] + E_-^o\ \hat{e}_-(0)\exp\left[-i\frac{2\pi}{p}z\right]\\ &= \sum_{i=\pm} E_i^o\ \hat{e}_i(0)\exp\left[ik_i(0)z\right]\end{aligned} \qquad (24)$$

where we have defined

$$E_+^{\,o} = E_-^{\,o} = \frac{E^o}{\sqrt{2}}$$

$$\hat{e}_{\pm}(0) = \frac{1}{\sqrt{2}}\,(\hat{\xi} + i\hat{\eta}\,)$$

$$k_{\pm}\ (0) = \pm\,\frac{2\pi}{p} \qquad (25)$$

Using Eq. (17-a), $\vec{P}_T^{\,NLS}$ can be calculated and Eq. (22) can then be integrated to give

$$E_+(2\omega) = 4\pi\left(\frac{2\omega}{c}\right)^2 \frac{D\hat{e}_+^{*}(2\omega) - B\hat{e}_-^{\,*}(2\omega)}{AD - BC} \cdot \overleftrightarrow{\Gamma}_T : \sum_{i,j,k=\pm} \hat{e}_i(\omega)\hat{e}_j(\omega)\hat{e}_k(0)\ \times$$

$$E_i(\omega)\,E_j(\omega)\,E_k(0)$$

$$\times\ \frac{\mathrm{Sin}\left[\frac{1}{2}(\Delta k)_{+ijk} z\right]}{\frac{1}{2}(\Delta k)_{+ijk}}\ \exp\left[-i\frac{1}{2}(\Delta k)_{+ijk} z\right] \qquad (26)$$

$$E_-(2\omega) = 4\pi\left(\frac{2\omega}{c}\right)^2 \frac{A\hat{e}_-^{\,*} - C\hat{e}_+^{\,*}}{AD - BC} \cdot \overleftrightarrow{\Gamma}_T : \sum_{i,j,k=\pm} \hat{e}_i(\omega)\hat{e}_j(\omega)\hat{e}_k(0)\ \times$$

$$E_i(\omega)\,E_j(\omega)\,E_k(0)$$

$$\times\ \frac{\mathrm{Sin}\left[\frac{1}{2}(\Delta k)_{-ijk} z\right]}{\frac{1}{2}(\Delta k)_{-ijk}}\ \exp\left[-i\frac{1}{2}(\Delta k)_{-ijk} z\right] \qquad (27)$$

When $(\Delta k)_{+ijk}$ or $(\Delta k)_{-ijk}$ is zero, phase-matching is achieved.

AD-A095 368 NORTHWESTERN UNIV EVANSTON IL F/G 7/4
NONLINEAR OPTICAL EFFECTS IN LIQUID CRYSTALS.(U)
DEC 80 G K WONG DAAG29-77-G-0009

UNCLASSIFIED ARO-14280.4-P NL

2 OF 2
AD
A095 368

END
DATE
FILMED
3-81
DTIC

Thus the general phase-matching condition for d. c.-field-induced second-harmonic generation is

$$k_i(\omega)+k_j(\omega)+ k_k(0) - k_{\pm}(2\omega) = 0 \qquad (28)$$

where i,j,k can be + or - . Knowing $\bar{\varepsilon}(\omega)$, $\bar{\varepsilon}(2\omega)$ and α of a given cholesteric liquid crystal, we can then use Eq. (11) to examine which of the above mode combinations can satisfy the phase-matching condition.

A simple physical interpretation of Eq. (28) is possible if $\lambda'^2 >> \alpha^2$. Under this condition, Eq. (11) gives

$$k_{\pm} = k_o \pm \frac{2\pi}{p}$$

where $k_o(\omega) = \frac{\omega}{c}\bar{\varepsilon}^{1/2}(\omega)$. Then the phase-matching condition for the mode combination

$$k_+(\omega) + k_+(\omega) + k_+(0) - k_+(2\omega) = 0$$

is equivalent to

$$k_0(2\omega) - 2k_o(\omega) = \frac{2\pi}{p}$$

which shows that the momentum mismatch between the fundamental and second harmonic photons is compensated by the lattice momentum associated with the helical structure.

4.2 Experiments

The phase-matching conditions for d. c.-field-induced second-harmonic generation in cholesteric liquid crystal was tested experimentally using a mixture of 1.75:1.00 by weight of cholesteryl chloride and cholesteryl myristate [5]. These materials were obtained from Eastman Kodak and then purified with standard techniques [6]. These materials were first dissolved in heptane. The insoluble impurity residues were then filtered out. After these materials were recovered by recrystallization out of the solution, they were kept in a dessicator which was continuously pumped to remove traces of solvent. The correct amount of each material was then weighed out to form the desirable mixture. The helical pitch of this mixture is variable from $-1.7\ \mu m$ to $\pm\ \infty$ to $2\ \mu m$ by varying the temperature from 20 to $68^{\circ}C$. (A negative pitch denotes a left-handed twisted structure.) The inverse pitch as a function of temperature is shown in Fig. 2. The temperature dependence of the pitch is described very well by $p = \frac{42.86\ \mu m}{T-T_N}$ where T_N is the temperature at which the pitch goes to impurity. T_N for our sample was $42.35^{\circ}C$. The dielectric constant $\bar{\epsilon}(1.064\ \mu m)$, $\bar{\epsilon}(5320 Å)$ and α had been determined in Ref. 4 to be 2.18, 2.24 and 0.03 respectively. Using these values in Eq. (13), we determined that out of all the mode combinations, only

$$k_+(\omega) + k_+(\omega) + k_{\pm}^{o}(\omega) = k_+(2\omega) \qquad (29)$$

$$k_+(\omega) + k_-(\omega) + k_{\pm}^{o}(\omega) = k_+(2\omega) \qquad (30)$$

are phase matchable. The first mode combination shown in Eq. (29) is phase matchable at $p = \pm 42.5\ \mu m$ and that shown in Eq.(30) at $p = \pm 220 \mu m$. Using the results shown in Fig.2, we determined $p = 42.5\ \mu m$ occurs at $43.35^{\circ}C$ and $p = 42.5\ \mu m$ at $41.35^{\circ}C$. For $p = \pm\ 220\ \mu m$, phase-matching should occur at $T = T_N + 0.2^{\circ}C$. Since the condition of sample alignment is usually very poor near T_N, we expect to be able to observe phase-matching at $43.35^{\circ}C$ and $41.35^{\circ}C$ only.

Our experiments were performed on a $60\ \mu m$ thick sample. Alignment of the sample was achieved by placing the mixture between two clean, unidirectionally rubbed glass spacers. Fig. 3 shows the observed second-harmonic intensity as a function of temperature. Two peaks appear at temperatures within $0.1^{\circ}C$ of the predicted values of $43.35^{\circ}C$ and $41.35^{\circ}C$. The solid theoretical curve was calculated from

$$I(2\omega) = \frac{\sin^2\left(\frac{1}{2}\,(\Delta k)\text{++++}\ell\right)}{\left(\frac{1}{2}\,(\Delta k)\text{++++}\ell\right)^2}$$

using Eq. (10) and the measured temperature dependence of $\bar{\varepsilon}(1.064\ \mu m)$, $\bar{\varepsilon}(5320\mathring{A})$, α and p^4. The sample length ℓ for our sample is $60\ \mu m$. The calculated full width at half-maximum (FWHM) is $0.4^{\circ}C$ which is narrower than the observed FWHM of $1^{\circ}C$. This discrepancy is probably mainly due to the fact that the orientation of molecules on the surface of the glass spacer are determined by the interaction of molecules and the rubbed surface. This anchoring force is sufficiently strong that the molecular orientation on the boundary layers remain unchanged as the temperature is varied. This constraint would not allow a perfect helical structure of arbitrary pitch to fit between the two interfaces.

Thus there would in general be a distortion of the helical structure amounting to ~ $\frac{1}{2}p$ over the sample thickness. This implies a pitch distribution with a width $\frac{\delta p}{p} \sim \frac{p}{2\ell}$. For ℓ = 60 μm and p = 42.5 μm, δp is $\sim 15\,\mu m$. Using the temperature dependence of p, this δp amounts to an additional broadening of $0.4^{o}C$ in the FWHM of the observed peaks. The additional broadening is probably due to the presence of domains with somewhat different orientations of the helical axis.

In summary, we have studied theoretically the phase-matching conditions for d. c.-field-induced second-harmonic generation in a cholesteric liquid crystal. The experimental results obtained with a cholesteric mixture of cholesteryl choloride and cholesteryl myristate agree well with the theoretical predictions.

REFERENCES

Chapter 4

1. J. W. Shelton and Y. R. Shen, Phys. Rev. Lett. 25, 23 (1970).

2. C. W. Oseen, Trans. Faraday Soc. 29, 883 (1933).

3. H. de Vries, Acta Cryst. 4, 219 (1951).

4. J. W. Shelton and Y. R. Shen, Phys. Rev. A5, 1867 (1972).

5. E. Sackmann, S. Meilboom, L. C. Snyder, A. E. Meixner, and R. E. Dietz, J. Am. Chem. Soc. 90, 3567 (1968).

6. K. Miyano, Ph.D. Thesis, Northwestern University, 1975 (unpublished).

FIGURE CAPTIONS

Chapter 4

1. Molecular arrangement in a cholesteric liquid crystal ξ and η are the molecular alignment axes.
2. Temperature dependence of inverse pitch of a cholesteric liquid crystal.
3. Variation of the second-harmonic intensity as a function of temperature. The solid line is the theoretical phase-matching curve and the circles are experimental data points.

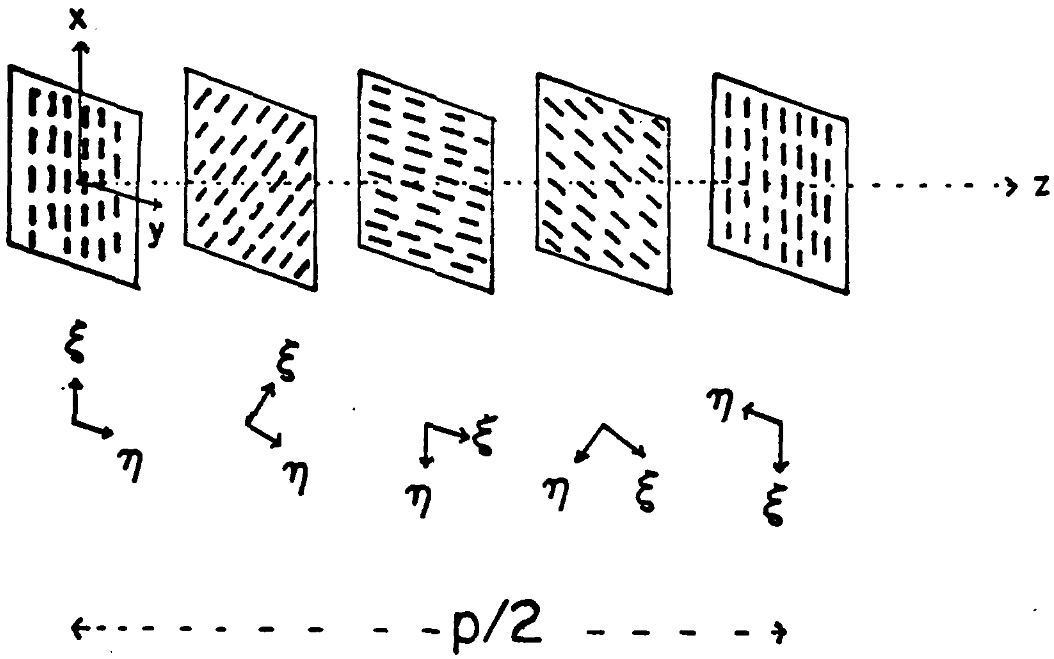

FIG. 1

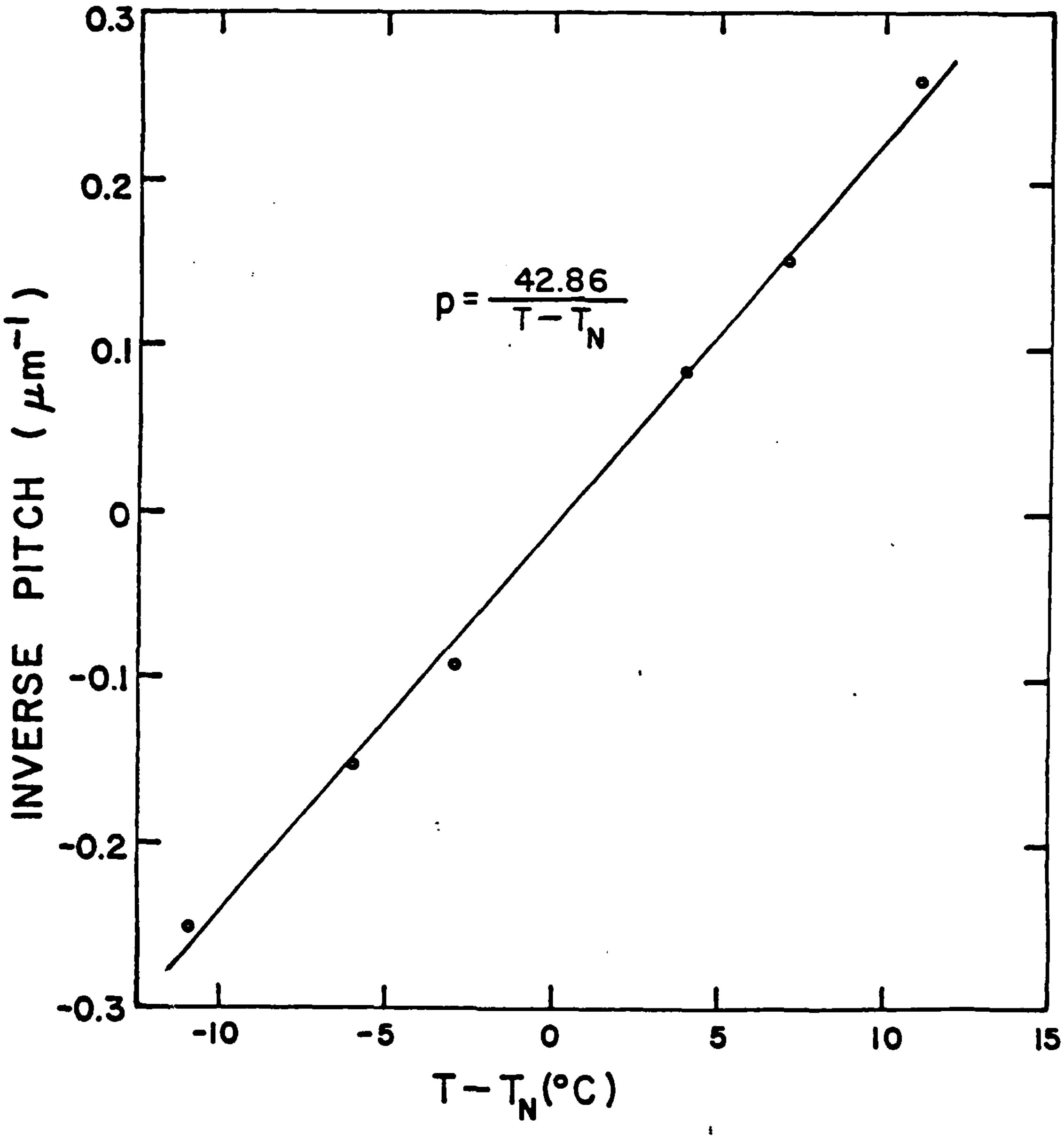
0.3
0.2
0.1
0
-0.1
-0.2
-0.3
INVERSE PITCH (μm⁻¹)
$p = \frac{42.86}{T - T_N}$
-10
-5
0
5
10
15
T − T_N(°C)

FIG. 2

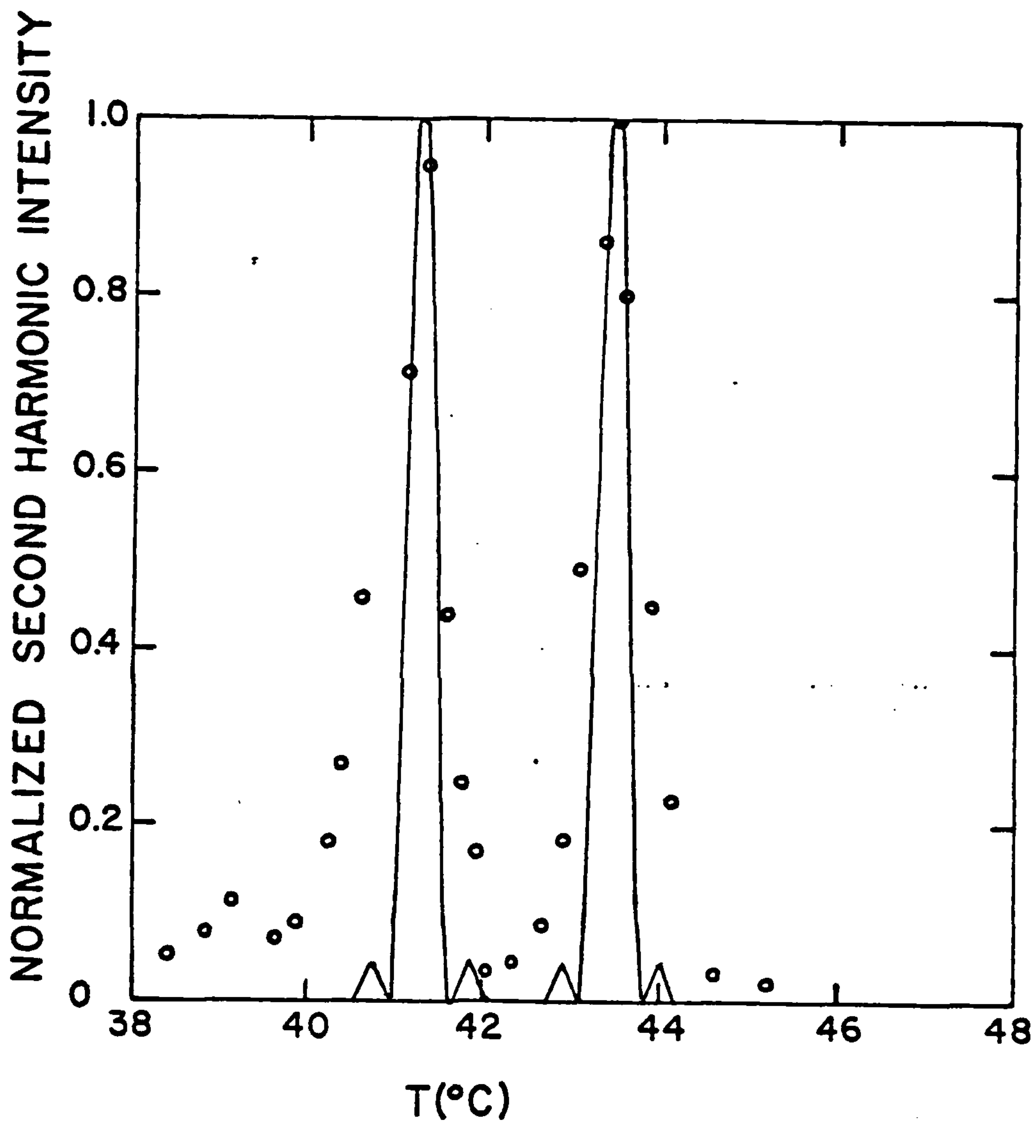
NORMALIZED SECOND HARMONIC INTENSITY
1.0
0.8
0.6
0.4
0.2
0
38
40
42
44
46
48
T(°C)

FIG. 3

5. FLEXOELECTRIC INDUCED SECOND-HARMONIC GENERATION IN A NEMATIC LIQUID CRYSTAL

5.1 Introduction

Liquid crystals exhibit many interesting third-order nonlinear optical effects.[1] Unusually large optical Kerr effect[2,3] and strong self-focusing[4] have been observed near the isotropic to nematic phase transition. Phase-matched third harmonic generation[5] and d. c.-field-induced second harmonic generation[6,7] have also been observed in cholesteric (CLC) and nematic (NLC) liquid crystals. However, second-order nonlinear processes are not expected to occur in NLC and CLC because these two phases possess overall inversion symmetry[8], i.e., the physical equivalence of the director direction $\hat{n}$ and $-\hat{n}$. In fact, the absence or presence of optical second-harmonic generation (SHG) provides a reliable determination of the presence or absence of centrosymmetry in crystal structures.[9] The method is especially useful when X-ray results do not provide unambiguous conclusions. Earlier experiments [10,11] on CLC and NLC indicate SHG is indeed absent in these two phases, providing strong support that $\hat{n}$ and $-\hat{n}$ are physically equivalent in CLC and NLC. However, Arakelyan et.al.[12] recently reported that they had observed SHG in well aligned samples of nematic liquid crystal MBBA (P-methoxy benzylidene p-n-butylanilane). These authors, therefore, questioned the generally accepted view that $\hat{n}$ and $-\hat{n}$ are physically indistinguishable in NLC and CLC. In view of the fundamental importance of this question, we have performed SHG experiments on aligned samples of NLC MBBA. Our results show that SHG can be observed only in samples with distortion in its director field. No SHG is present in samples which exhibit sharp conoscopic figures. Analysis based on our experimental results indicates that flexoelectric effect is responsible for the observed SHG. Our results reaffirm that NLC and CLC possess overall centrosymmetry.

5.2 Experiment

The MBBA used in our experiments was purchased from Atomergic Chemetals Corp. and was used without further purification. The nematic to isotropic transition (N-I) temperature of freshly prepared thin film samples was $43^{o}C$. In our experiment, we used only homogeneously aligned samples. The alignment was achieved either by unidirectional rubbing of carefully cleaned microscopic slides or by using fused quartz plates coated with SiO_2 evaporated obliquely onto the plates.[13] The quality of the alignment was checked by monitoring the conoscopic figure obtained with a focussed He-Ne laser beam.[14] Distortion in the director field over areas as small as 20 μm across could be readily detected. The thickness of samples used in the experiments ranged from a few tens to about 200 microns.

5.3 Results and discussion

In samples with satisfactory alignment as evidenced by the presence of a clear conoscopic figure of families of hyperbola-like fringes in these samples, no SHG was detected. However, strong SHG was observed in samples with distortion in the director field. These samples did not show a clear conoscopic figure and they were prepared by rubbing with unidirectional "hard" strokes. Additional information about the director distortion was obtained from the following observation. When an unfocussed He-Ne laser beam linearly polarized along the rubbing direction was sent through these thin film samples, the beam was scattered into a streak perpendicular to the rubbing direction. However, for He-Ne laser beam linearly polarized perpendicular to the rubbing direction, virtually no scattering was observed. These observations indicate that the director of these samples prepared by rubbing with "hard" strokes tilts away from the substrate surface with the director lying in the plane formed by the rubbing direction and the normal of the substrate surface. The degree of tilting, however, varies randomly across the substrate surface making the thin film sample appear as a random grating for light polarized parallel to the rubbing direction.

The SHG observed in these samples was strongly polarized perpendicular to the rubbing direction with extinction ratio $\gtrsim 10$. For a linearly polarized fundamental beam, the observed SHG intensity $I^{2\omega}$ varied as a function of θ, the angle between the polarization direction. As shown in Fig. 1, the angular variation closely followed a $\sin^2 2\theta$ dependence. This indicates the dominant contribution to the SHG is due to an effective nonlinear susceptibility Γ^{eff}_{xxz}, where we have taken z to be along the rubbing direction, x to be in the plane of the substrate surface, and y to be the beam propagation direction which is normal to the substrate surface. For a linearly polarized fundamental beam, this nonlinear susceptibility leads to a nonlinear polarization $P_x^{2\omega} \propto \Gamma_{xxz}^{eff} E_x E_z = \Gamma_{xxz}^{eff} E^2 \sin\theta\cos\theta$ and hence the observed θ dependence of $I_x^{2\omega}$ since $I_x^{2\omega} \propto P_x^{2\omega\,2} \propto \sin^2 2\theta$. The temperature dependence of $I_x^{2\omega}$ is shown in Fig. 2. In the nematic phase, the SHG intensity decreased slightly with increasing temperature but dropped rapidly to zero at the N-I transition temperature. We have also measured the sample length dependence of the SHG intensity. Within $\pm$ 10%, the SHG intensity was independent of sample thickness and did not exhibit any clear coherence length effect. This indicates that the observed SHG is gen ated in a region whose thickness is thinner than or comparable to a coherence length which is a few microns for MBBA.

From the above observations, it is clear that the observed SHG is due to a flexoelectric effect. Rubbing with "hard" strokes produces aligned sample with distortion in its director field near the substrate surface. This distortions leads to a linear polarization that destroys the overall centrosymmetry of nematic phase and hence gives rise to SHG. From the polarization dependence of the scattering of the He-Ne laser beam, we know that the director field near the substrate surface is of the form

$$
\begin{aligned}
n_z &= \cos\Phi\ (x,y) \\
n_y &= \sin\Phi\ (x,y) \qquad\qquad (1) \\
n_x &= 0
\end{aligned}
$$

While the exact form of $\phi(x,y)$ may be complicated, it suffices for a qualitative analysis to assume that

$$\Phi(x,y) = A \sin kx \, e^{-\alpha y} \tag{2}$$

with $A \ll 1$. Due to the flexoelectric effect, this director field leads to a linear polarization given by[8]

$$\vec{P}^d = e_1 \hat{n}(\nabla\cdot\hat{n}) + e_3(\nabla \times \hat{n}) \times \hat{n} \tag{3}$$

where e_1 and e_3 are the flexoelectric coefficients. To first order in A, we obtain from Eqs. (1), (2) and (3) a linear polarization

$$P_z^d = -e_1 \alpha \, A \sin kx \, e^{-\alpha y} \tag{4}$$

The nematic medium then becomes effectively a uniaxial system without centrosymmetry. From symmetry consideration,[15] the only nonvanishing second-order nonlinear susceptibilities for this medium are $\Gamma^{eff}_{xxz} = \Gamma^{eff}_{xxz} = \Gamma^{eff}_{zxx} = \Gamma^{eff}_{zyy}$ and Γ^{eff}_{zzz}. The fact that we only observed significant SHG from Γ^{eff}_{xxz} is probably due to the following two reasons. First, the SHG due to Γ^{eff}_{zzz} and Γ^{eff}_{zxx} would be polarized along the rubbing direction and hence would be scattered by the random grating effect of the director distortion. A large part of the SHG signal would have missed the photomultiplier. Second, using the refractive indices of MBBA at 5320Å and 1.064 μm[16], we calculated the SHG coherent length to be 0.8μm for Γ^{eff}_{zxx} geometry, 2.2μm for Γ^{eff}_{zzz}, and 7.2μm for Γ^{eff}_{xxz}. Thus, if $1/\alpha$ is ≤7.2μm but ≫ 2.2 μm, the SHG generated will be dominated due to Γ^{eff}_{xxz} as was observed in our experiments.

5.4 Conclusion

We have observed SHG from MBBA thin film samples which have distortion in their director field. We have shown that our experimental results can be explained well by the flexoelectric effect and the observed SHG in NLC MBBA is not due to the lack of centrosymmetry in the nematic phase. We notice that Arakelyan et.al.[12] used in their experiment NLC samples prepared by rubbing technique and they did not check the quality of alignment by monitoring the conoscopic figures. We, therefore, believe the SHG observed in their experiment is also due to the flexoelectric effect and not due to the lack of centrosymmetry in NLC.

REFERENCES

Chapter 5

1. See, for a review, Y. R. Shen, Rev. Mod. Phys. 48, 1 (1976).
2. G. K. Wong and Y. R. Shen, Phys. Rev. Lett. 30, 895 (1973); Phys. Rev. A10, 1277 (1974).
3. J. Prost and J. R. Lalanne, Phys. Rev. A8, 2090 (1973).
4. E. G. Hanson, Y. R. Shen and G. K. Wong, Appl. Phys. 14, 65 (1977).
5. J. W. Shelton and Y. R. Shen, Phys. Rev. A5, 1867 (1972).
6. S. K. Saha and G. K. Wong, Appl. Phys. Lett. 34, 432 (1979).
7. S. K. Saha and G. K. Wong, Optics Comm., 30, 119 (1979).
8. See, for example, P. G. de Gennes, "Physics of Liquid Crystals", (Clarendon Press, Oxford, 1974).
9. A. Coda and F. Pandarese, J. Appl. Crystl. 9, 193 (1976).
10. G. Durand and C. H. Lee, Compt. Rend. 264, series B, 1397 (1967) and Mol. Crystl. 5, 171 (1968).
11. L. S. Goldberg and J. S. Schnur, Appl. Phys. Lett. 14, 306 (1969) and Radio Electronic Engr. 39, 279 (1970).
12. S. M. Arakelyan et.al., JETP Lett. 28, 202 (1978).
13. W. Urbach, M. Boix and E. Guyon, Appl. Phys. Lett. 25, 479 (1974).
14. S. Jen, N. A. Clark, P. S. Pershan, and E. B. Priestly, J. Chem. Phys. 66, 4635 (1977).
15. P. N. Butcher, "Nonlinear Optical Phenomena" (Ohio State University Engineering Publications, Columbus, Ohio, 1965).
16. Extrapolated from the data of M. Germain, C. R. Acad. Sc. Paris 271, series B, 1075 (1970).

FIGURE CAPTIONS

Chapter 5

1. Variation of second-harmonic intensity as a function of the angle (θ) between the rubbing direction and the polarization vector of the fundamental beam. The solid line is the plot of $\sin^2 2\theta$.

2. Relative second-harmonic intensity as a function of temperature.

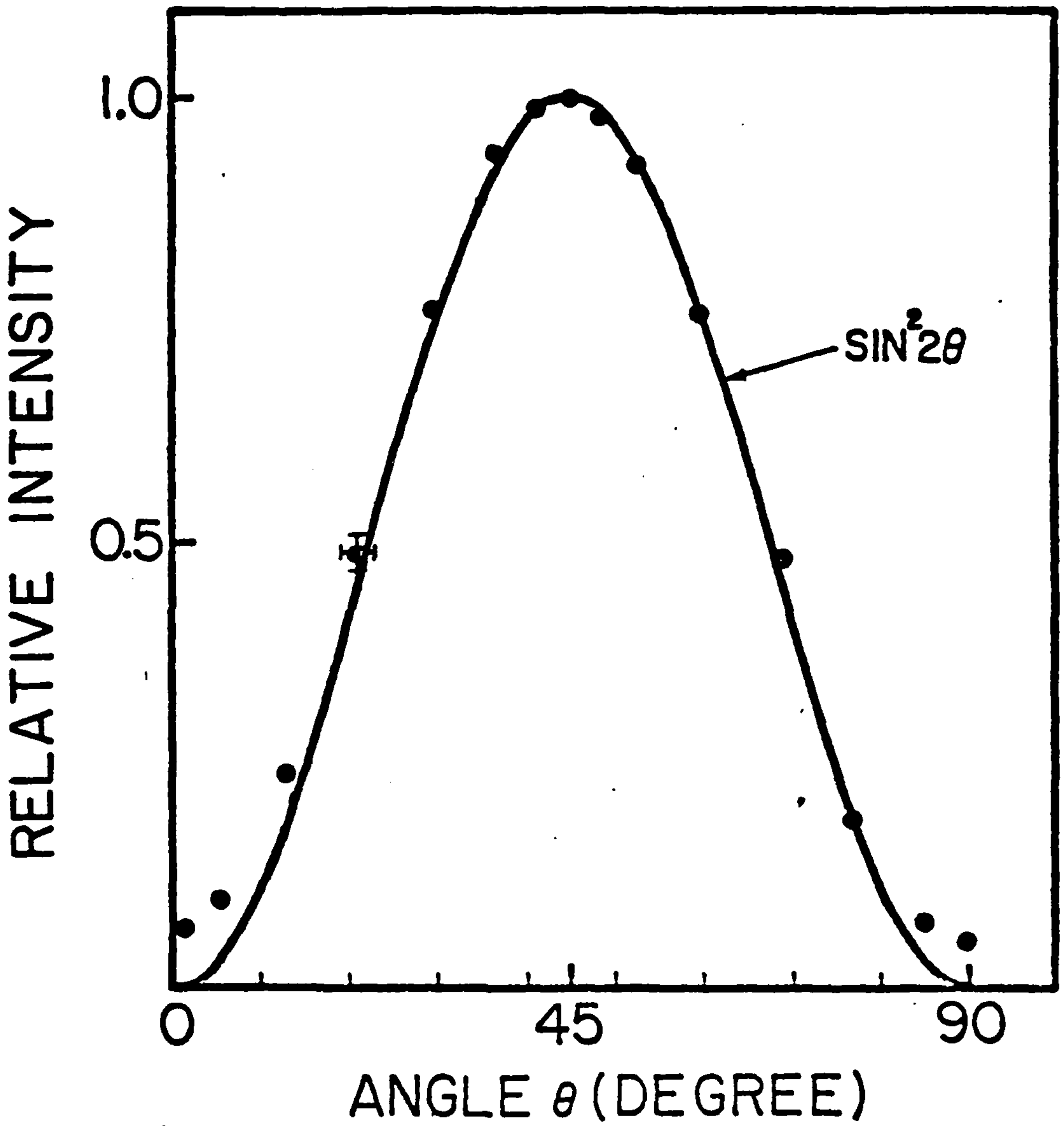
RELATIVE INTENSITY
1.0
0.5
$SIN^2 2\theta$
0
45
90
ANGLE θ (DEGREE)

FIG. 1

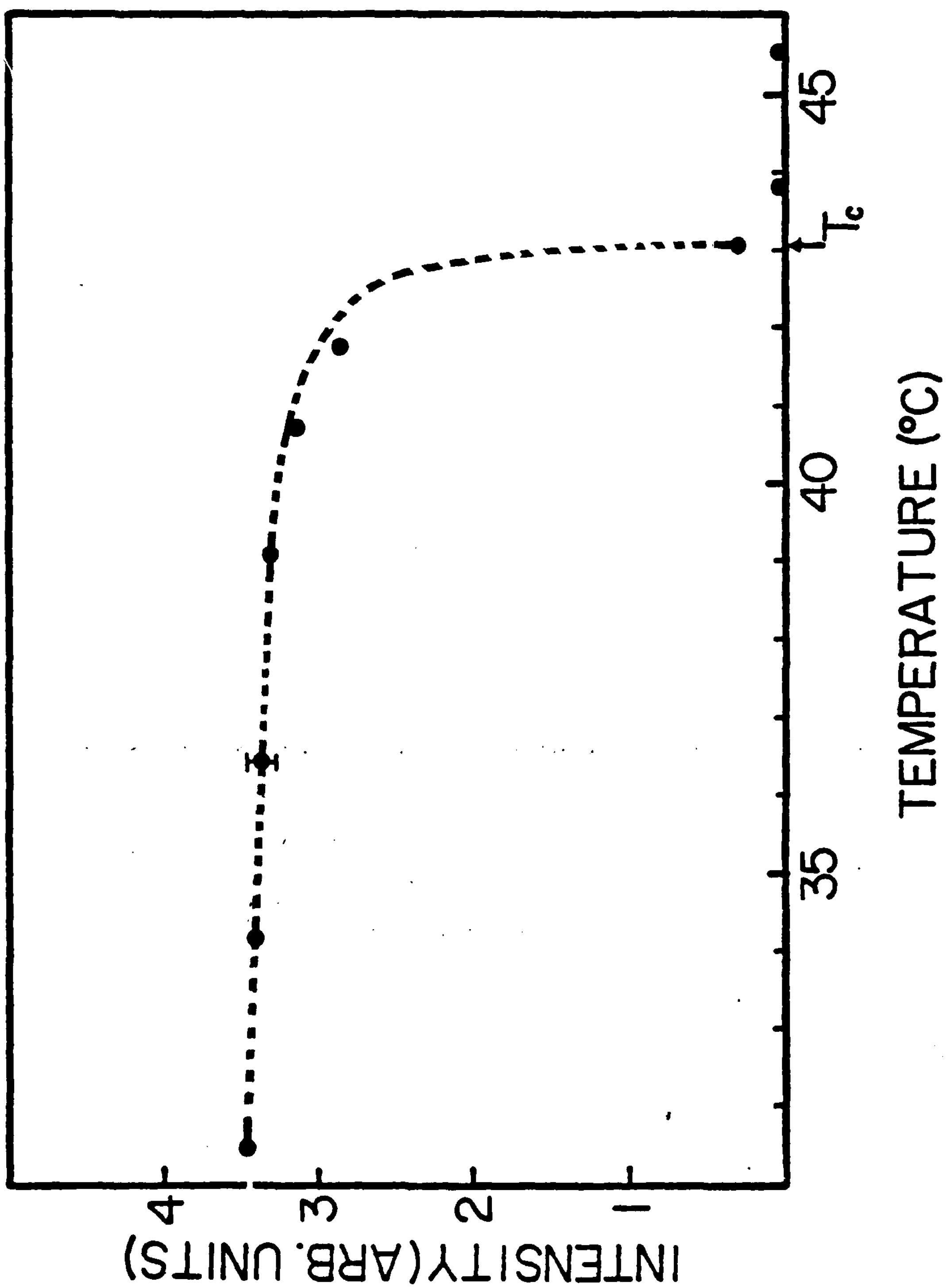

FIG. 2

LMED

8